

NO-A100 000

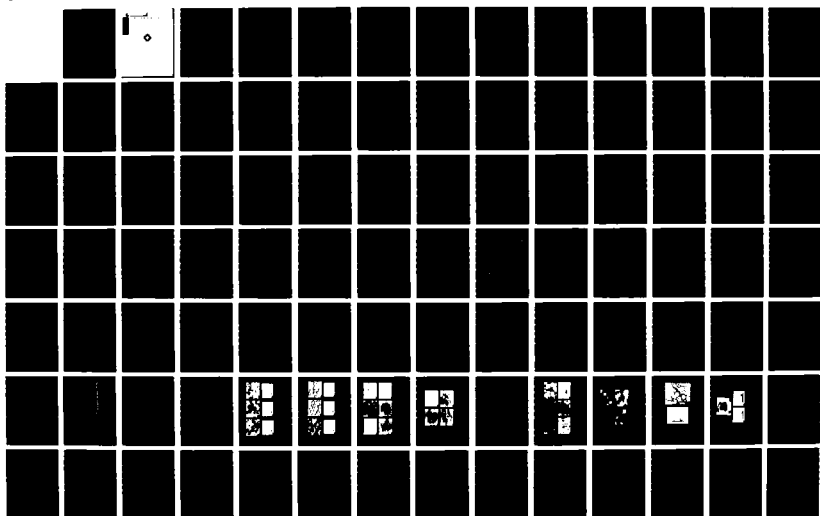
ULTRA-LOW EXPANSION METAL MATRIX COMPOSITES(U)
MASSACHUSETTS INST OF TECH CAMBRIDGE LAB FOR MFG AND
PRODUCTIVITY N P SUN ET AL. APR 81 LNP/MTLS-81-84
NDAS83-78-C-0417

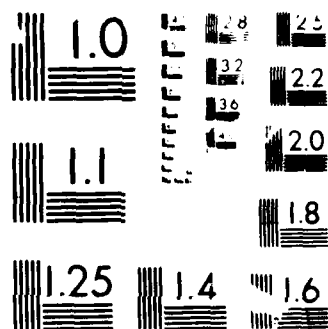
1/2

UNCLASSIFIED

F/G 11/4

NL





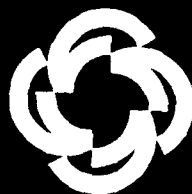
1919-1920 RESOLUTION TEST CHART

AD-A188 000

Ultra-Low Expansion Metal Matrix Composites

Final Report to
The Defense Advanced Research Projects Agency
Contract No. MDA 903-78-C-0417

Nam P. Suh
Nannaji Saka
Joseph Boustani



Laboratory for Manufacturing and Productivity
School of Engineering
Massachusetts Institute of Technology
Cambridge, Massachusetts 02139

April 1981

①

ULTRA-LOW EXPANSION METAL MATRIX COMPOSITES

Final Report to
The Defense Advanced Research Projects Agency
Contract No. MDA 903-78-C-0417



Accession For	
NTIS	<input checked="" type="checkbox"/>
DTIC	<input type="checkbox"/>
Unannounced	<input type="checkbox"/>
Justification	
By	
Distribution/	
Availability Codes	
Dist	Avail and/or Special
A-1	

Nam P. Suh
Nannaji Saka
Joseph Boustani

DTIC
ELECTE
DEC 03 1987
S E D

Laboratory for Manufacturing and Productivity

School of Engineering
Massachusetts Institute of Technology
Cambridge, Massachusetts 02139

April 1981

This report is the property of the
Department of Defense and is to be
returned to the organization to which it
is loaned.

87 11 18 082

REPORT DOCUMENTATION PAGE		READ INSTRUCTIONS BEFORE COMPLETING FORM
1. REPORT NUMBER	2. GOVT ACCESSION NO.	3. RECIPIENT'S CATALOG NUMBER
-----		-----
4. TITLE (and Subtitle) Ultra-Low Expansion Metal Matrix Composites		5. TYPE OF REPORT & PERIOD COVERED August 4, 1978 - Sept. 30, 1980
		6. PERFORMING ORG. REPORT NUMBER LMP/MTLS-81-04
7. AUTHOR(s) Nam P. Suh, Nannaji Saka and Joseph Boustani		8. CONTRACT OR GRANT NUMBER(s) MDA-903-78-C-0417
9. PERFORMING ORGANIZATION NAME AND ADDRESS Laboratory for Manufacturing and Productivity Massachusetts Institute of Technology 77 Mass. Ave, Cambridge, MA 02139		10. PROGRAM ELEMENT, PROJECT, TASK AREA & WORK UNIT NUMBERS -----
11. CONTROLLING OFFICE NAME AND ADDRESS Office of Naval Research Department of the Navy Arlington, VA 22217		12. REPORT DATE April, 1981
		13. NUMBER OF PAGES 140
14. MONITORING AGENCY NAME & ADDRESS (if different from Controlling Office) MIT Resident Representative Office of Naval Research Room E19-628, MIT, Cambridge, MA 02139		15. SECURITY CLASS. (of this report) Unclassified
		15a. DECLASSIFICATION/DOWNGRADING SCHEDULE -----
16. DISTRIBUTION STATEMENT (of this Report) Approved for public release; distribution unlimited		
17. DISTRIBUTION STATEMENT (of the abstract entered in Block 20, if different from Report) -----		
18. SUPPLEMENTARY NOTES -----		
19. KEY WORDS (Continue on reverse side if necessary and identify by block number) High Altitude Large Optics (HALO), High Energy Laser Optics (HELO) Ultra-low CTE Materials, Metal-Ceramic Composites Thermoelastic Analysis, Powder Metallurgy Processing		
20. ABSTRACT (Continue on reverse side if necessary and identify by block number) (See summary)		

SUMMARY

The satisfactory performance of mirror substrates of High Energy Large Optics (HALO) and High Energy Laser Optics (HELLO) requires that the distortion of these substrates (due to temperature variations) be less than $0.1 \mu\text{m}$ per meter (ideally zero thermal expansion) in the temperature range 150-300K. In addition they should have high thermal conductivity, high microyield strength and low density. Moreover, they should be extremely resistant to outgasing.

A literature survey has been conducted to identify currently available materials that satisfy the above criteria. After many discussions with other investigators and a thorough screening of the published literature, it has been found that there exists no material, commercial or experimental, that satisfies the above requirements.

Indeed, the material that will have the optimum properties is a metal matrix particle dispersed composite. Accordingly, theoretical and experimental work has been conducted on such composites.

A thermoelastic analysis has been carried out to compute the coefficient of thermal expansion (CTE). Exact equations for stresses, strains and CTE have been derived for a two-phase composite. The results indicate that the thermal expansion coefficient of the composite is a sensitive function of the CTE's of the constituent phases and insensitive to the elastic moduli and Poisson's ratios. It is shown that to produce ultra low or zero CTE materials two phases, one with a low positive CTE and the other with large negative CTE, are required. Further, the amount of the matrix and dispersed phases should be controlled to within a few percent.

Experimental work on the $\text{Ni-Nb}_2\text{O}_5$ and superinvar- Nb_2O_5 composites was carried out using powder metallurgy techniques. Thermal expansion coefficients measured by laser interferometry in the temperature range 200-300K indicate that the Nb_2O_5 has a positive thermal expansion coefficient ($0.52 \times 10^{-6} \text{K}^{-1}$). The composites have a thermal expansion coefficient an order of magnitude smaller than common metals and comparable to invar and superinvar. The agreement between theoretically predicted values and the experimentally measured values was excellent.

However, the experimentally measured CTE values of $\text{Ni-Nb}_2\text{O}_5$, Superinvar- Nb_2O_5 were much higher than that are required for HALO/HELLO applications. On the basis of this work a few suggestions can be offered to produce zero or ultra-low CTE materials. It is absolutely necessary to use a metal

that has a low thermal expansion coefficient and a ceramic phase that has the largest possible negative CTE. Unfortunately, literature search has shown that not many ceramics have large negative CTE. In fact, most negative CTE values reported for ceramics in the literature are suspect because of micro-cracking during CTE measurement. The most reliable CTE values are those obtained by low-temperature x-ray diffraction. Further literature search has shown that La_2O_3 has a negative thermal expansion coefficient of about $-4.0 \times 10^{-6} \text{ K}^{-1}$ at room temperature. Currently we are working on La_2O_3 and TaVO_5 to obtain a negative CTE ceramic.

Moreover, it is necessary to improve the bonding between the metal and ceramic phase. This can be done by coating metal which forms an oxide that has lowest free energy of formation than the ceramic phase. Zr is ideal for this purpose, for it forms a stable Oxide (ZrO_2) when reacted with oxide ceramic phase and, therefore, bonding is expected to improve. We are also working on this problem at present.

Acknowledgments

This research was sponsored by the Defense Advanced Research Projects Agency under contract No. MDA 903-78-C-0417. The authors are grateful to Major Harry V. Winsor and Dr. E. Joseph Friebele for their support and guidance throughout the course of this research. Thanks are due Dr. Ernest G. Wolff of the Aerospace Corporation for his help in the measurement of CTE by laser interferometry and low temperature dilatometry.

TABLE OF CONTENTS

	<u>Page</u>
TITLE PAGE.....	1
SUMMARY	3
ACKNOWLEDGEMENTS.....	5
TABLE OF CONTENTS.....	6
LIST OF TABLES	8
LIST OF FIGURES.....	9
NOMENCLATURE.....	13
CHAPTER I - INTRODUCTION.....	14
CHAPTER II - LITERATURE REVIEW.....	16
A. Thermal Expansion Coefficient.....	16
B. Other Properties.....	22
CHAPTER III- THEORETICAL ANALYSIS.....	32
A. Thermoelastic Analysis.....	33
A.1 General Thermoelastic Equation for an Inhomogeneous Sphere.....	33
A.2 Multilayered Sphere.....	35
A.3 Two-phase Sphere.....	39
B. Composite Design.....	47
CHAPTER IV - EXPERIMENTAL PROCEDURES.....	54
A. Flame Spraying.....	55
B. Electroless Plating.....	55
C. Mechanical Mixing.....	56
D. Hot Pressing.....	56
E. Optical Metallography.....	57

		<u>Page</u>
	F. Scanning Electron Microscopy.....	57
	G. X-Ray Diffraction.....	57
	H. Chemical Analysis.....	57
	I. CTE Measurements.....	58
CHAPTER V	- RESULTS.....	59
	A. Chemical Analysis.....	59
	B. X-Ray Diffraction.....	65
	C. Scanning Electron Microscopy.....	71
	D. CTE Measurements.....	76
CHAPTER VI	- DISCUSSION.....	95
CHAPTER VII	- CONCLUSIONS.....	107
	REFERENCES.....	109
APPENDIX I	- THERMAL EXPANSION COEFFICIENT OF COMPOSITES: LITERATURE REVIEW.....	114
APPENDIX II	- FLAME SPRAYING.....	122
APPENDIX III	- ELECTROLESS PLATING.....	125
APPENDIX IV	- HOT PRESSING.....	130
APPENDIX V	- CTE MEASUREMENTS.....	137

LIST OF TABLES

<u>Table Number</u>	<u>Title</u>	<u>Page</u>
1	Materials with Negative CTE.....	19
2	Thermal and Mechanical Properties of Various Polymers.....	23
3	Thermal and Mechanical Properties of Various Metals.....	24
4	Thermal and Mechanical Properties of Various Ceramics.....	25
5	Values of $(\sigma_r - \sigma_g)_{\max}$ for $\Delta T = 250K$ and Yield Stress of Various Metals.....	53
6	Semiquantitative Chemical Analysis.....	60
7	Carbon Weight Percent.....	62
8	Composition of Superinvar.....	63
9	Weight and Volume Percent of Ni in Ni-Nb ₂ O ₅ Composites.....	64
10	CTE Predictions of Ni-Nb ₂ O ₅ Composites at 300K.....	102
III-1	Composition of the Niposit 468 Electroless Plating Bath.....	126
III-2	Plating Time vs Nickel Volume Fraction.....	127

LIST OF FIGURES

<u>Figure Number</u>	<u>Title</u>	<u>Page</u>
1	Materials with Positive CTE.....	13
2	Thermal Conductivity versus CTE.....	27
3	Modulus of Elasticity versus CTE.....	28
4	Tensile Strength versus CTE.....	29
5	Density versus CTE.....	30
6	Multilayered Composite Sphere.....	36
7	Dimensionless Plot of the Composite's CTE vs the Volume Fraction of the Dispersoid (Material 1).....	48
8	Coefficient of Thermal Expansion of the Composite at 300K vs Volume Fraction of Nb_2O_5	50
9	Semi-Log Plot of the Composite's CTE vs Volume Fraction of Nb_2O_5 at 300K.....	51
10	X-Ray Diffraction Pattern of as Received Nb_2O_5 Powder. Ni-Filtered Copper Radiation, 35 kV, 15 mA.....	66
11	X-Ray Diffraction Pattern of Flame Sprayed Nb_2O_5 Powder. Ni-Filtered Copper Radiation, 35 kV, 15 mA.....	67
12	X-Ray Diffraction Pattern of Hot Pressed Nb_2O_5 and Ni-90.5 Nb_2O_5 Composite. Ni-Filtered Copper Radiation, 35 kV, 15 mA..	68
13	X-Ray Diffraction Pattern of Ni-87.3 Nb_2O_5 after Plating. Ni-Filtered Copper Radiation, 35 kV, 15 mA.....	69

<u>Figure Number</u>	<u>Title</u>	<u>Page</u>
14	X-Ray Diffraction Pattern of Superinvar Powder. Chromium Radiation, 35 kV, 15 mA.....	70
15	SEM Micrographs of Aldrich Nb ₂ O ₅ Powder: (a) As received, (b) Flame Sprayed and (c) Ni-coated; (d), (e) and (f) are EDAX Analysis of (a), (b) and (c) Repsectively.....	72
16	SEM Micrographs of A.D. McKay Nb ₂ O ₅ Powder: (a) As received, (b) Flame Sprayed and (c) Ni-coated; (d), (e) and (f) are EDAX Analysis of (a), (b) and (c) Respectively.....	73
17	SEM Micrographs of Ni-Nb ₂ O ₅ and Nb ₂ O ₅ , Hot Pressed and Polished Specimens: (a) Ni-20.5 Nb ₂ O ₅ , (b) Ni-33.5 Nb ₂ O ₅ , (c) Ni-63.15 Nb ₂ O ₅ , (d) Ni-87.3 Nb ₂ O ₅ , (e) Ni-90.5 Nb ₂ O ₅ and (f) Nb ₂ O ₅	74
18	SEM Micrographs of Superinvar and Superinvar-Nb ₂ O ₅ , Hot Pressed and Polished Specimens: (a) Superinvar, (b) Superinvar-10 Nb ₂ O ₅ , (c) Superinvar-20 Nb ₂ O ₅ and (d) Superinvar 50 Nb ₂ O ₅	75
19	Optical Micrographs of Ni-Nb ₂ O ₅ and Nb ₂ O ₅ , Hot Pressed and Polished Specimens: (a) Ni-20.5 Nb ₂ O ₅ , (b) Ni-33.5 Nb ₂ O ₅ , (c) Ni-63.15 Nb ₂ O ₅ , (d) Ni-87.3 Nb ₂ O ₅ , (e) Ni-90.5 Nb ₂ O ₅ and (f) Nb ₂ O ₅	77
20	Optical Micrographs of Superinvar and Superinvar-Nb ₂ O ₅ , Hot Pressed and Polished Specimens: (a) Superinvar, (b) Superinvar-10 Nb ₂ O ₅ , (c) Superinvar-20 Nb ₂ O ₅ and (d) Superinvar-50 Nb ₂ O ₅	78
21	SEM Micrograph and EDAX Analysis of Superinvar Powder.....	79

<u>Figure Number</u>	<u>Title</u>	<u>Page</u>
22	SEM and EDAX Analysis of Hot Pressed Superinvar: (a) bulk superinvar sample and (b) segregated particle.....	80
23	Thermal Expansion of Ni-20.5 Nb ₂ O ₅ vs Temperature.....	81
24	Thermal Linear Expansion of Ni-33.5 Nb ₂ O ₅ vs Temperature.....	82
25	Thermal Linear Expansion of Ni-63.15 Nb ₂ O ₅ vs Temperature.....	83
26	First Measurement of the Thermal Linear Expansion of Ni-87.3 Nb ₂ O ₅ vs Temperature..	84
27	Second Measurement of the Thermal Linear Expansion of Ni-87.3 Nb ₂ O ₅ vs Temperature..	85
28	Thermal Linear Expansion of Ni-90.5 Nb ₂ O ₅ vs Temperature.....	86
29	Thermal Linear Expansion of Nb ₂ O ₅ vs Temperature.....	87
30	Thermal Linear Expansion of Superinvar vs Temperature.....	88
31	Thermal Linear Expansion of Superinvar- 10 Nb ₂ O ₅ vs Temperature.....	89
32	Thermal Linear Expansion of Superinvar- 20 Nb ₂ O ₅ vs Temperature.....	90
33	Thermal Linear Expansion of Superinvar- 50 Nb ₂ O ₅ vs Temperature.....	91
34	CTE of Ni-Nb ₂ O ₅ Composites vs Temperature...	93
35	CTE of Superinvar-Nb ₂ O ₅ Composites vs Temperature.....	94
36	CTE of Ni-Nb ₂ O ₅ and Superinvar-Nb ₂ O ₅ Com- posites vs Volume Fraction of Nb ₂ O ₅	100
II.1	Schematic Diagram of the Thermospray System.	123

<u>Figure Number</u>	<u>Title</u>	<u>Page</u>
III.1	Schematic Diagram of the Electroless Nickel Plating Apparatus.....	129
IV.1	Hot Pressing Apparatus.....	131
IV.2	Schematic Diagram of Hot Pressing Die.....	132
IV.3	Hot Pressing Conditions.....	135
V.1	Double Michelson Interferometer for Small Sample CTE Measurements.....	138
V.2	Apparatus for Heating Cylindrical Samples..	138

NOMENCLATURE

E	Modulus of elasticity
G	Shear modulus
K	Bulk modulus
k	Thermal conductivity
L	Length
T	Temperature
u	Displacement
V	Volume
α	Linear coefficient of thermal expansion
β	Bulk coefficient of thermal expansion
Δ	Change of
ϵ	Strain
ρ	Density
σ	Stress
ν	Poisson's ratio

Subscripts

d	Dispersoid
i	Interfacial
m	Matrix
r	Radial direction
θ, ϕ	Tangential direction
y	Yield

CHAPTER I

INTRODUCTION

The satisfactory operation of a variety of high technology systems where thermal strains no more than a few micrometers per meter are permissible require ultra-low thermal expansion coefficient materials. Examples [1] of these systems include a variety of spacecraft components (e.g. primary housing/structure, metering shells, telescope housings, mirror substrates, microwave components, etc.), ultra-high precision machine tools, high precision dilatometers and laser mirror substrates.

A particularly demanding component is the mirror substrate for High Altitude Large Optics (HALO) and High Energy Laser Optics (HELO) because mirrors that distort more than $0.1\text{-}10\text{ }\mu\text{m}$ per meter lose image resolution. A previous feasibility study [2,3] on the fabrication of substrates of these optical systems has shown that these substrates shall have Zero (or nearly Zero) Coefficient of Thermal Expansion (ZCTE) in the temperature range of operation 150-400K. In addition they should have high thermal conductivity, high elastic modulus, high microyield strength and low density.

The thermal strain of a structural member is directly proportional to the temperature change, ΔT , and the coefficient of thermal expansion, α . To minimize thermal distortion, therefore, it

is necessary to reduce the temperature fluctuations, both temporal and spatial. This is accomplished by minimizing temperature fluctuations in the environment and by choosing materials that have high thermal conductivity. Another approach is to use materials which have zero or ultra-low thermal expansion materials. Because it is difficult to control temperature variations in outerspace, the most promising approach appears to be the use of materials that have ultra-low thermal expansion coefficients and high thermal conductivity.

At present only a few materials that have ultra-low expansion are available. Unfortunately these materials have low modulus and low thermal conductivity. Examples of these materials include graphite-epoxy composites and Ultra-Low Expansion (ULE) glasses.

Accordingly, the objective of this thesis is to produce metal-matrix composites that have high thermal conductivity and ultra-low (or even zero) thermal expansion coefficient in the temperature range 150-400K. To accomplish this goal literature search, thermo-elastic analysis and experimental work have been carried out. Ni-Nb₂O₅ and Superinvar-Nb₂O₅ composites have been developed using the powder metallurgy (PM) technique. The materials have been characterized by optical metallorgraphy, Scanning Electron Microscope (SEM), X-ray diffraction and chemical analysis. The thermal expansion coefficients have been measured in the temperature range 100-300K using the laser interferometer and low temperature dilatometer. The CTE values of these composites are presented and discussed.

CHAPTER II

LITERATURE REVIEW

The principal objective of this thesis is to produce materials which will be used as substrates of High Altitude Large Optics (HALO) and High Energy Laser Optics (HELO). To that end literature was searched to find out if there exist any materials, commercial or experimental, that satisfy all the requirements (low thermal expansion, high elastic modulus, high strength, high thermal conductivity and low density) of HALO and HELO substrates. Further, because low coefficient of thermal expansion is the crucial requirement of these substrates, the literature was reviewed to explore the physical principles underlying the ultra-low thermal expansion coefficient. In addition, thermal expansion coefficients, elastic modulus, ultimate tensile strength and density were also collected for a variety of polymers, metals and ceramics.

A. Thermal Expansion Coefficient

The coefficient of linear thermal expansion, α , of materials is defined as

$$\alpha = \frac{1}{L} \left(\frac{\partial L}{\partial T} \right)_p \quad (1)$$

Similarly, the volume thermal expansion coefficient, β , is defined as

$$\beta = \frac{1}{V} \left(\frac{\partial V}{\partial T} \right)_p \quad (2)$$

It can be easily shown that for isotropic materials and for a single crystal having cubic symmetry

$$\beta = 3\alpha \quad (3)$$

Because this equation is the result of isotropy in a material, it will also hold for annealed glasses, amorphous materials and even for non-cubic polycrystalline solids that have randomly oriented grains [4].

Literature has been searched to collect CTE values for as many materials as possible. Figure 1 [5 -35] lists a number of polymers, metals and ceramics. Although this list is by no means exhaustive, it includes a wide range of CTE values for a variety of solids. Materials with negative CTE values are listed in Table 1.

From Figure 1 and Table 1 the following observations can be made:

- (a) For polymers, CTE's range $\sim 50 \times 10^{-6} \text{K}^{-1}$ for polyphenylene sulfide, to $\sim 200 \times 10^{-6} \text{K}^{-1}$ for polyethylenes.
- (b) For metals, except for invar and superinvar ($\alpha \sim 1 \times 10^{-6} \text{K}^{-1}$), the CTE's range from $5 \times 10^{-6} \text{K}^{-1}$ for tungsten and molybdenum to near $24 \times 10^{-6} \text{K}^{-1}$ for aluminum and tin.
- (c) For ceramics the range is much wider; it spans over three order of magnitude from $\sim 3 \times 10^{-8} \text{K}^{-1}$ for ULE Corning 7971, to $\sim 10 \times 10^{-6} \text{K}^{-1}$ for MgO.

An important conclusion that can be drawn from Figure 1 and Table 1 is that there is no commercial material at present that has zero CTE over the range of temperatures 150-400K. Some materials (e.g. ULE, invar), however, exhibit zero CTE at some temperatures and negative CTE values over a small range of temperatures.

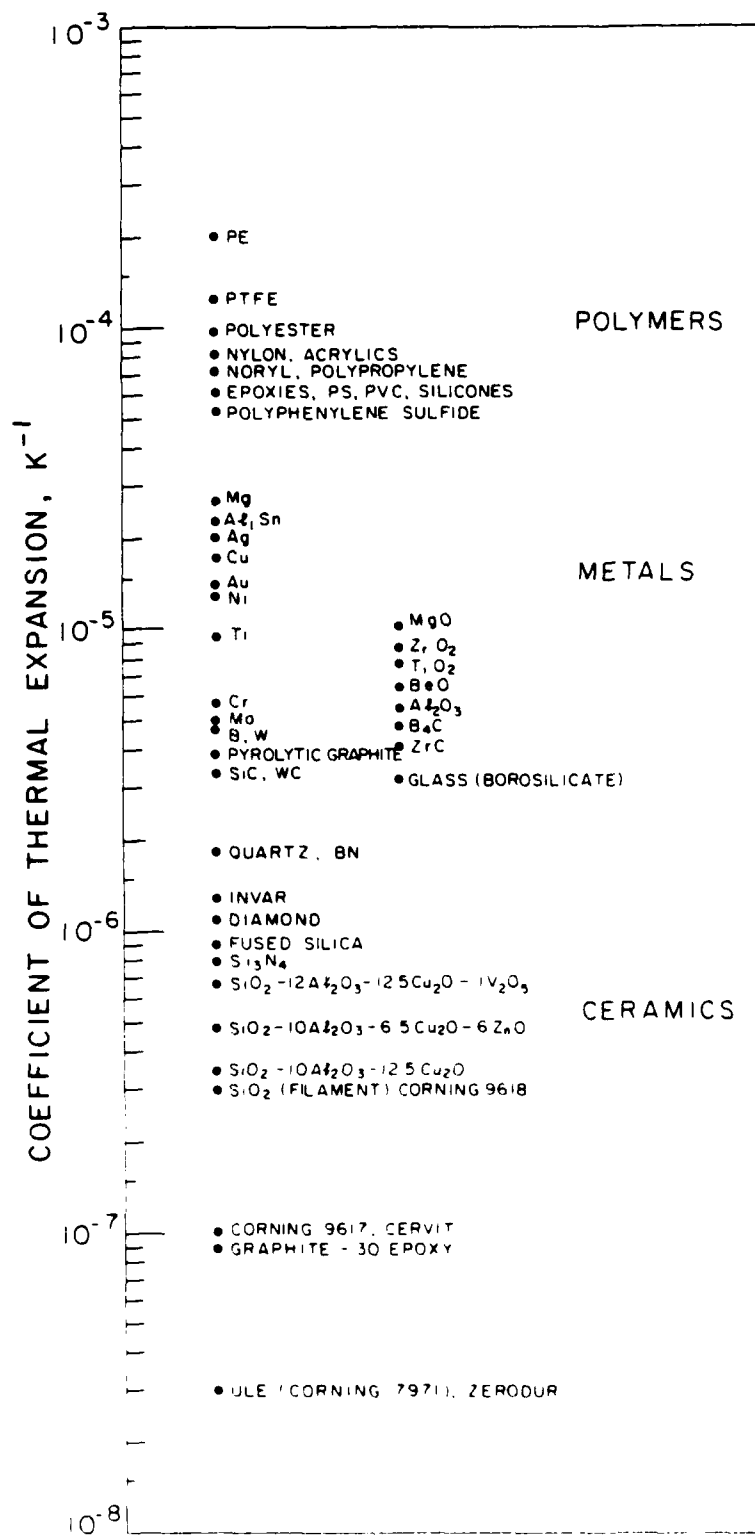


FIGURE 1. MATERIALS WITH POSITIVE CTE

TABLE 1. MATERIALS WITH NEGATIVE CTE

MATERIAL	CTE, K^{-1}		REFERENCE
	300K	150K	
1. Supertemp(Pycobond)graphite pitch material	-4.5×10^{-6}	-4.5×10^{-6}	3
2. Corning #9617	————	-0.72×10^{-6}	3
3. Nb_2O_5 (Sintered)	-2.0×10^{-6}	————	3,8
4. Nb_2O_5 (hot pressed)	-0.7×10^{-6}	————	3,8-12
5. β -eucryptite($Li_2O \cdot Al_2O_3 \cdot 2SiO_2$)	-6.0×10^{-6}	————	16-21
6. β -spodumene($Li_2O \cdot Al_2O_3 \cdot 4SiO_2$)	-1.0×10^{-6}	————	16,18-21
7. Keatite	-2.66×10^{-6}	————	20
8. SiO_2 -12 Li_2O -8 Al_2O_3 -1 GeO_2	-2.8×10^{-6}	————	7
9. Petalite-40($Al_2O_3 \cdot TiO_2$)	-1.0×10^{-6}	————	7
10. SiO_2 -8 Al_2O_3 -7 Li_2O -5 MgO	$-1.0 \sim -8.0 \times 10^{-6}$	————	7
11. Zinc petalite(SiO_2 -23.25 Al_2O_3 -23.25 ZnO)	-0.5×10^{-6}	————	22
12. β -Quartz(64.68 SiO_2 -19.9 ZnO -14.9 Al_2O_3)	-0.3×10^{-6}	————	22
13. Li_2O - Ta_2O_5 (sintered)//c-axis	-11.0×10^{-6}	————	7
14. 3(SiO_2 -36.7 Al_2O_3 -12.3 Li_2O)-(NiO -20 CaF_2)	-1.2×10^{-6}	————	3,32
15. $Ta_{16}W_{18}O_{94}$	-5.0×10^{-6}	————	7,15
16. Ta_2WO_8	-2.5×10^{-6}	————	7,15
17. $Ta_2O_5 \cdot V_2O_5$	-4.0×10^{-6}	————	7
18. PbO - TiO_2	-2.4×10^{-6}	1.2×10^{-6}	13
19. La_2O_3	-4.03×10^{-6}	1.87×10^{-6}	14

Negative CTE values in some temperature range insure zero or ultra-low CTE at least at one temperature, since the thermal expansion at high temperature is generally positive (α increases with temperature increase). Some well-known materials that have negative thermal expansion coefficients are: (a) elastomers (e.g. rubber), (b) "open" structures like those of ice and water, (c) solids that have a diamond cubic lattice where α becomes negative at very low temperatures (e.g. 20K) and (d) in structures that have relatively low shear moduli [3,5]. Elemental and compound semiconductors satisfy some of these requirements and in all cases negative expansion is observed over a range of low temperatures. Studies on fused silica show that at low temperature the α is negative, becomes positive at high temperature and again negative at still higher temperatures. Similar behavior was observed with $\text{SiO}_2 - \text{TiO}_2$, and with enough TiO_2 the maximum in α between the negative CTE regions can be eliminated to get an extended region of ultra-low CTE (ULE glasses $\sim 3 \times 10^{-8} \text{K}^{-1}$). However, obtaining even lower CTE in single phase materials appears to be a difficult problem. Current theories of thermal expansion cannot provide any guidance for developing such materials.

Nevertheless, low enough CTE can generally be achieved in homogeneous-isotropic and anisotropic materials. CTE in homogeneous materials is inversely proportional to the strength of the binding forces [6]. Low atomic weight, high melting temperature, high modulus materials have low CTE. Although it may not be possible to get zero or

or ultra-low CTE at a given temperature, metals with high melting point, ionic compounds and covalent compounds are the best choices. Indeed from Figure 1 it can be seen that diamond, SiC, BN and Si_3N_4 have low coefficients of thermal expansion.

There is a possibility of achieving a very low CTE, and even zero CTE, for at least one direction in anisotropic materials providing that they have at least one negative α component in one of the directions. Often these structures have near-zero CTE for a range which is fixed by the crystal physics of the material.

The thermal expansion of coefficients of materials are essentially structure insensitive; i.e., minor variations in microstructure do not significantly affect the coefficient of thermal expansion [4]. For example, stoichiometry, impurities (<1 percent), porosity, dislocation density and grain boundary area have virtually no effect on α . On the other hand, oriented grains, second phases (in small quantities) cracks, etc. do affect the thermal expansion somewhat (~40 percent), but not substantially. Starting with the single phase materials the thermal expansion coefficient cannot be changed over several orders of magnitude by the minor microstructural modifications.

The best approach for obtaining ultra-low or zero CTE materials, then, is through the development of polyphase materials or composites. Composites made of a highly anisotropic material with others, can have zero or ultra-low CTE for a range of temperatures.

This range could also be increased depending on the constituent phases. Examples of this kind include graphite-epoxy, graphite-carbon composites and low expansion glasses [2]. However, these composites (except the glasses) have anisotropic thermal expansion coefficient and, thus, cannot be used in many applications. To obtain a material with isotropic ultra-low thermal expansion coefficient it is necessary to produce particle reinforced composites.

B. Other Properties

Although it may not be apparent at first glance, the HALO/HELO requirements (high elastic modulus, low thermal expansion coefficient, high thermal conductivity, low density) are to some extent conflicting requirements. These properties cannot be obtained in a single material. This can be explored further by plotting, as shown in Figures 2-5, one property at a time against the thermal expansion coefficient for the materials listed in Tables 2-4. The intent of this approach is to explore the correlations, if any, between various properties and the thermal expansion coefficient. Needless to say, this approach is not rigorous. However, because the theories of CTE, thermal conductivity etc. are very complex, this empirical approach helps us identify useful correlations without extensive review of the theories.

From Tables 2-4 and Figures 2-5 the following conclusions can be drawn.

TABLE 2. THERMAL AND MECHANICAL PROPERTIES OF VARIOUS POLYMERS

MATERIAL	COEFFICIENT OF THERMAL EXPANSION $\alpha, K^{-1} \times 10^{-6}$ 300K	THERMAL CONDUCTIVITY K, W/(m, k) 300K	MODULUS OF ELASTICITY E, Pax10 ⁹ 300K	TENSILE STRENGTH Pax10 ⁶ 300K	DENSITY ρ kg/m ³
Acrylics	81	0.21	2.41-3.1	41.4-62.1	1,170-1,190
Epoxies (cast rigid)	59.4	0.17-0.52	3.11	65.6-79.4	1,150
Nylons (General Pur- pose molding)	81.8	0.25	2.66-3.28	—	1,130-1,150
Polyester (General Pur- pose grade)	95.4	0.16	—	55.2	1,310
Phenylenes oxides (Noryl)	68.4	0.16	2.62	—	1,100
Polypropylene (general purpose)	68.4-104.4	0.17-0.2	1.1-1.52	—	900-910
Polyphenylene Sulfide (standard)	54	0.29	3.3	—	1,340
Polyethylene	149.4-300	0.33	0.15-0.19	9.66-27.6	910-965
Polystyrenes	59.4-86.4	0.1-0.16	3.17-3.45	—	1,040-1,070
Polyvinyl Chloride (rigid)	50.4-59.4	0.12-0.17	2.42-2.76	24.5-55.2	1,200-1,500
Silicones	57.1-58.1	0.31	—	45.5	1,880

TABLE 3. THERMAL AND MECHANICAL PROPERTIES OF VARIOUS METALS

MATERIAL	COEFFICIENT OF THERMAL EXPANSION $\alpha, \text{K}^{-1} \times 10^{-6}$		THERMAL CONDUCTIVITY K, (W/(m.k))	MODULUS OF ELASTICITY E, Pax10 ⁹	TENSILE STRENGTH Pax10 ⁶	DENSITY ρ Kg/m ³
	300K	150K				
Aluminum	23.5	17.85	283.4	68.3,69	207-276	2,700
Boron	4.8	—	1.2	228	—	2,340
Chromium	4.4	4.2	69	248	82.8	7,100
Copper	17	13.6	393.2	124.1-131	413.8-482.5 (Hard)	8,960
Gold	14.1	12.8	292.8	78.6-82.8	137.9-219.7	19,300
Invar	0.2	1.38	10.5	141	448	8,055
Molybdenum	4.8	3.8	145.6	289.5	178	10,200
			at 393K			
Nickel	12.9	9.2	87.8	206.8	1060 (Hard drawn)	8,900
Silver	18.73	15.85	418.3	75.9	289.6 (Cold drawn)	10,500
			at 100K			
Tin	23.5	17.4	64.8	46.8	59.2	7,300
			at 160K			
Titanium	8.48	6.35	7.1	110	—	4,430
Tungsten	4.37	3.52	166.5	358.5	1520	19,300
			at 373K			

TABLE 4. THERMAL AND MECHANICAL PROPERTIES OF VARIOUS CERAMICS

MATERIAL	COEFFICIENT OF THERMAL EXPANSION α , $K^{-1} \times 10^{-6}$		THERMAL CONDUCTIVITY K, W/(m.k)	MODULUS OF ELASTICITY E, $Pax10^9$	TENSILE STRENGTH $Pax10^6$	DENSITY ρ kg/m ³
	300K	150	300K	300K	300K	
Al_2O_3	5.4	1.9	19.7	375	260	3,500-3,900
B_e	6.4	—	71.1-301.2	379.8	95-135	3,025
MgO	10.4	4.95	53.1	294-303	96.5	3,570
Nb_2O_5	-2.0 (sintered)	—	—	153	—	4,470
	-0.7 (hot pressed)	—	—	—	—	—
Si_3O_2 Filament	0.3	—	0.9	68.6-172	1029-4119	2,000-2,330
Fused Silica	0.9	—	1.26	72.6	275	2,200
Quartz	1.8	—	5.86	75.5	—	2,650
Glass (Borosilicate)	3.2	—	1.0	67.6	68.9	2,230
TiO_2	7.5	6.8	10.0	282	51	4,250
ZrO_2	8.8	—	1.9	137	146	5,600
BN	1.8	1.0	—	—	—	—
11 to pressing direction	—	—	15.1	75.9-84	621-109	Borazone 3,4500(β)
1 to pressing direction	—	—	28.9	33.7	50	3,490(γ)
Si_3N_4	0.8	—	17.2	47.7-213.7	14.7-27	3,400

TABLE 4 (con't)

MATERIAL	COEFFICIENT OF THERMAL EXPANSION $\alpha, K^{-1} \times 10^6$		THERMAL CONDUCTIVITY K, W/(m.k)	MODULUS OF ELASTICITY E, Pax10 ⁹	TENSILE STRENGTH Pax10 ⁶	DENSITY ρ kg/m ³
	300K	150				
B ₄ C	4.8	—	27.6	448	155	2,500
SiC	3.4	0.4	42.7	386.3	137.9	3,217
TiC	6.4	—	18-20.5	316-451	6.5-118	4,930
WC	3.7	—	87.9	648	377.7	15,630
7rC	4.0	—	20.5	348.1	110	6,730

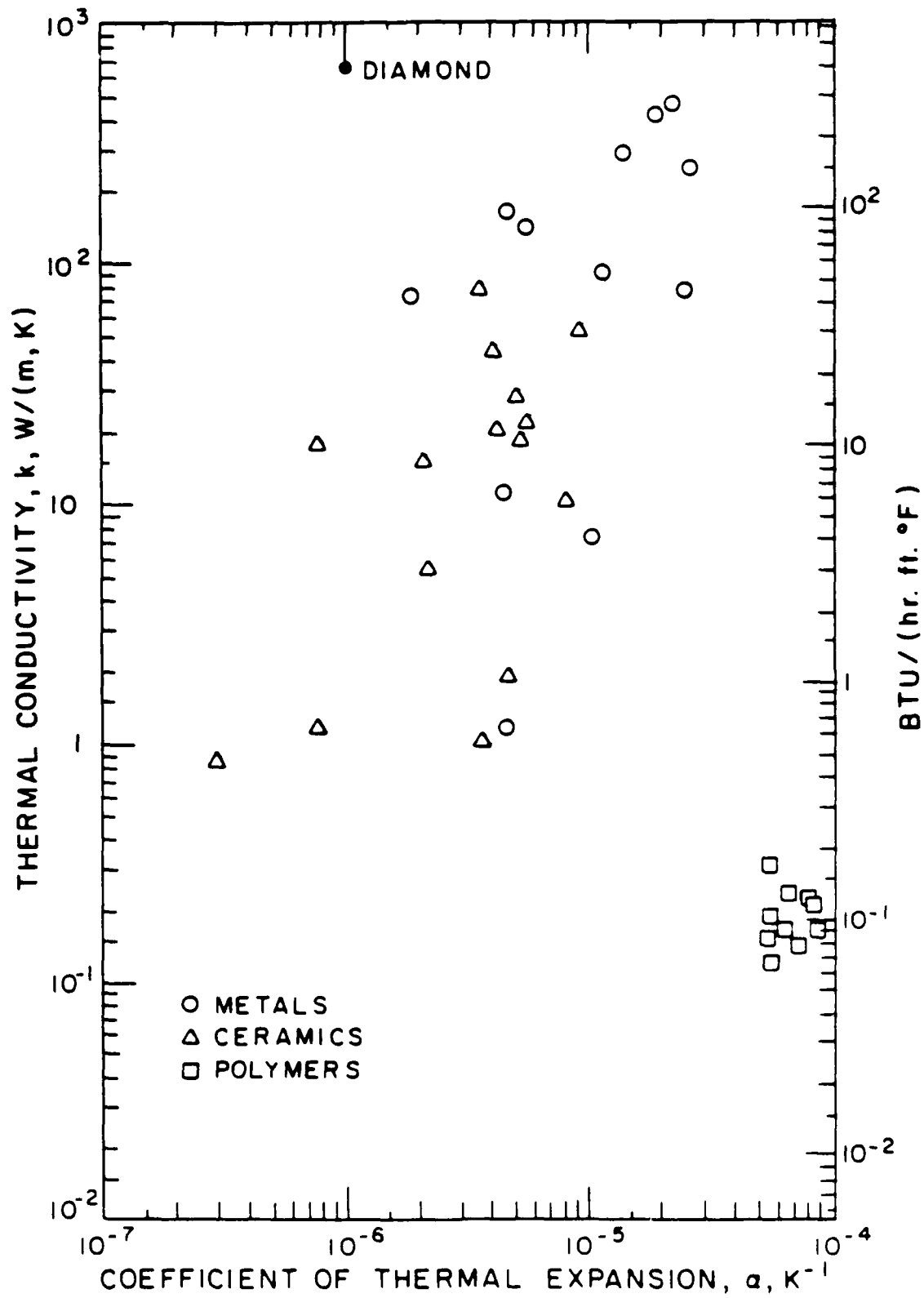


FIGURE 2. THERMAL CONDUCTIVITY VERSUS CTE

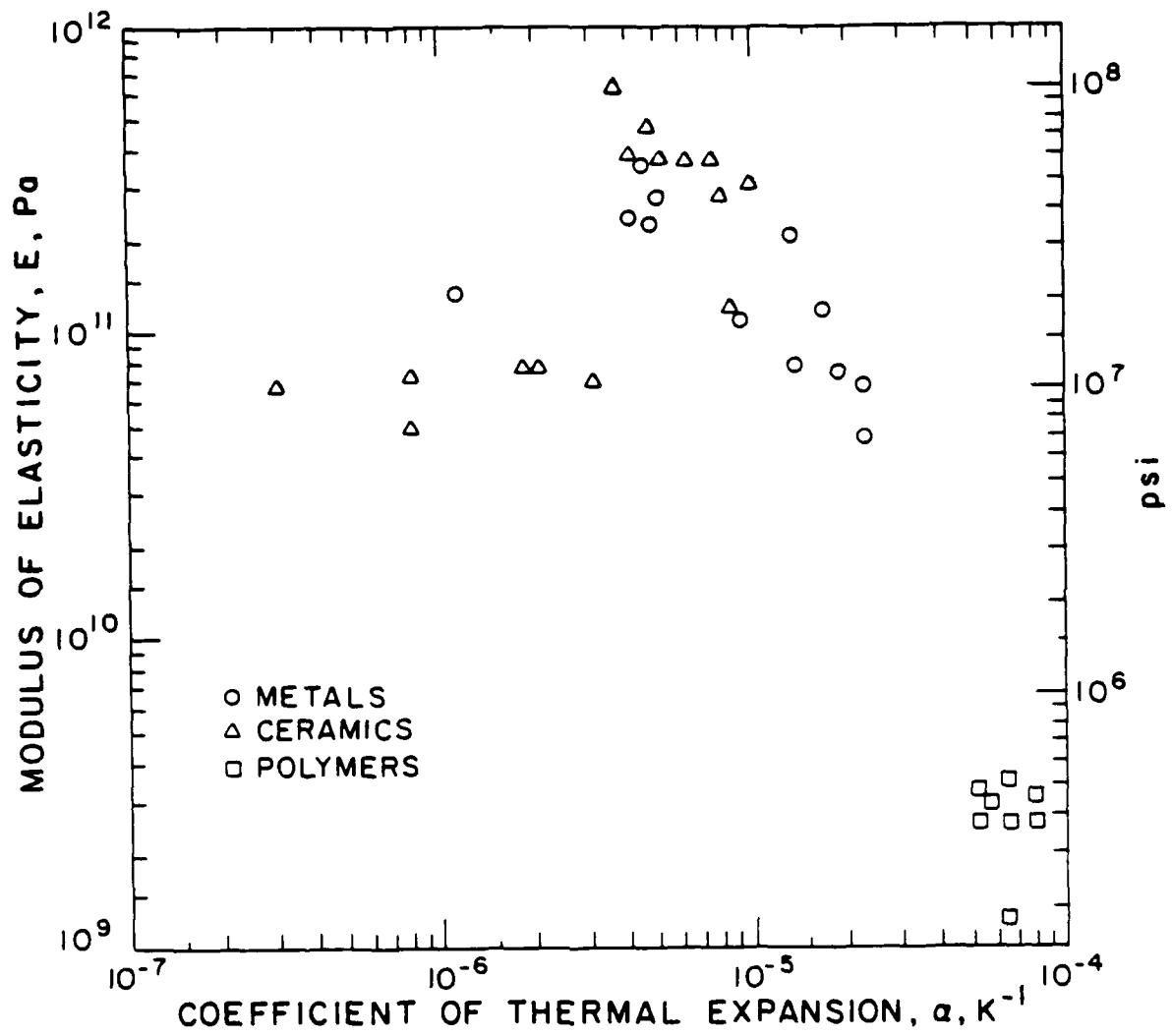


FIGURE 3. MODUDLUS OF ELASTICITY VERSUS CTE

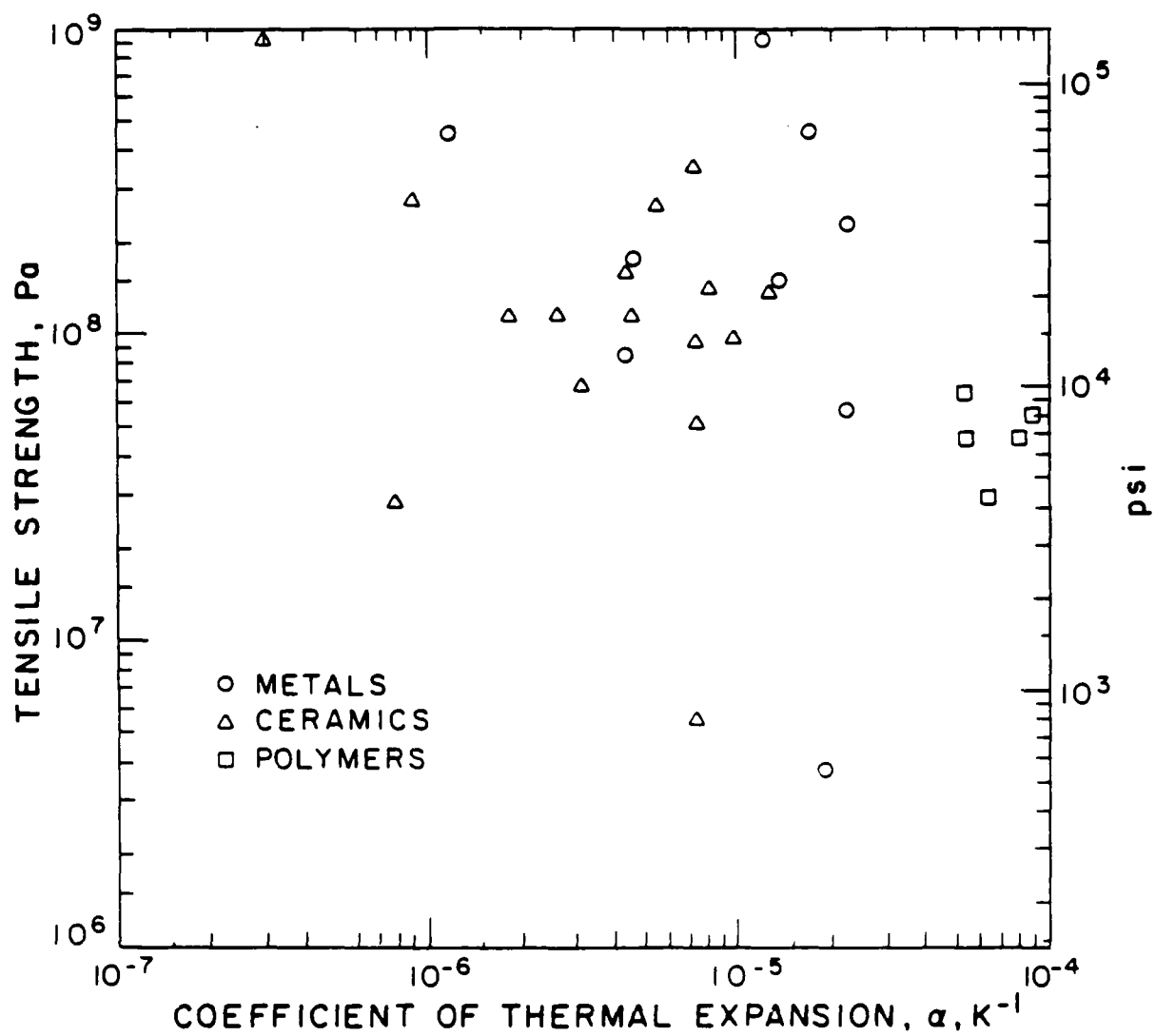


FIGURE 4. TENSILE STRENGTH VERSUS CTE

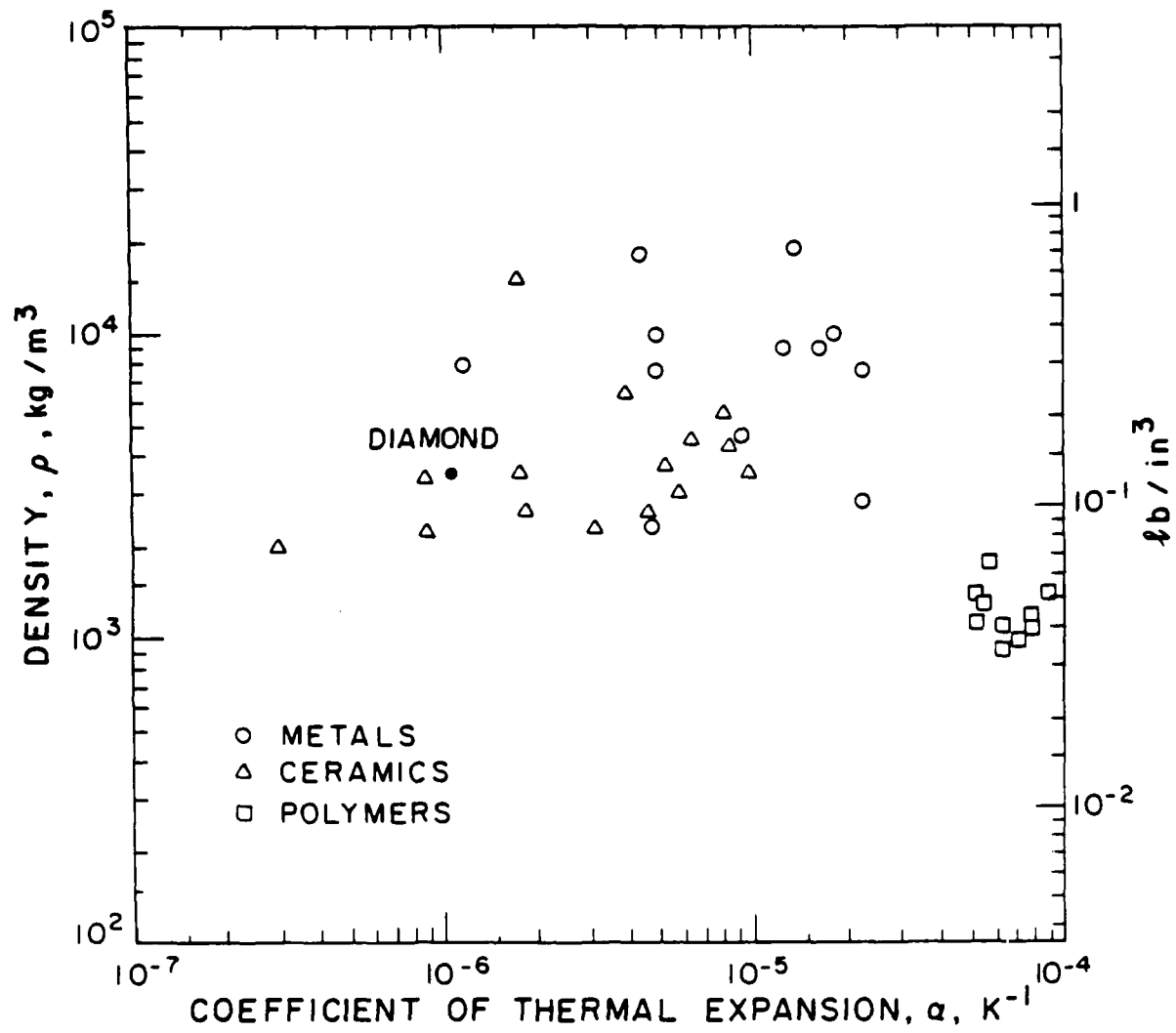


FIGURE 5. DENSITY VERSUS CTE

- (a) polymers [33]: In general they have high CTE, low modulus of elasticity and low thermal conductivity, which means that they are not suited for HALO/HELO applications.
- (b) metals [7,34]: In general they have high conductivity, high strength but also high CTE. Invar and superinvar are the only metallic alloys with relatively low CTE ($\sim 0.2 \cdot 10^{-6} \text{K}^{-1}$) but they also have low thermal conductivity.
- (c) Ceramics [7,35]: In general they have high modulus, low CTE, low density but very low thermal conductivity. Also they are very weak in tension (i.e., they are brittle) although usually they are very strong in compression.

In summary, it appears that no one material will satisfy all the requirements of HALO and HELO substrates. It is evident that the candidate material selected will be one which offers the best compromise between various properties, even though not showing the ultimate value in each property. Indeed a material that will optimize all the properties will be a particle-dispersed composite. Accordingly, development of metal-matrix composites has been chosen for investigation in this work.

CHAPTER III

THEORETICAL ANALYSIS

As shown in the previous chapter, only metal-matrix composites meet all the requirements of HALO and HELO substrates. Such composites shall have a continuous metallic phase, because metals have high thermal conductivity, and a dispersed ceramic phase, because ceramics have either very low or negative CTE. Moreover, only particle-dispersed composites will give isotropic thermal expansion coefficient. The theoretical calculation of the coefficient of thermal expansion of the particle-dispersed composite and a discussion of the choice of its constituents will be taken up in this chapter.

In the past many reseachers [36-44] addressed the problem of calculating the thermal expansion coefficients of particle-dispersed composites. The geometries considered, the assumptions made, and the equations derived are summarized in Appendix I. However, many of these equations are not applicable to the present problem. The principal drawback is the lack of explicit equations for the stresses and strains developed in the matrix and dispersed phases. Yielding of the matrix, fracture of the dispersed phase and debonding at particle-matrix interface can give rise to spurious thermal expansion coefficients when subjected to a large cyclic temperature fluctuations, as in the HALO/HELO substates.

Accordingly, the thermal expansion coefficient of particle-dispersed composites is calculated in this chapter by a rigorous thermo-

elasticity approach. Using this approach new results for composites that contain hollow and multilayered spherical particles are obtained. Further, the conditions for matrix yielding, particle fracture and interfacial debonding are also identified and discussed.

A. Thermoelastic Analysis

In the following analysis, the composite material is assumed to be an assembly of spherical composite particles that contain all the constituents present in the composite material. The volume fractions of these constituents are the same in each spherical composite as in the composite material. Hence, the coefficient of thermal expansion of each spherical composite and the composite material are approximately equivalent.

First the analysis is performed for a single spherical composite particle in which all the phases are assumed to be isotropic, linear elastic, homogeneous (within each phase) and the interfaces perfectly bonded. Then the thermal expansion coefficient of the two-phase composite material is calculated.

A.1 General Thermoelastic Equation for an Inhomogeneous Sphere

Let us consider first the more general case of a sphere whose properties (α , E and ν) are functions of the radius, r , and subjected to a temperature rise, ΔT , which is also a function of the radius.

From Timoshenko [45] the condition of equilibrium is given by

$$\frac{d\sigma_r}{dr} + \frac{2}{r} (\sigma_r - \sigma_\phi) = 0 \quad (4)$$

and the stress-strain relations are given by

$$\sigma_r = \frac{E}{(1+\nu)(1-2\nu)} [(1-\nu)\epsilon_r + 2\nu\epsilon_\phi - (1+\nu)\alpha\Delta T] \quad (5)$$

$$\sigma_\phi = \sigma_\theta = \frac{E}{(1+\nu)(1-2\nu)} [\epsilon_\phi + \nu\epsilon_r - (1+\nu)\alpha\Delta T] \quad (6)$$

$$\text{and } \epsilon_r = \frac{du_r}{dr} \quad (7)$$

$$\epsilon_\phi = \epsilon_\theta = \frac{u_r}{r} \quad (8)$$

Substituting (5), (6), (7) and (8) into Equation (4) we get

$$\begin{aligned} & \frac{d^2 u_r}{dr^2} + \left[\frac{1}{E} \frac{dE}{dr} + \frac{2\nu(2-\nu)}{(1+\nu)(1-\nu)(1-2\nu)} \frac{d\nu}{dr} + \frac{2}{r} \right] \frac{du_r}{dr} \\ & + \left[\frac{2\nu}{E(1-\nu)r} \frac{dE}{dr} + \frac{2}{(1-\nu)r} \frac{d\nu}{dr} - \frac{2}{r^2} \right] u_r = \\ & - \frac{(1+\nu)}{(1-\nu)} \left[\frac{1}{E} \frac{dE}{dr} + \frac{2(1+\nu)}{(1+\nu)(1-2\nu)} \frac{d}{dr} \right] \alpha\Delta T + \frac{d(\alpha\Delta T)}{dr} \end{aligned} \quad (9)$$

The solution of this non-linear differential equation subject to the appropriate boundary conditions provides displacements, strains and stresses in the inhomogeneous sphere. Once the radial displacement, u_r ,

is known, the equivalent thermal expansion coefficient of this inhomogeneous sphere, α , can be easily calculated.

Equation (9) is completely general. It can be used for both inhomogeneous, multilayered and homogeneous spheres subjected to both uniform and nonuniform temperature changes. A more practical case where the physical properties in each phase are constant and the temperature rise is uniform, is considered next.

A.2 Multilayered Sphere

Consider a multilayered composite sphere (Figure 6) where each phase is isotropic, linear elastic and homogeneous. Also assume that the temperature rise, ΔT , is constant for the entire multilayered spherical particle. Then equation (9) becomes

$$\frac{d^2 u_r}{dr^2} + \frac{2}{r} \frac{du_r}{dr} - \frac{2u_r}{r^2} = \frac{1+\nu}{1-\nu} \alpha \Delta T \quad (10)$$

which can be written as

$$\frac{d}{dr} \left[\frac{1}{r^2} \frac{d}{dr} (r^2 u_r) \right] = \frac{1+\nu}{1-\nu} \alpha \Delta T \quad (11)$$

and the solution is [45]

$$u_r = \frac{1+\nu}{1-\nu} \alpha \Delta T \frac{r^3 - r_0^3}{3r^2} + c_1 r + \frac{c_2}{r^2} \quad (12)$$

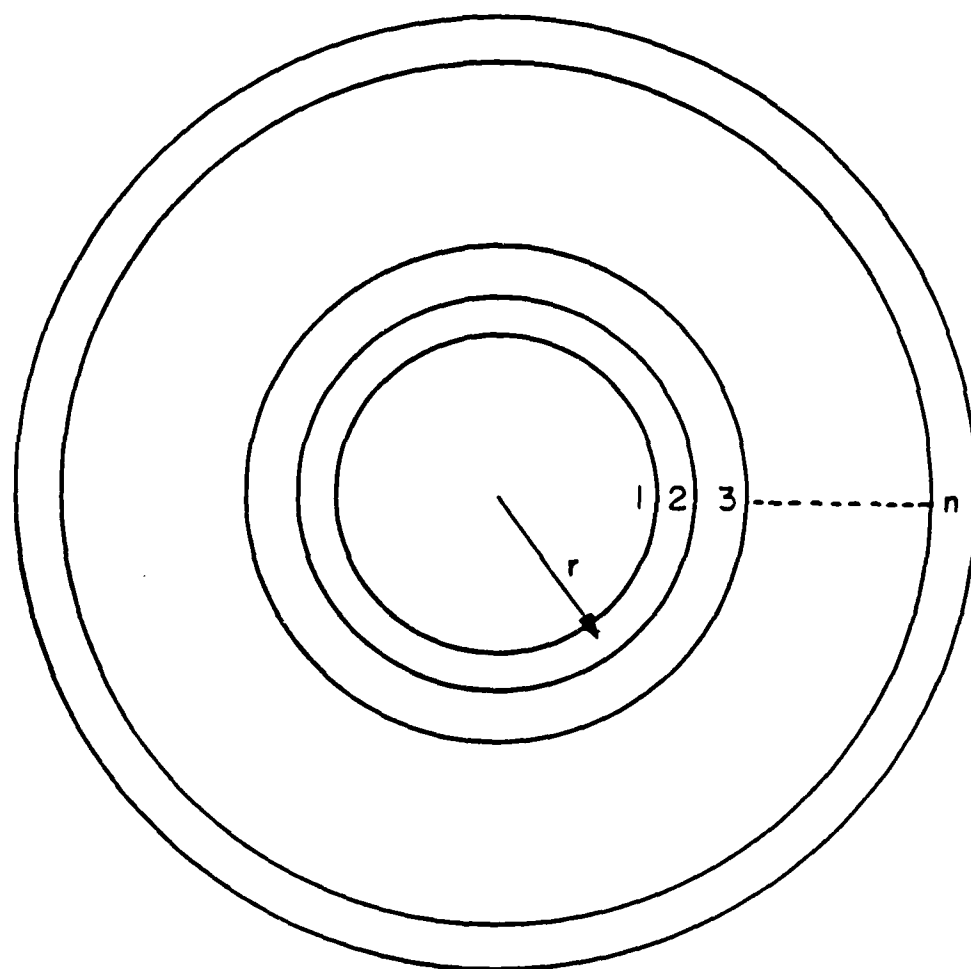


FIGURE 6. MULTILAYERED COMPOSITE SPHERE

here C_1 and C_2 are constants of integration and r_0 is any convenient lower limit for the integral.

This solution is used to find the stresses in the composite. Again from Timoshenko [45]

$$\sigma_r = - \frac{2E}{(1-\nu)} \alpha \Delta T \frac{r^3 - r_0^3}{3r^3} + \frac{E}{(1-2\nu)} C_1 - \frac{2E}{1+\nu} \frac{C_2}{r^3} \quad (13)$$

$$\sigma_\theta = \sigma_\phi = \frac{E}{(1-\nu)} \alpha \Delta T \frac{r^3 - r_0^3}{3r^3} + \frac{E}{(1-2\nu)} C_1 + \frac{E}{1+\nu} \frac{C_2}{r^3} - \frac{E \alpha \Delta T}{1-\nu} \quad (14)$$

Equations (12), (13) and (14) describe the displacement and the state of the stress in each phase where the boundary conditions are:

- (a) $\sigma_r = 0$ on the outer surface,
- (b) σ_r and u_r are the same in the adjacent consecutive phases at the common interfaces,
- (c) $\sigma_r = 0$ at the inside surface for a hollow inner sphere, i.e. at $r=r_1$, and
- (d) $u_r = 0$ at $r = r_0 = 0$ for a solid inner sphere.

Using these boundary conditions and Equations (12) and (13) the following relations for the integration constants for an n-phase composite sphere are obtained

$$\begin{aligned} \frac{E_{i-1}}{1-2\nu_{i-1}} C_{2i-3} - \frac{2E_{i-1}}{(1+\nu_{i-1})r_{i-1}^3} C_{2i-2} - \frac{E_i}{1-\nu_i} C_{2i-1} + \frac{2E_i}{(1+\nu_i)r_{i-1}^3} C_{2i} \\ = - \frac{2\Delta T \alpha_{i-1} E_{i-1}}{3(1-\nu_{i-1})} \end{aligned} \quad (15)$$

$i = 2, \dots, n$

$$\frac{E_n}{1-\nu_n} C_{2n-1} + \frac{2E_n}{(1+\nu_n)r_n^3} C_{2n} = \frac{2\Delta T \alpha_n E_n}{3(1-\nu_n)} \frac{r_n^3 - r_{n-1}^3}{r_n^3} \quad (16)$$

$$C_{2i-3} + \frac{C_{2i-2}}{r_{i-1}^3} - C_{2i-1} - \frac{C_{2i}}{r_{i-1}^3} = - \frac{1+\nu_{i-1}}{1-\nu_{i-1}} \frac{\alpha_{i-1}}{3} \frac{r_{i-1}^3 - r_{i-2}^3}{r_{i-1}^3} \quad (17)$$

$$i = 2, \dots, n$$

and for a solid inner sphere

$$C_2 = 0 \quad (18)$$

or for hollow inner sphere

$$\frac{E_1}{1-2\nu_1} C_1 - \frac{2E_2}{(1+\nu_1)r_1^3} C_2 = 0 \quad (19)$$

For a multilayered n -phase composite particle, we have $2n$ equations and $2n$ unknowns. Solving for these unknowns and substituting in Equations (7), (8), (12), (13) and (14), equations for the displacements, strains and stresses can be obtained.

To find the coefficient of thermal expansion of the composite sphere, α_c , we note that at $r=r_n$

$$u_r(r_n) = \alpha_c \Delta T r_n \quad (20)$$

But $u_r(r_n)$ is also obtained from Equation (12) which becomes

$$u_r(r_n) = \frac{1+\nu_n}{1-\nu_n} \alpha_n \Delta T \frac{r_n^3 - r_{n-1}^3}{3 r_n^2} + r_{2n-1} r_n + \frac{C_{2n}}{r_n^2} \quad (21)$$

A.3 Two-Phase Sphere

For this thesis we are interested in a two phase composite. In this section the thermal expansion coefficient for a two-layer composite is calculated using the equations derived so far. Hence, if we consider a two-phase composite with a solid inner sphere then Equations (15), (16), (17) and (18) will be reduced to

$$\frac{E_1}{1-2\nu_1} C_1 - \frac{E_2}{1-2\nu_2} C_3 + \frac{2E_2}{a^3(1+\nu_2)} C_4 = \frac{2E_1\alpha_1\Delta T}{3(1-\nu_1)} \quad (22)$$

$$\frac{E_2}{1-2\nu_2} C_3 + \frac{2E_2}{b^3(1+\nu_2)} C_4 = \frac{2E_2\alpha_2\Delta T}{3(1-\nu_2)} \frac{b^3-a^3}{b^3} \quad (23)$$

$$C_1 - C_3 - \frac{1}{a^3} C_4 = - \frac{1+\nu_1}{1-\nu_1} \frac{\alpha_1\Delta T}{3} \quad (24)$$

Solving for C_1 , C_3 , and C_4 and substituting into Equations (7), (8), (12), (13) and (14) and further substituting $x = \frac{a^3}{b^3}$, the volume fraction of the inner sphere where $r_1=a$ and $r_2=b$, we get for the inner sphere, i.e. for $0 \leq r \leq a$

$$u_r = r \Delta T \frac{\alpha_1 E_1 [(1+\nu_2)+2(1-2\nu_2)x] + 2\alpha_2 E_2 (1-x)(1-2\nu_1)}{2E_2(1-2\nu_1)(1-x) + 2E_1(1-2\nu_2)x + E_1(1+\nu_2)} \quad (25)$$

$$\epsilon_r = \epsilon_\phi = \epsilon_\theta = \Delta T \frac{\alpha_1 E_1 [(1+\nu_2)+2(1-2\nu_2)x] + 2\alpha_2 E_2 (1-x)(1-2\nu_1)}{2E_2(1-2\nu_1)(1-x) + 2E_1(1-2\nu_2)x + E_1(1+\nu_2)} \quad (26)$$

$$\sigma_r = \sigma_\phi = \sigma_\theta = \Delta T \left[\frac{2E_1 E_2 (\alpha_2 - \alpha_1)(1-x)}{2E_2(1-2\nu_1)(1-x) + 2E_1(1-2\nu_2)x + E_1(1+\nu_2)} \right] \quad (27)$$

For the outer sphere, i.e. for $a \leq r \leq b$

$$\begin{aligned} u_r = & \Delta T \left[\frac{1+\nu_2}{1-\nu_2} \alpha_2 \left(r - \frac{a^3}{r^2} \right) \right] \\ & + \frac{\Delta T a^3}{3(1-\nu_2)r^2} \frac{2\alpha_2(1-x)(1+\nu_2)[E_2(1-2\nu_1)-E_1(1-2\nu_2)]+3\alpha_1 E_1(1-\nu_2)(1+\nu_2)}{2E_2(1-2\nu_1)(1-x) + 2E_1(1-2\nu_2)x + E_1(1+\nu_2)} \\ & + \frac{\Delta T r}{3(1-\nu_2)} \frac{2\alpha_2(1-2\nu_2)(1-x)[E_1(1+\nu_2)+2E_2(1-2\nu_1)]+6\alpha_1 E_1(1-2\nu_2)(1-\nu_2)x}{2E_2(1-2\nu_1)(1-x) + 2E_1(1-2\nu_2)x + E_1(1+\nu_2)} \end{aligned} \quad (28)$$

$$\begin{aligned} \varepsilon_r = & \Delta T \left[\frac{1+\nu_2}{1-\nu_2} \alpha_2 \left(1 + \frac{2a^3}{r^3} \right) \right] \\ & - \frac{2\Delta T a^3}{3(1-\nu_2)r^3} \frac{2\alpha_2(1-x)(1+\nu_2)[E_2(1-2\nu_1)-E_1(1-2\nu_2)]+3\alpha_1 E_1(1-\nu_2)(1+\nu_2)}{2E_2(1-2\nu_1)(1-x) + 2E_1(1-2\nu_2)x + E_1(1+\nu_2)} \\ & + \frac{\Delta T}{3(1-\nu_2)} \frac{2\alpha_2(1-2\nu_2)(1-x)[E_1(1+\nu_2)+2E_2(1-2\nu_1)]+6\alpha_1 E_1(1-2\nu_2)(1-\nu_2)x}{2E_2(1-2\nu_1)(1-x) + 2E_1(1-2\nu_2)x + E_1(1+\nu_2)} \end{aligned} \quad (29)$$

$$\begin{aligned}
\varepsilon_{\theta} = & \Delta T \left[\frac{1 + \nu_2}{1 - \nu_2} \alpha_2 \left(1 - \frac{a^3}{r^3} \right) \right] \\
& + \frac{\Delta T a^3}{3(1-\nu_2)r^3} \frac{2\alpha_2(1-x)(1+\nu_2)[E_2(1-2\nu_1)-E_1(1-2\nu_2)]+3\alpha_1 E_1(1-\nu_2)(1+\nu_2)}{2E_2(1-2\nu_1)(1-x)+2E_1(1-2\nu_2)x+E_1(1+\nu_2)} \\
& + \frac{\Delta T}{3(1-\nu_2)} \frac{2\alpha_2(1-2\nu_2)(1-x)[E_1(1+\nu_2)+2E_2(1-2\nu_1)]+6\alpha_1 E_1(1-2\nu_2)(1-\nu_2)x}{2E_2(1-2\nu_1)(1-x)+2E_1(1-2\nu_2)x+E_1(1+\nu_2)}
\end{aligned}
\tag{30}$$

$$\begin{aligned}
\sigma_r = & \Delta T \frac{2\nu_2 E_2}{3(1-\nu_2)} \left(\frac{a^3}{r^3} - 1 \right) \\
& - \frac{2\Delta T E_2 a^3 / r^3}{3(1-\nu_2)} \frac{2\nu_2(1-x)[E_2(1-2\nu_1)-E_1(1-2\nu_2)]+3\alpha_1 E_1(1-\nu_2)}{2E_2(1-2\nu_1)(1-x)+2E_1(1-2\nu_2)x+E_1(1+\nu_2)} \\
& + \frac{\Delta T E_2}{3(1-\nu_2)(1-2\nu_2)} \frac{2\alpha_2(1-x)(1-2\nu_2)[E_1(1+\nu_2)+2E_2(1-2\nu_1)]+6\alpha_1(1-2\nu_2)(1-\nu_2)x}{2E_2(1-2\nu_1)(1-x)+2E_1(1-2\nu_2)x+E_1(1+\nu_2)}
\end{aligned}
\tag{31}$$

$$\begin{aligned}
\sigma_\phi = \sigma_\theta = & -\Delta T \frac{\alpha_2 E_2}{3(1-\nu_2)} \left(2 + \frac{a^3}{r^3} \right) \\
& + \frac{\Delta T E_2 (a^3/r^3)}{3(1-\nu_2)} \frac{2\alpha_2(1-x)[E_2(1-2\nu_1)-E_1(1-2\nu_2)]+3\alpha_1 E_1(1-\nu_2)}{2E_2(1-2\nu_1)(1-x)+2E_1(1-2\nu_2)x + E_1(1+\nu_2)} \\
& + \frac{\Delta T E_2}{3(1-\nu_2)(1-2\nu_2)} \frac{2\alpha_2(1-2\nu_2)(1-x)[E_1(1+\nu_2)+2E_2(1-2\nu_1)]+6\alpha_1 E_1(1-2\nu_2)(1-\nu_2)x}{2E_2(1-2\nu_1)(1-x) + 2E_1(1-2\nu_2)+E_1(1+\nu_2)}
\end{aligned} \tag{32}$$

The coefficient of thermal expansion of the composite sphere, α_c , is given by

$$u_{r=b} = \alpha_c \Delta T b$$

Substituting into Equation (28)

$$\alpha_c = \alpha_2 + \frac{3(1-\nu_2)(\alpha_1 - \alpha_2) E_1 x}{2E_2(1-2\nu_1)(1-x)+2E_1(1-2\nu_2)x+E_1(1+\nu_2)} \tag{33}$$

Dividing by E_1

$$\alpha_c = \alpha_2 + \frac{3(1-\nu_2)(\alpha_1 - \alpha_2)x}{2 \frac{E_2}{E_1} (1-2\nu_1)(1-x)+2(1-2\nu_2)x+(1+\nu_2)} \tag{34}$$

From Equation (34) a few results can be readily obtained. First, when $E_1 = E_2$ and $\nu_1 = \nu_2$ we have that

$$\alpha_c = \alpha_1 x + \alpha_2 (1-x) \tag{35}$$

which is the rule of mixture for the thermal expansion coefficient of a composite.

Second, from Equation (34) it can be easily shown that for α_c to be zero, α_1 and α_2 must have opposite signs; i.e. one of the phases must have positive CTE whereas the other should have negative CTE.

The term

$$R = \frac{3(1 - \nu_2)x}{2 \frac{E_2}{E_1} (1 - 2\nu_1)(1-x) + 2(1-2\nu_2)x + (1+\nu_2)} \quad (36)$$

is always positive (because ν_1 and ν_2 are generally less than 0.5 and x is always less than unity) and varies between 0 and 1. So

$$\alpha_c = \alpha_1 R + \alpha_2 (1-R) \quad (37)$$

will be zero if and only if α_1 and α_2 have opposite signs. However, if only an ultra-low CTE is required then α_1 and α_2 could be both positive providing that at least one of them has an ultra-low values (10^{-8} - 10^{-9}K^{-1}).

Now let us consider some interesting implications of Equations (25-34) when α_1 is positive and α_2 negative. On heating sphere 1 will expand and sphere 2 will contract. On cooling, however, sphere 1 will contract and sphere 2 will expand, which means unless strong bonding exists between the two phases, debonding is going to occur. Once debonding occurs the composite will show a CTE as that

of material 2. On the other hand if α_1 is negative and α_2 positive, debonding may be encountered on heating but not on cooling. To avoid debonding, the composite should be designed so that it has zero CTE at the "critical temperature" (i.e. if α_1 is negative the critical temperature will be the upper limit of the design range of temperature and if α_1 is positive the critical temperature will be the lower limit). Since it has already been decided to use a metal phase and a ceramic phase in the composite and since the composite should have good thermal conductivity, it is clear that the inner sphere should be the ceramic phase with negative CTE and the outer sphere should be the metallic phase with positive CTE. For the case of an ultra-low CTE, composite the phase with the negative CTE can be replaced by a phase with ultra-low CTE.

In this analysis the value of α was assumed to be constant over the temperature range ΔT . Although this assumption is not realistic, since α varies with temperature, it does not affect the design much, since the different values of α at different temperature will just change the range of temperature where α_c is zero or ultra-low.

Two other aspects of concern in the design of the composites are yielding of the metallic phase and fracture of the ceramic phase. According to the von Mises criterion [46] yielding begins when

$$\sigma_y = \frac{1}{\sqrt{2}} [(\sigma_r - \sigma_\theta)^2 + (\sigma_\theta - \sigma_\phi)^2 + (\sigma_\phi - \sigma_r)^2]^{1/2} \quad (38)$$

But for a sphere

$$\sigma_{\theta} = \sigma_{\phi}$$

so

$$\sigma_y = |\sigma_r - \sigma_{\theta}|$$

that is for the metallic phase we should have that

$$|(\sigma_r - \sigma_{\theta})_{\max}| < \sigma_y$$

substituting for σ_r and σ_{θ} from Equation (31) and (32)

$$\left| \frac{\Delta T E_2}{(1-\nu_2)} a^3/r^3 \alpha_2 - \left[\frac{2\alpha_2(1-x)[E_2(1-2\nu_1)-E_1(1-2\nu_2)]+3\alpha_1 E_1(1-\nu_2)}{2E_2(1-2\nu_1)(1-x)+2E_1(1-2\nu_2)x+E_1(1+\nu_2)} \right] \right| < \sigma_y \quad (39)$$

It can be clearly seen from above that $|(\sigma_r - \sigma_{\theta})_{\max}|$ occurs at $r=a$. For the ceramic phase it can be easily shown that stress state is hydrostatic compression and therefore yielding does not occur.

Further, the stress at the interface should be preferably compressive; if the stresses were tensile, however, it should not exceed the interfacial strength, σ_i , i.e.,

$$\Delta T \left[\frac{2E_1 E_2 (\alpha_2 - \alpha_1)(1-x)}{2E_2(1-2\nu_1)(1-x)+2E_1(1-2\nu_2)x+E_1(1+\nu_2)} \right] < \sigma_i \quad (40)$$

If σ_i is high enough, that is if bonding is strong, then fracture may occur in the ceramic phase. And the criterion for the ceramic not to fracture is

$$\Delta T \left[\frac{2E_1E_2(\alpha_2 - \alpha_1)(1-x)}{2E_2(1-2\nu_1)(1-x) + 2E_1(1-2\nu_2)x + E_1(1+\nu_2)} \right] < \sigma_f \quad (41)$$

where σ_f is the fracture stress of the ceramic phase. Equations (39) (40) and (41) will determine how high ΔT could be without inducing plastic deformation in the metal matrix, debonding at the interface and fracture of the ceramic dispersoid.

In summary, it is assumed that the composite material behaves as a two-layer composite sphere whose phases are isotropic, homogeneous within each phase, and elastic. Expressions for the displacements, strains and stresses throughout the sphere were derived. From those expressions, the coefficient of thermal expansion of the composite, α_c , the yielding, debonding and fracture criteria were obtained.

The limitations of this analysis are that it was assumed that the phases are isotropic, elastic and homogeneous within each phase. The isotropy requirements will apply if we have a good number of randomly oriented grains in each phase. Another requirement is that bonding between the two phases should be sufficiently strong so that the interface can support tensile stresses. A major assumption, of course, was that the coefficient of thermal expansion of the spherical composite is the same as that of the composite material. This assumption does not appear to be correct since practically the assembly of spheres of the same size will leave the composite with about 25% porosity.

B. Composite Design

In the previous section it has been shown that two constituents, one with a positive CTE and another with a negative CTE, are needed to achieve a zero or ultra-low CTE composite. The choice of those two constituents will be discussed in this section.

From Equation (34) it can be seen that the coefficient of thermal expansion of the composite is a function of the coefficients of thermal expansion, moduli of elasticity, Poisson's ratios and, more importantly, the volume fractions of the constituents. It is obvious that the Poisson's ratios have almost no effect on α_c since for most materials the value of the Poisson's ratio is about 0.3. To study the modulus effect, Figure 7 was plotted using Equation (36), where the Poisson's ratios were taken as 0.3. The value $(\alpha_c - \alpha_2)/(\alpha_1 - \alpha_2)$ is plotted vs the volume fraction of the dispersed phase for different values of the moduli ratio, E_2/E_1 . It can be seen that the CTE of the constituents should be the principal design parameter, because for most combinations of metals and ceramics E_2/E_1 varies from 0.5 to 2. If we first consider that the values of α_1 and α_2 are fixed then for a certain value α_c the effect of E_2/E_1 (between 0.5 to 2) is marginal ($\pm 6\%$) whereas for a value E_2/E_1 between 0.5 to 2 a change in x_1 means a drastic change in α_c . Also it should be mentioned that the line $E_2/E_1 = 1$ is the rule of mixtures.

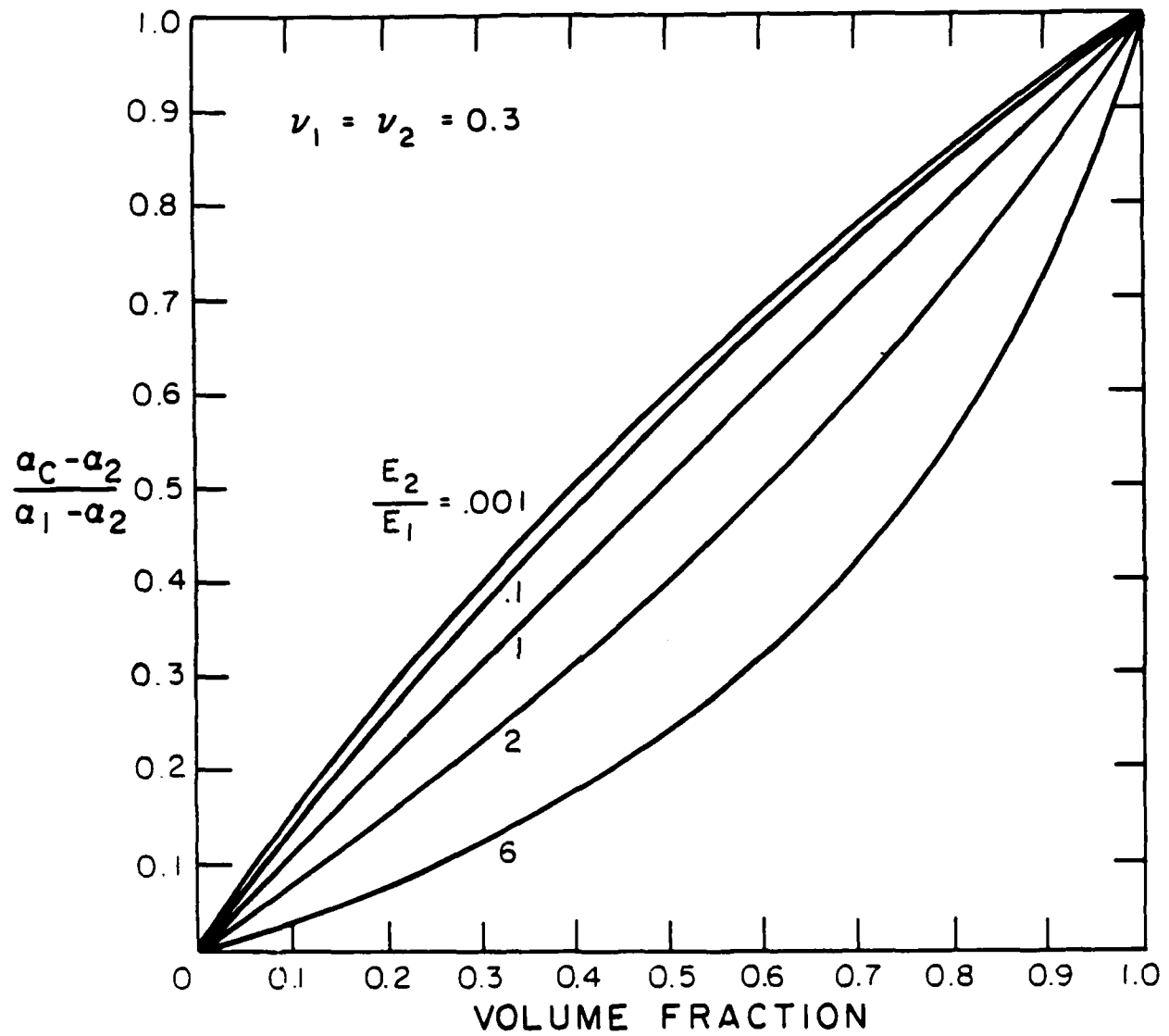


FIGURE 7. DIMENSIONLESS PLOT OF THE COMPOSITE'S CTE vs THE VOLUME FRACTION OF THE DISPERSOID (Material 1)

The design objective is to have as much metal in the composite as possible so that the thermal conductivity of the composite will be high. To achieve this, the ideal combination would be to have a ceramic with large negative CTE and a metal with a small positive CTE. Unfortunately, not many ceramics have large negative CTE. As can be seen in Table 1, the most promising ceramic appears to be Nb_2O_5 . Accordingly Nb_2O_5 was chosen as the dispersoid. As for the matrix material, several metals and alloys can be used.

Using Equation (30) Figure 8 was plotted for the CTE of the composite at 300K with superinvar, titanium, nickel, copper and aluminum as matrices. The value of α_c is plotted vs the volume fraction of Nb_2O_5 . It can be shown as predicted that the composite with superinvar is the most promising composite in that it requires a small amount of Nb_2O_5 . The next promising composites are the ones with titanium and nickel matrices.

Figure 9 is a semi-log plot of Equation (34). The value of $\log \alpha_c$ is plotted vs the volume fraction of Nb_2O_5 . The figure has two sets of curves: the ones on the left are when α_c is positive and the ones on the right are when α_c is negative. It is clear that the volume fraction should be tightly controlled ($\pm 2\%$) to produce a composite with ZCTE ($\sim 10^{-8} \text{K}^{-1}$).

Further, Equations (39), (40) and (41) should be satisfied so that we should have no yielding of the matrix or debonding at the inter-

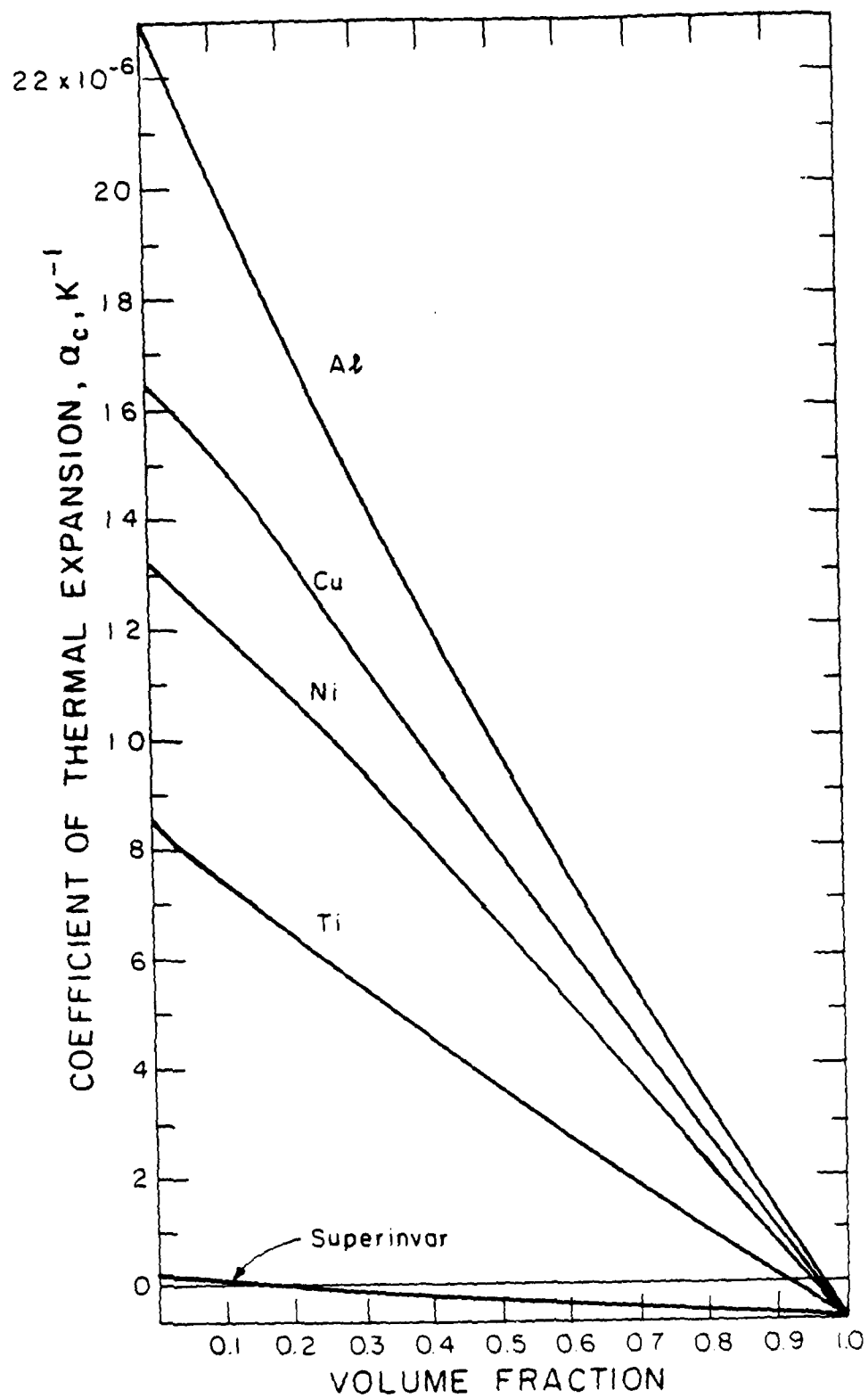


FIGURE 8. COEFFICIENT OF THERMAL EXPANSION OF THE COMPOSITE AT 300K vs VOLUME FRACTION OF Nb_2O_5

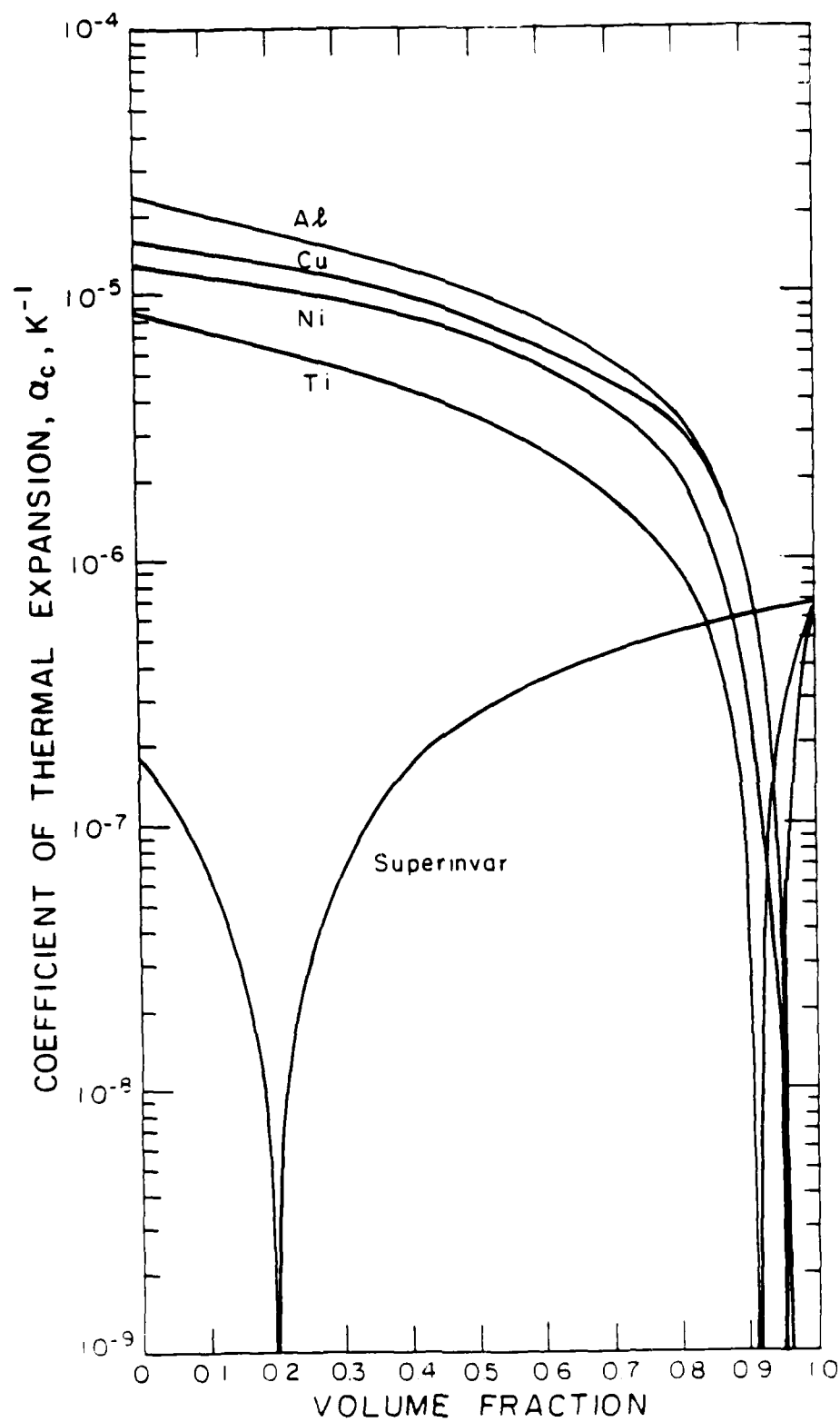


FIGURE 9. SEMI LOG PLOT OF THE COMPOSITE'S CTE vs VOLUME FRACTION OF Nb_2O_5 AT 300K

face or fracture of the ceramic phase. From equation (39) it can be seen that $(\sigma_r - \sigma_\theta)_{\max}$ occurs when $r=a$, i.e. at the interface

$$(\sigma_r - \sigma_\theta)_{\max} = \frac{\Delta T E_2}{(1 - \nu_2)} \alpha_2 - \left[\frac{2\alpha_2(1-x)[E_2(1-2\nu_1) - E_1(1-2\nu_2)] + 3\alpha_1 E_1(1-\nu_2)}{2E_2(1-2\nu_1)(1-x) + 2E_1(1-2\nu_2)x + E_1(1+\nu_2)} \right] \quad (42)$$

This equation is also maximum for high x when $E_2(1-2\nu_1) - E_1(1-2\nu_2) > 0$ and vice-versa. Table 5 gives the values of $(\sigma_r - \sigma_\theta)_{\max}$ for a temperature change, ΔT , of 250K and the yield stress of various metals. From that table it can be seen that only composites with electroless nickel and superinvar would satisfy the requirement of Equation (39). It should be noted that the coefficient of thermal expansion was assumed to be constant in that temperature range. Although this assumption is not valid, it gives an approximate value of $(\sigma_r - \sigma_\theta)_{\max}$ since the coefficient of thermal expansion varies by $\pm 20\%$ of the value used; and this change will not affect the values in Table 5 by more than 20%, which means that nickel and superinvar composites will still deform elastically.

TABLE 5: VALUES OF $(\sigma_r - \sigma_\theta)_{\max}$ for $\Delta T = 250K$ and
YIELD STRESS OF VARIOUS METALS

METAL	$(\sigma_r - \sigma_\theta)_{\max}$ MPa	σ_y MPa
Al	746	27.6-300
Cu	794	69-345
Ni*	1070	2490
Ti	424	400-600
Superinvar	49	276-414

*Electroless Ni with Hardness = $63R_c$

CHAPTER IV

EXPERIMENTAL PROCEDURES

The traditional technique of producing particle-reinforced composites is by mechanically mixing powders of the matrix and reinforcing phases and subsequently hot pressing them (or by cold pressing and sintering) to obtain a dense composite. The composite so produced will have continuous matrix and dispersed reinforcing phases, provided the volume fraction of the reinforcing phase is small. But when the volume fraction is large, such as in the Ni-Nb₂O₅ composite ($x_{\text{Nb}_2\text{O}_5} \sim 0.95$, see Figure 9), the compacted composite will have continuous reinforcing and dispersed metallic phases. Such a composite will be both brittle and thermally insulating. In an attempt to disperse Nb₂O₅ particles in Ni matrix each Nb₂O₅ particle was coated with the required amount of nickel by electroless plating. The composite spheres so produced were then hot pressed in an argon atmosphere. A brief description of these procedures is given in the following sections.

Although the primary objective of this thesis is one of making low expansion metal-matrix composites, characterizing those composites is a necessary complementary task. Scanning Electron Microscopy (SEM), chemical analysis and γ -ray diffraction were used to identify the different elements and phases in the composites. Accordingly, a brief description of these techniques is also included in this section.

A. Flame Spraying

The commercial Nb_2O_5 powder purchased from Aldrich^{*} and A.D. McKay^{**} was porous, flaky, and had a wide size distribution. The powder was sieved and sent to General Plasma Associates^{***} for flame spraying.

The thermospray system used was MetCo 6P-H hand-held manual spray gun. Nb_2O_5 particles, 38-63 μm , were fed to the gun at a rate of 450-900g per hour. The particles emerged through the center of the head where the flame temperature was of the order of 4000K. The molten Nb_2O_5 particles were sprayed into a water bath and then collected and dried at 373K for two hours. A detailed description of this procedure is given in Appendix II.

B. Electroless Plating

The coating technique employed for making $\text{Ni-Nb}_2\text{O}_5$ composites was electroless nickel plating, a commercial process^{****} used for plating high purity nickel on metals, semiconductors and insulators.

The Nb_2O_5 spherical particles were soaked in a catalyst (1g PdCl_2 per 500 ml of distilled water) for 15 minutes, rinsed with

^{*} Aldrich Chemical Co., Milwaukee, WI.

^{**} A.D. McKay, Darien, CT.

^{***} General Plasma Associates, East Windsor, CT.

^{****} Shipley Co., Danvers, MA.

distilled water and then put into an already prepared electroless plating solution in a Pyrex beaker.. The plating was carried out at 338K for 2-18 hours depending on the volume fraction of nickel required. The powder particles were then collected, washed with distilled water and acetone and dried in air. Other details of this procedure are given in Appendix III.

C. Mechanical Mixing

In the case of superinvar-Nb₂O₅ composites, the volume fraction of Nb₂O₅ required to obtain an ultra-low or zero CTE is only about 0.2. This means that mechanical mixing of Nb₂O₅ and superinvar powder will insure continuous metal matrix. The mechanical mixing was carried out by placing spherical particles of superinvar and Nb₂O₅ of the same size (44-53 μ m) in a ball milling jar and rotating the jar for an hour.

This method was used for all the superinvar-Nb₂O₅ composites even though the final composite is not expected to have the ideal structure (metal surrounding the oxide). There is no simple method of coating superinvar on the Nb₂O₅ particles.

D. Hot Pressing

Both the coated and the mixed powders were compacted by hot pressing in a graphite die which was inductively heated. Hot-pressing was carried out at 1473K at a pressure of 34.5 MPa (5000 psi) for 3 minutes in an argon atmosphere. The sample was then furnace cooled,

i.e., by turning the power off. This procedure is described in Appendix IV in greater detail.

E. Optical Metallography

After hot pressing, the samples were cut by a diamond saw, mounted in Bakelite, polished with 0.3 and 0.05 μm alumina in water. All the samples were photographed without etching. Although many etchants (HF , HCl , HNO_3 , H_2SO_4 , NaOH , KOH) were tried, it was not possible to etch the Nb_2O_5 specimen.

F. Scanning Electron Microscopy

Scanning electron microscopy was carried out on both the particles and the mounted samples. The powder particles were coated with gold by vapor deposition. Energy dispersive X-ray analysis (EDAX) was carried out to identify the impurities present in the powder particles and in the superinvar sample.

G. X-ray Diffraction

X-ray diffraction was used to identify the different phases of Nb_2O_5 present before and after flame spraying, after nickel plating, and hot pressing. Nickel-filtered copper radiation was used. For the superinvar powder chromium radiation was used.

H. Chemical Analysis

A semi-quantitative chemical analysis was performed after each procedure to identify the elements in the samples and to make sure that no major compositional changes took place. Further, since

the samples were hot pressed in a graphite die, the carbon content in the samples was also determined.

Also, the volume fraction of the $\text{Ni-Nb}_2\text{O}_5$ composite was found by dissolving the nickel in the composite into a solution of hydrofluoric and nitric acid; subsequently the Ni content in the composite was obtained.

I. CTE Measurement

The hot pressed samples were cut to a size of approximately 1.5 cm x 0.5 cm x 0.5 cm, with a diamond saw at low speed with copious quantities of cutting liquid. They they were cleaned with acetone and dried. These samples were sent to the Aerospace Corporation^{*} where they were polished and coated with a thin film of aluminum to insure better reflection of the laser beam. The CTE measurements were carried out in the temperature range 150-300K by the laser interferometric technique. Appendix V describes this technique.

^{*}Aerospace Corporation, El Segundo, CA.

CHAPTER V

RESULTS

In many instances the properties of a composite are irreversibly influenced by impurities. The only way to avoid the complications due to compositional changes is by monitoring and tightly controlling the composition of the constituents of the composite during processing. Similarly, the size, shape, crystal structure and, more importantly, the volume fraction of various phases also affect the properties of a composite. Again it is necessary to keep track of these microstructural features to meaningfully interpret the properties of the final product.

Accordingly, chemical analysis, X-ray diffraction and scanning electron microscopy have been used in this work to identify different elements and phases in the composites. In the following sections the results of these analyses and the coefficient of thermal expansion of $N_i-Nb_2O_5$ and superinvar- Nb_2O_5 composites in the temperature range 180-300K are presented.

A. Chemical Analysis

Semiquantitative chemical analysis was performed after each treatment (electroless plating, flame spraying, etc.) to identify the impurities in the samples and to insure that no major changes in chemical composition took place during processing. It can be seen from Table 6 that the Nb_2O_5 powder purchased from two different companies, Aldrich Chemicals and A.D. McKay, had the same composition

TABLE 6. SEMIQUANTITATIVE CHEMICAL ANALYSIS

SAMPLE	Al	B	Ca	Co	Cr	Cu	Fe	Mg	Mo	Nb	Ni	Si	Ti
1. Aldrich Nb ₂ O ₅	Ft	—	Vft-t	—	—	t	Vft	Vft	—	H	—	Ft	Vft
2. A.D. McKay Nb ₂ O ₅	Vft	—	Ft-t	—	—	t	Vft	Ft	—	H	Ft	Vft	Vft
3. Aldrich Nb ₂ O ₅ , flame sprayed	Ft	—	Vft-t	—	Ft	t	Vft	Vft	—	H	t	Ft	Vft
4. A.D. McKay Nb ₂ O ₅ , flame sprayed	Vft	—	Ft-t	Vft	—	Ft	Ft	Ft	—	H	Ft	Ft	Ft
5. Nb ₂ O ₅ hot pressed	Vft	—	Vft	—	Vft	t	Ft	Vft	—	H	—	Ft	—
6. Ni-90.5 Nb ₂ O ₅ after plating	—	t	Ft-t	Vft	—	Ft	Vft	Ft	—	H	H	Vft	—
7. Ni-90.5 Nb ₂ O ₅ hot pressed	Ft	t	L	Vft	Vft	—	Ft	t	—	H	H	L	Vft
8. Superinvar	Ft	—	Wft	M	t	Ft-t	H	Vft	Ft	—	H	Ft	Ft-t

Key: VFt < 0.0001%

VFt 0.0001 - 0.001%

Ft 0.001 - 0.01%

t 0.01 - 0.1%

L 0.1 - 1.0%

M 1.0 - 10.0%

H > 10%

and the same concentration of impurities. There were no major compositional changes due to flame spraying, electroless plating, or hot pressing.

However, after flame spraying the Nb_2O_5 powder turned gray, which means that it could have been at least partially reduced. The carbon content was determined in the as received and flame sprayed sample to investigate whether the Nb_2O_5 was reduced. It can be seen from Table 7 that carbon content is about the same in all the Nb_2O_5 samples. Similarly, carbon content was also obtained for all the hot pressed samples to investigate if any reaction between the graphite die and the specimens took place. It can be seen from Table 6 again that the amount of carbon in the hotpressed samples is not unduly large. Hence, the effect of the carbon in the Ni - Nb_2O_5 composites can be disregarded.

In the superinvar- Nb_2O_5 composites, however, the carbon content is very important because the more carbon in the superinvar the higher is the CTE [47-53]. Further, since certain impurities (Si, Mn) [53] might affect the CTE of superinvar, chemical analysis was performed to find the composition of the superinvar powder used in this work (Table 8).

Finally, since the effect of volume fractions of various phases on the properties of the composite is very important, the weight fraction of nickel in the hot pressed Ni- Nb_2O_5 composites was determined. From these values (Table 9) the volume fraction of

TABLE 7. CARBON WEIGHT PERCENT

SAMPLE	% C
1. Aldrich Nb ₂ O ₅	0.05
2. A.D. MacKay Nb ₂ O ₅	0.02
3. Aldrich Nb ₂ O ₅ flame sprayed	0.05
4. A.D. McKay Nb ₂ O ₅ flame sprayed	0.07
5. Nb ₂ O ₅ -hot pressed	0.07
6. Ni-20.5 Nb ₂ O ₅ hot pressed	0.23
7. Ni-33.5 Nb ₂ O ₅ hot pressed	0.28
8. Ni-63.15 Nb ₂ O ₅ hot pressed	0.04
9. Ni-87.3 Nb ₂ O ₅ hot pressed	0.22
10. Ni-90.5 Nb ₂ O ₅ hot pressed	0.08
11. Superinvar powder	0.01
12. Superinvar-hot pressed	0.99
13. Superinvar-10 Nb ₂ O ₅ hot pressed	0.40
14. Superinvar-20 Nb ₂ O ₅ hot pressed	0.40
15. Superinvar-50 Nb ₂ O ₅ hot pressed	0.93

TABLE 2. COMPOSITION OF SUPERINVAR

ELEMENT	WEIGHT PERCENT
Al	0.23
C	0.01
Co	6.1
Cr	0.22
Cu	0.055
Fe	58.5
Mo	0.024
Mn	0.006
Ni	33.2
Si	0.035
Ti	0.013

TABLE 9. WEIGHT AND VOLUME PERCENT OF Ni
IN Ni-Nb₂O₅ COMPOSITES

SAMPLE	WEIGHT PERCENT	VOLUME PERCENT
1	17.0	9.50
2	22.2	12.70
3	53.3	36.85
4	79.5	66.50
5	88.3	79.50

nickel was calculated assuming there is no porosity in the composites. This method of finding the volume fraction of the various phases is accurate providing the final composites have negligible or no porosity.

B. X-Ray Diffraction

X-ray diffraction patterns of all the Nb_2O_5 samples (Figures 10-12) were taken to identify the changes in the crystal structure of Nb_2O_5 . It was found that the as received Aldrich Nb_2O_5 had both monoclinic and orthorhombic phases whereas the A.D. McKay Nb_2O_5 was monoclinic. After flame spraying, the Aldrich sample retained the same diffraction pattern and the A.D. McKay sample changed to orthorhombic Nb_2O_5 . However, both the hot pressed Nb_2O_5 (Aldrich sample) and the Ni-90.5 Nb_2O_5 , (from A.D. McKay) showed that the Nb_2O_5 was monoclinic. This is expected because the Nb_2O_5 when cooled from high temperature transforms at about 1273K and becomes a stable monoclinic phase [54-57]. Hence, it can be concluded that the Nb_2O_5 in all the hot pressed samples is monoclinic.

Figure 13 shows the diffraction pattern of nickel plated Nb_2O_5 . Since the diffraction pattern is mainly that of nickel, it can be concluded that the nickel is surrounding almost all the particles even though the volume fraction of nickel in that sample is only 0.127.

Finally, the diffraction pattern of the superinvar powder is given in Figure 14, which shows that the iron and nickel, in the super-

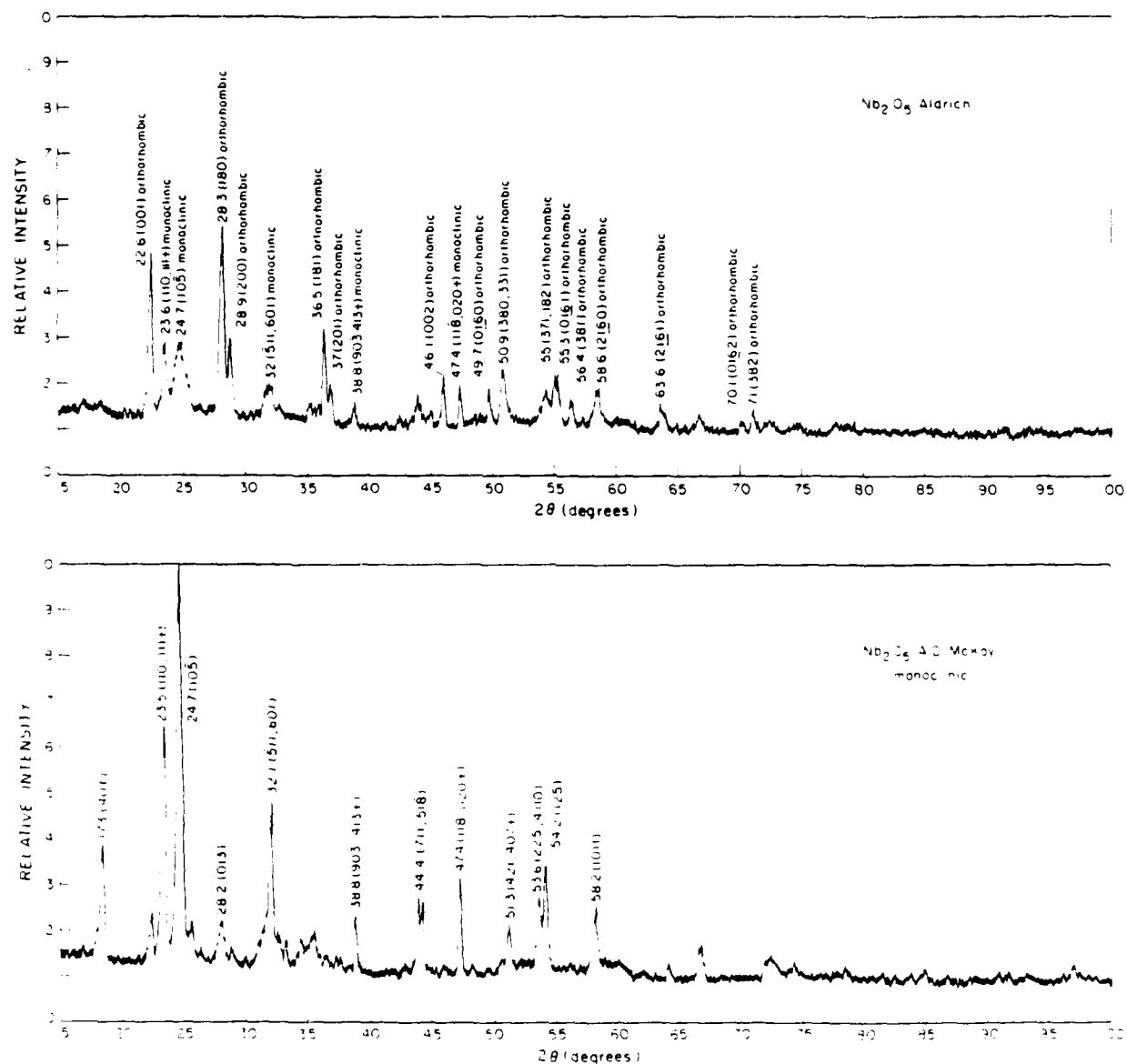


FIGURE 10. X-RAY DIFFRACTION PATTERN OF AS RECEIVED Nb₂O₅ POWDER. Ni-FILTERED COPPER RADIATION, 35 kV, 15 mA

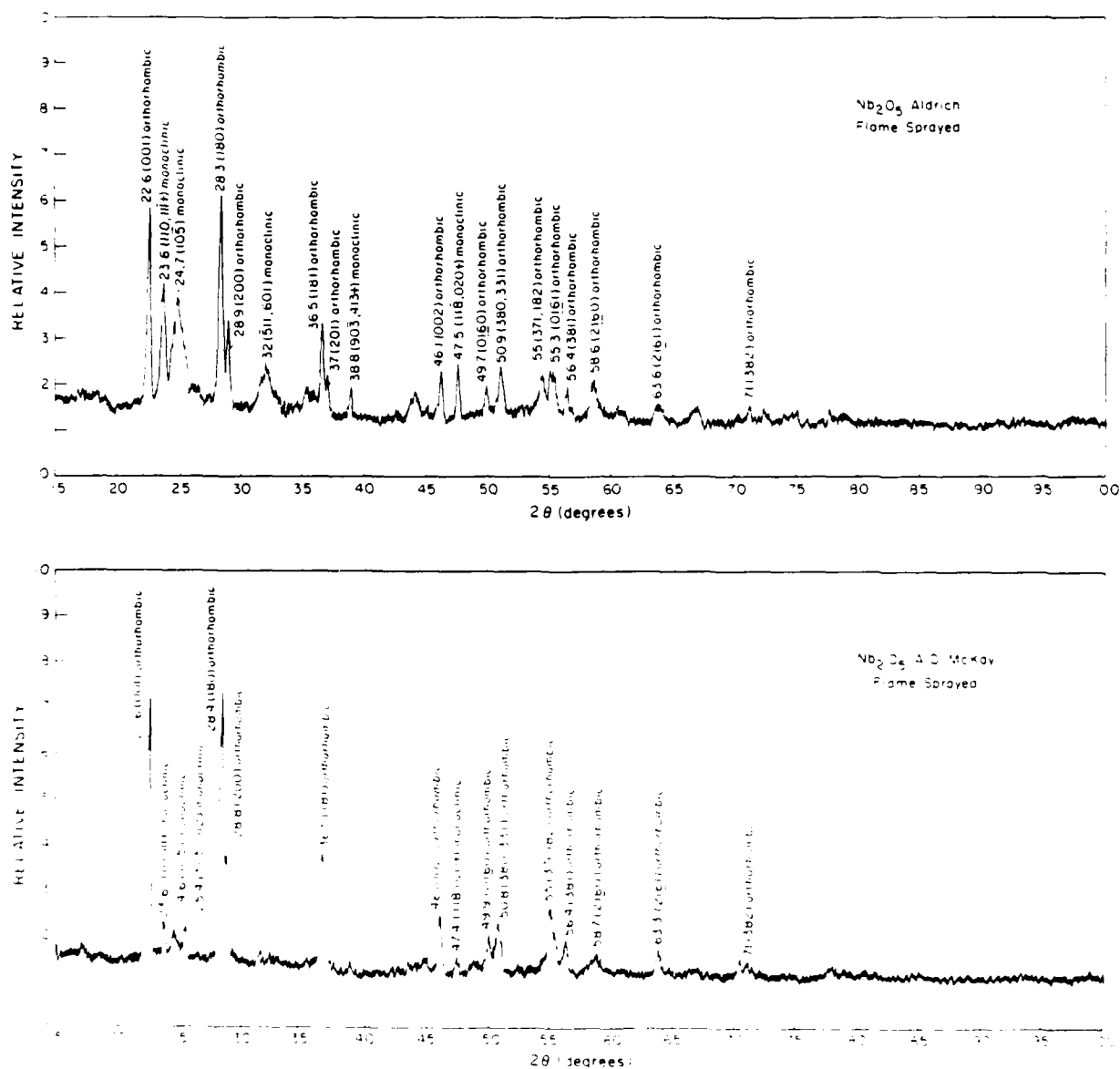


FIGURE 11. X-RAY DIFFRACTION PATTERN OF FLAME SPRAYED Nb_2O_5 POWDER. Ni-FILTERED COPPER RADIATION, 35 kV, 15 mA

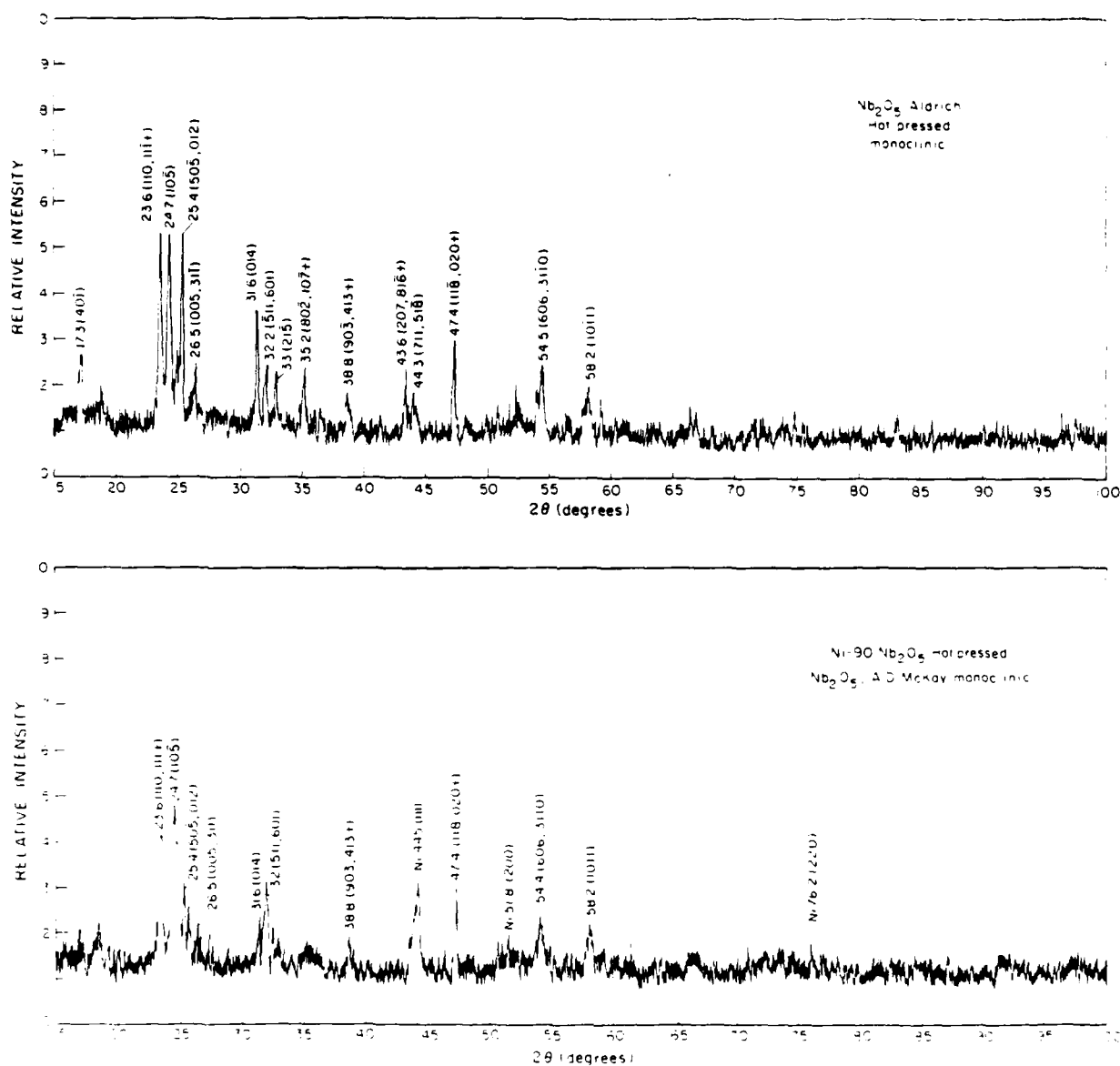


FIGURE 12. X-RAY DIFFRACTION PATTERN OF HOT PRESSED Nb_2O_5 AND Ni-90.5 Nb_2O_5 COMPOSITE. Ni-FILTERED COPPER RADIATION, 35 kV, 15 mA

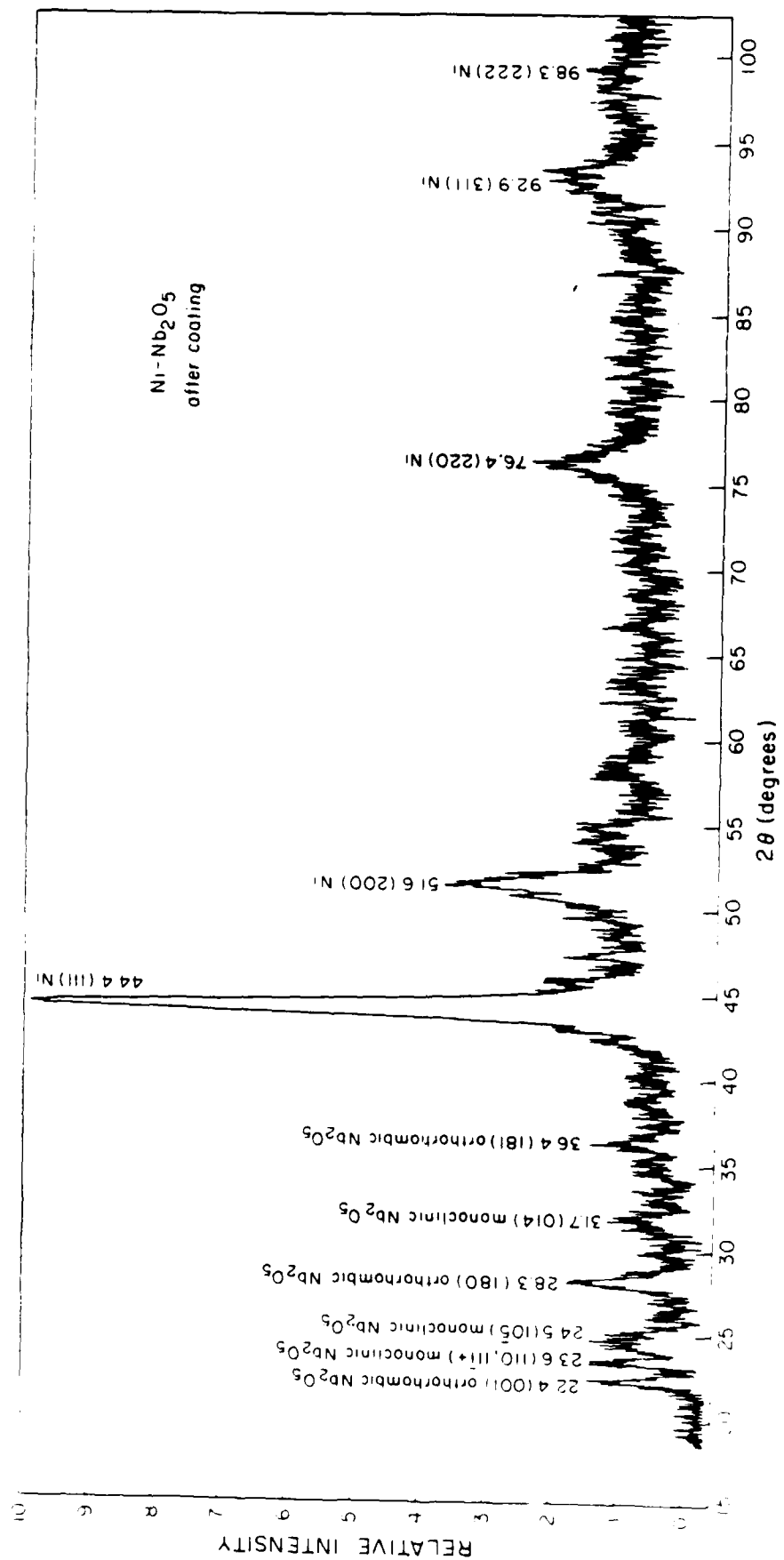


FIGURE 13. X-RAY DIFFRACTION PATTERN OF $\text{Ni-87.3 Nb}_2\text{O}_5$ AFTER PLATING.
 Ni-FILTERED COPPER RADIATION, 35 kV, 15 mA

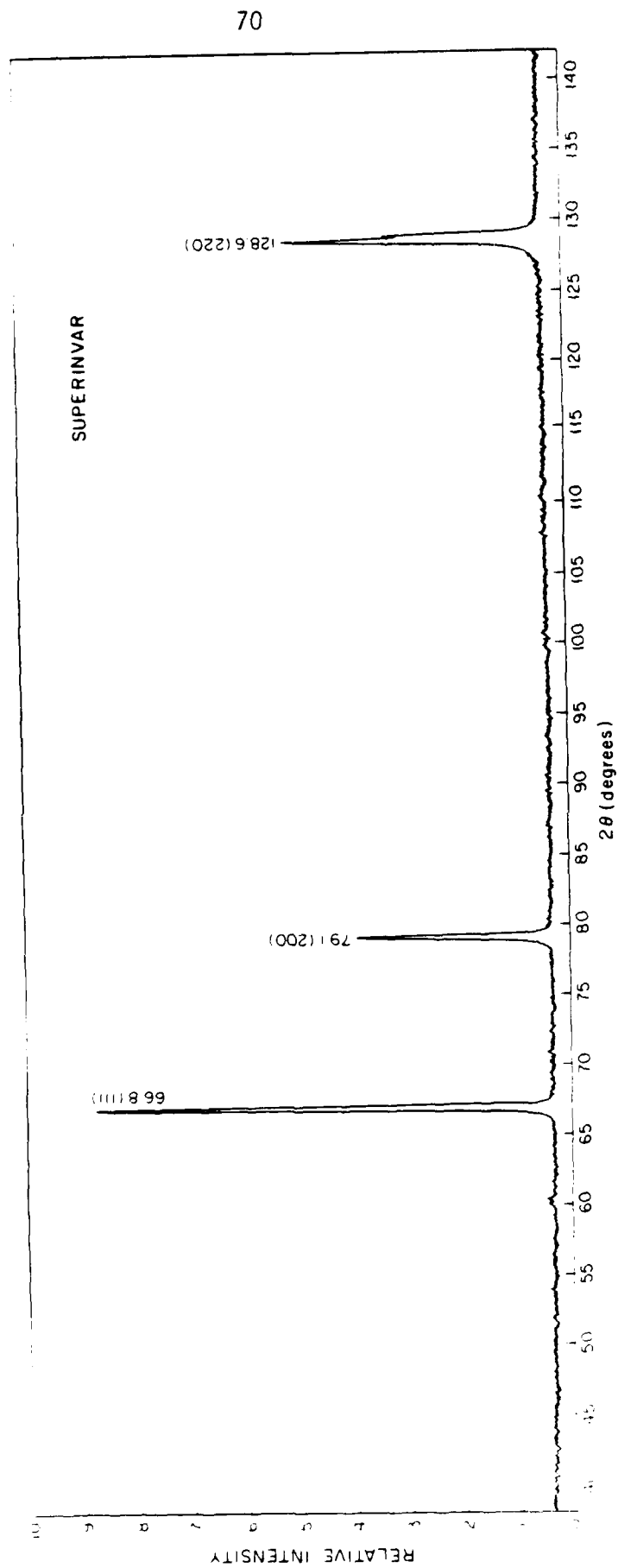


FIGURE 14. X-RAY DIFFRACTION PATTERN OF SUPERINVAR POWDER.
CHROMIUM RADIATION, 35 kV, 15 mA

invar, are in solid solution.

C. Scanning Electron Microscopy

All the powder samples and the hot pressed solid samples were observed in the SEM (Figures 15-18). Also, Energy Dispersive X-ray Analysis (EDAX) was done for the powder samples and the superinvar solid sample. From Figures 15 and 16 it can be seen that both powder samples, from Aldrich and A.D. McKay, were spherical after flame spraying. After plating, however, the Aldrich particle (Figure 15c) does not look spherical. A possible reason is that this sample was plated for 8 hours and most of the powder stuck to the magnetic stirrer after 4 hours which resulted in non-uniform plating on the particles. This problem is not present in Figure 16c since the powder there was only coated for 2 hours. Further, the EDAX spectra (Figures 15e and 16e) show that the powder was totally surrounded by nickel.

The SEM micrographs of the hot pressed samples (Figures 17,18) show that in composites where the Nb_2O_5 is low (Figures 17a,b,c and 18b, c), the metal surrounds the Nb_2O_5 , whereas in composites where the Nb_2O_5 volume fraction is high (Figures 7d,e), or low (~ 0.50) but mechanically mixed (Figure 18d), the metal matrix was discontinuous. Further, in some of the samples (Figures 17a,b,c,d and 18a,b,c,d) porosity was present in the Nb_2O_5 particles and in the metal matrix. Nb_2O_5 and $\text{Ni} - 90.5 \text{ Nb}_2\text{O}_5$ (Figures 17e, f) are almost pore-free. Also, in two of the samples (Figure 17c and d) there was evidence of interface debonding.

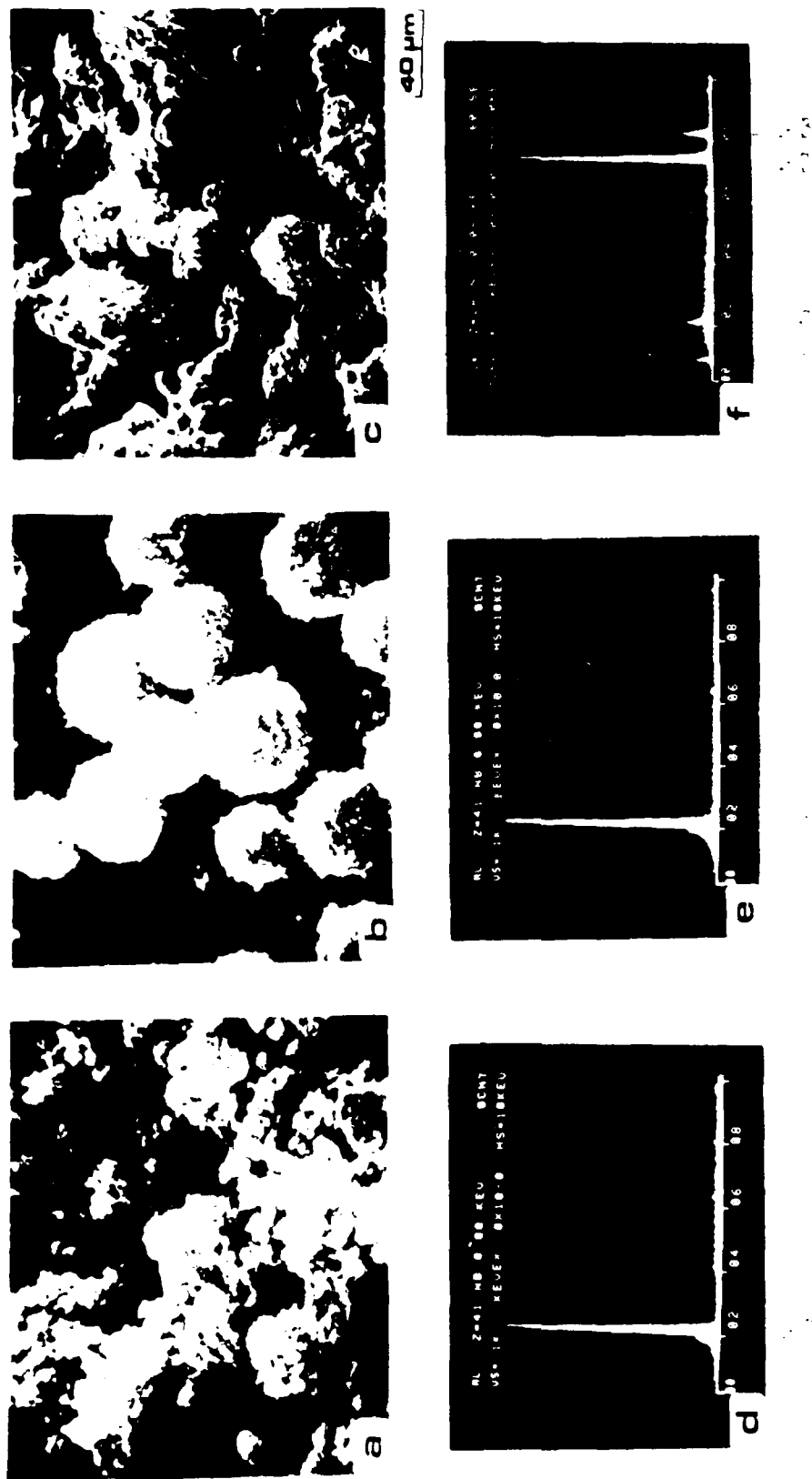


FIGURE 1. SEM micrographs of aluminum nitride powders: (a) as received, (b) flame sprayed and (c) plasma sprayed. (d), (e) and (f) are EDAX analysis of (a), (b) and (c) respectively.

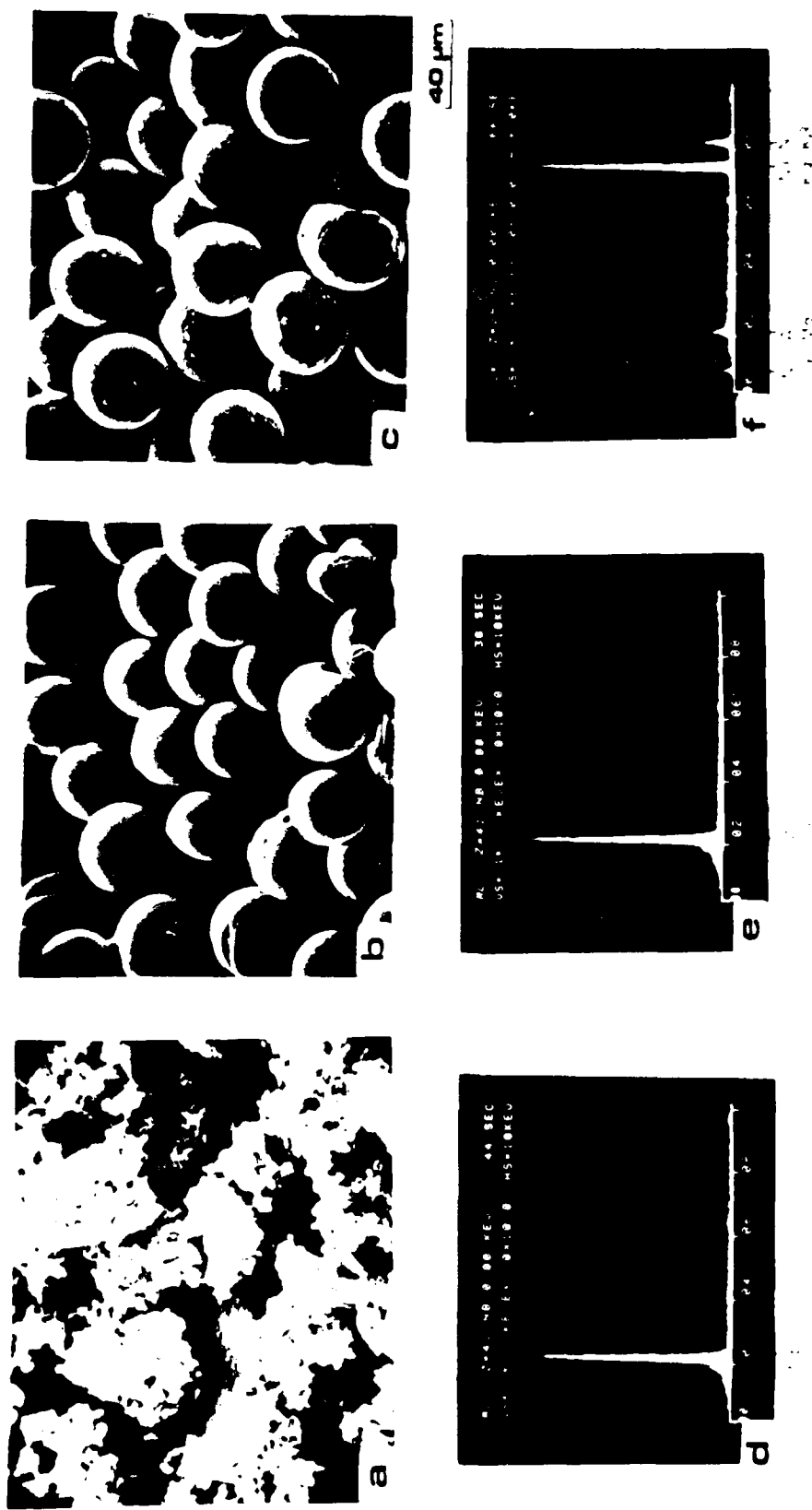


FIG. 16. SEM MICROGRAPHS OF (a) CLAY POWDER, (b) CLAY POWDER, (c) CLAY POWDER, (d) CLAY POWDER, (e) CLAY POWDER, (f) CLAY POWDER. (a), (b), and (c) ARE SEM MICROGRAPHS OF (a), (b), AND (c) RESPECTIVELY. (d), (e), AND (f) ARE EDS ANALYSIS OF (a), (b), AND (c) RESPECTIVELY.

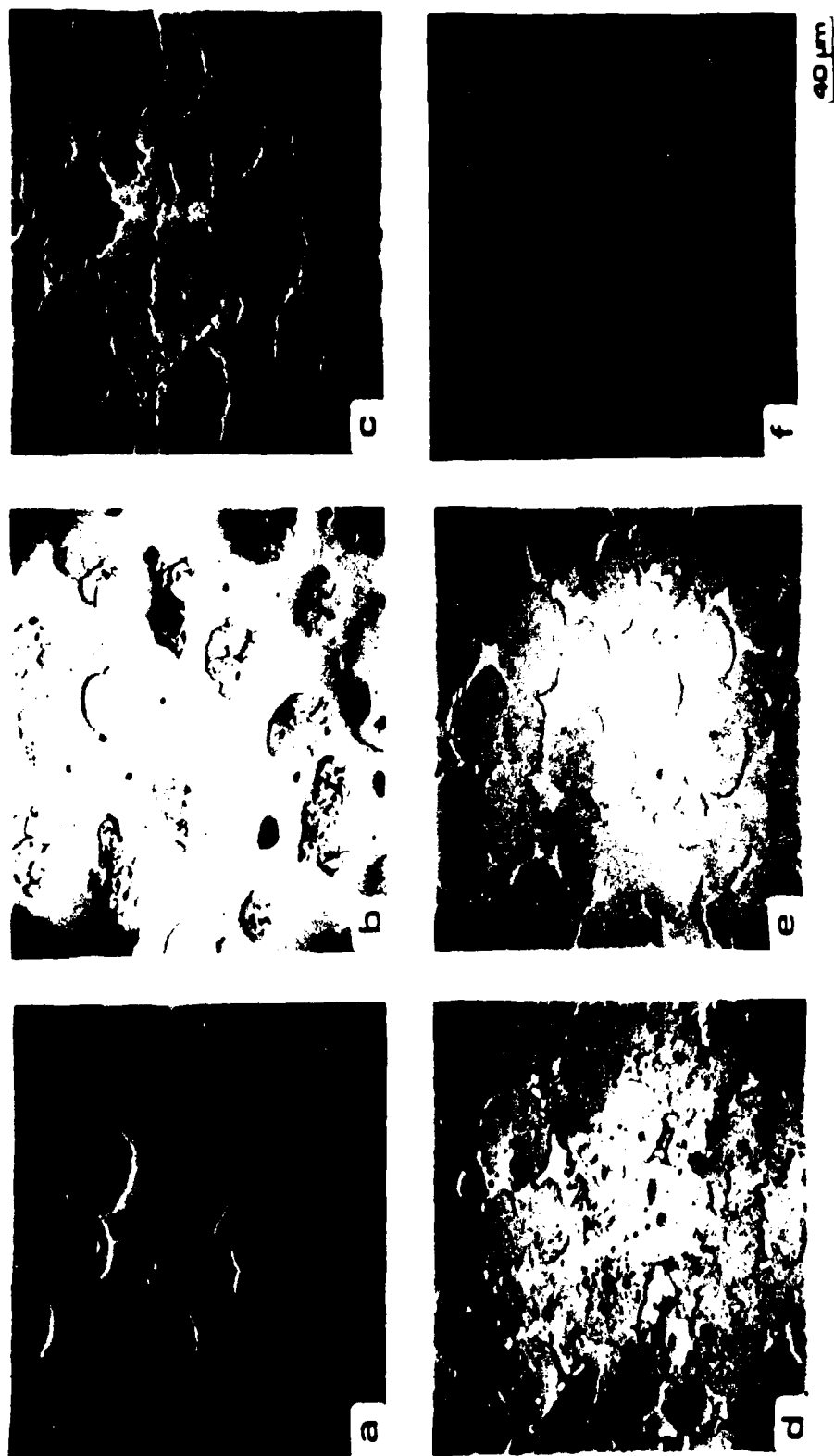


Figure 1. SEM micrographs of (a) NiO , (b) Ni_2O_3 , (c) Ni_3O_4 , (d) NiO , (e) Ni_2O_3 , and (f) Ni_3O_4 .
 (a) NiO , (b) Ni_2O_3 , (c) Ni_3O_4 , (d) NiO , (e) Ni_2O_3 , and (f) Ni_3O_4 .
 (a) NiO , (b) Ni_2O_3 , and (c) Ni_3O_4 .

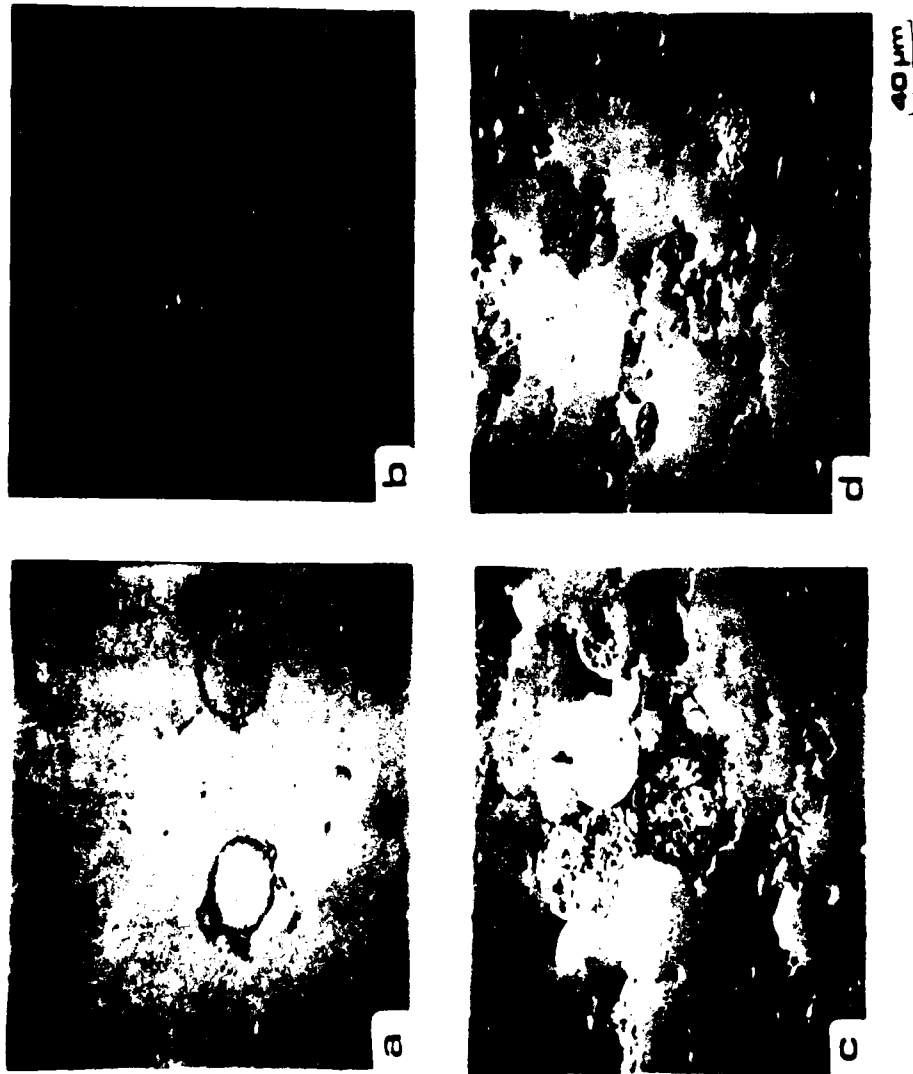


Fig. 1. Scanning electron micrographs of the surface morphology of the different materials: (a) pure PbO , (b) PbO - SnO_2 , (c) PbO - SnO_2 - ZnO , and (d) PbO - SnO_2 - ZnO - CuO .

All these samples were also observed with an optical microscope because the optical micrographs (Figures 19-20) accentuate the contrast between the two phases.

Finally, Figure 21 shows that some chromium was present in the superinvar powder sample. Figure 22b shows that most of the impurities such as chromium, sulfur and titanium and most of the cobalt were segregated in the hot pressed sample in form of spherical particles.

D. CTE Measurements

Figures 23-33 show the thermal linear expansion of all the hot pressed samples. The coefficients of thermal expansion of all the specimens, even that of Nb_2O_5 , were positive. The only sample that showed signs of zero and negative CTE is the Ni-87.3 Nb_2O_5 composite (Figure 26). That same sample, when measured a second time showed positive CTE (Figure 27). A possible explanation for this behavior will be discussed in the next chapter.

For the superinvar specimen, the thermal expansion measured was different for almost every run (Figure 30). This complex behavior could be due to phase change ($\gamma \rightarrow \alpha$) occurring in the material during cooling [49,53]. Also, the temperature at which the phase change occurs depends very much on the composition of the sample. Further since the α phase is more stable than the γ phase, the material seemed to stabilize after a few runs. The coefficient of thermal expansion of the material was $2.99 \times 10^{-6} \text{K}^{-1}$ on

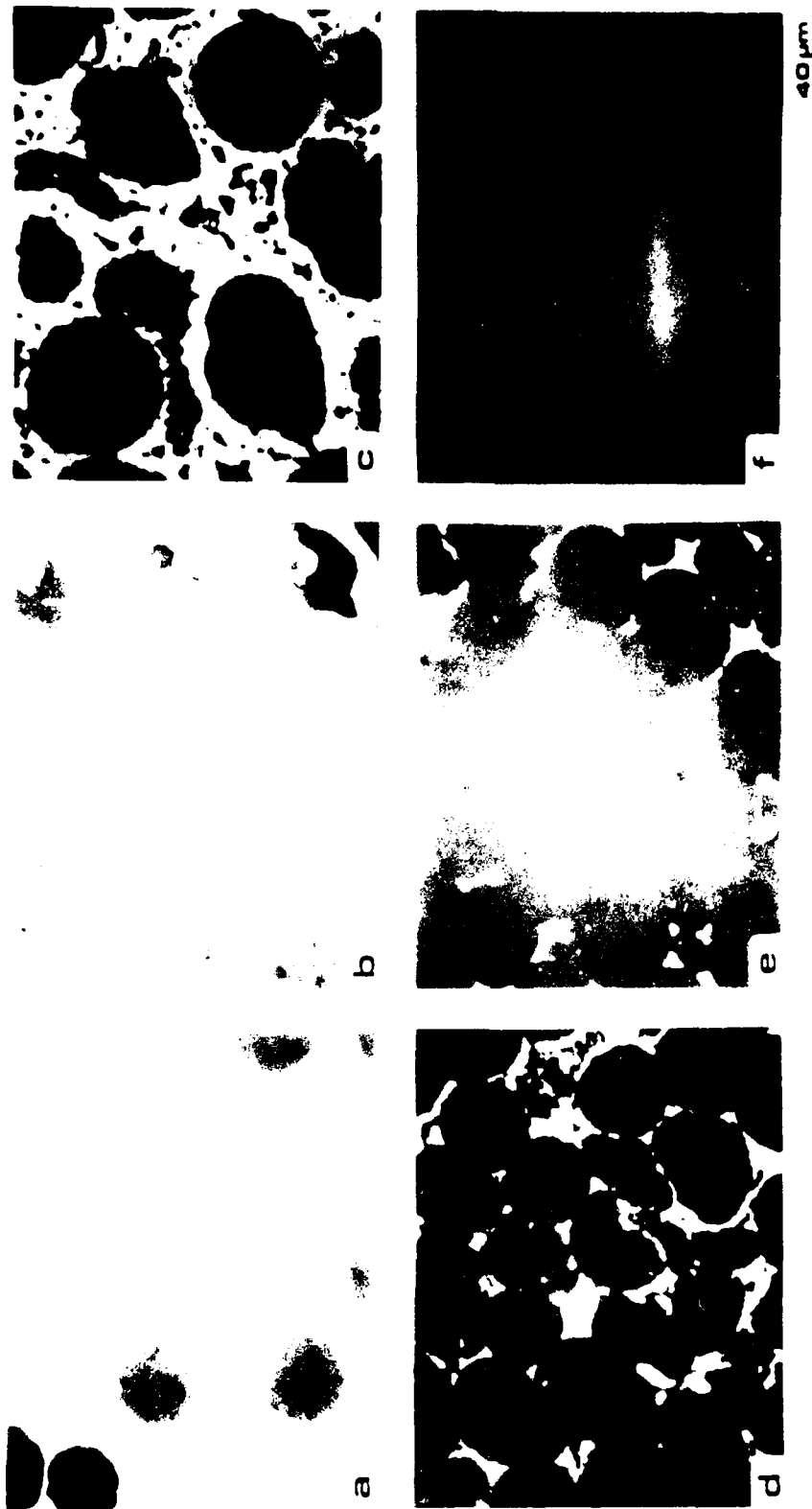


Fig. 1. Micrographs of the microstructure of the alloys: (a) 61-20.5Nb_{20.5}Cu, (b) 51-33.5Nb_{33.5}Cu, (c) 41-41.5Nb_{41.5}Cu, (d) 31-57.3Nb_{57.3}Cu, (e) 21-60.5Nb_{60.5}Cu, and (f) 11-62Cu.

(a) 61-20.5Nb_{20.5}Cu, (b) 51-33.5Nb_{33.5}Cu, (c) 41-41.5Nb_{41.5}Cu, (d) 31-57.3Nb_{57.3}Cu, (e) 21-60.5Nb_{60.5}Cu, and (f) 11-62Cu.

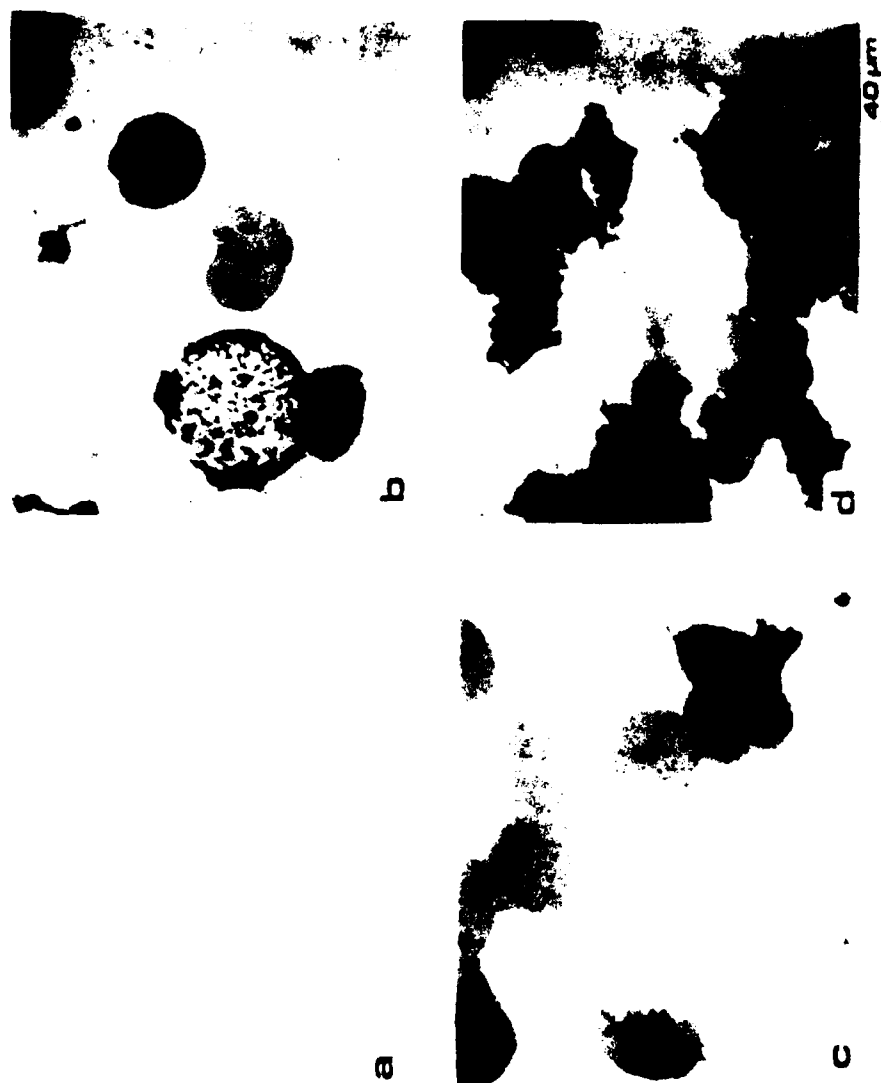
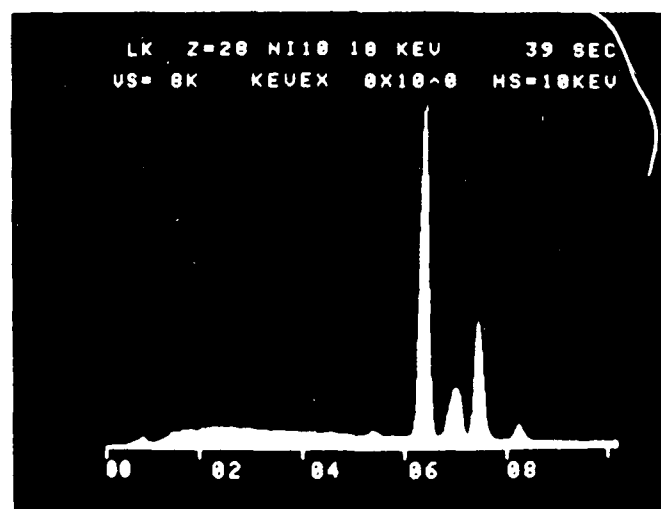
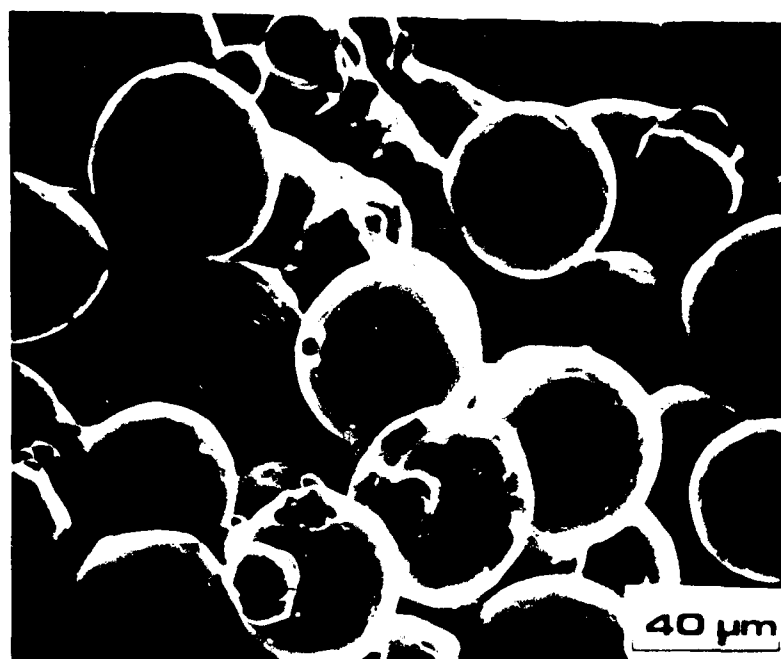
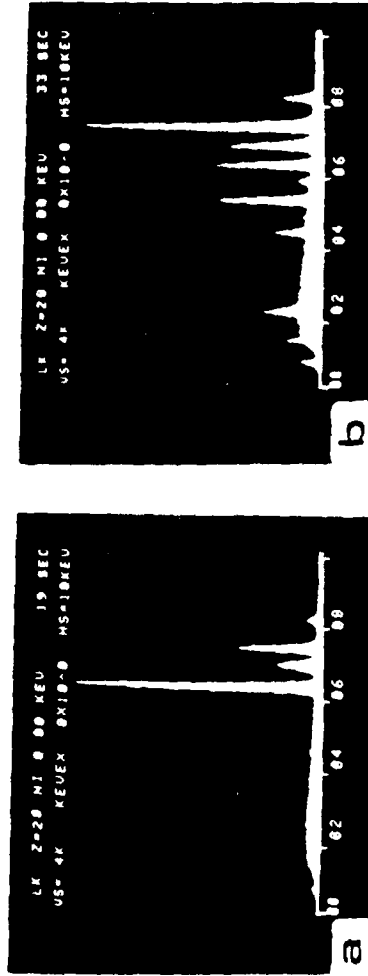
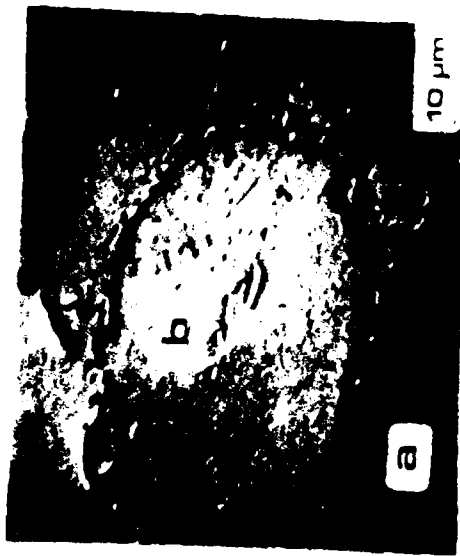


FIGURE 20. OPTICAL MICROGRAPHS OF SUPERINVAR AND SUPERINVAR-Nb₂O₅, HOT PRESSED AND POLISHED SPECIMENS: (a) SUPERINVAR, (b) SUPERINVAR-10 Nb₂O₅, (c) SUPERINVAR-20Nb₂O₅, (d) SUPERINVAR-50 Nb₂O₅





The spectra show the presence of various elements, including Ni, Fe, and Cu, which are consistent with the sample being analyzed. The scale bar in the SEM image indicates a length of 10 μm.

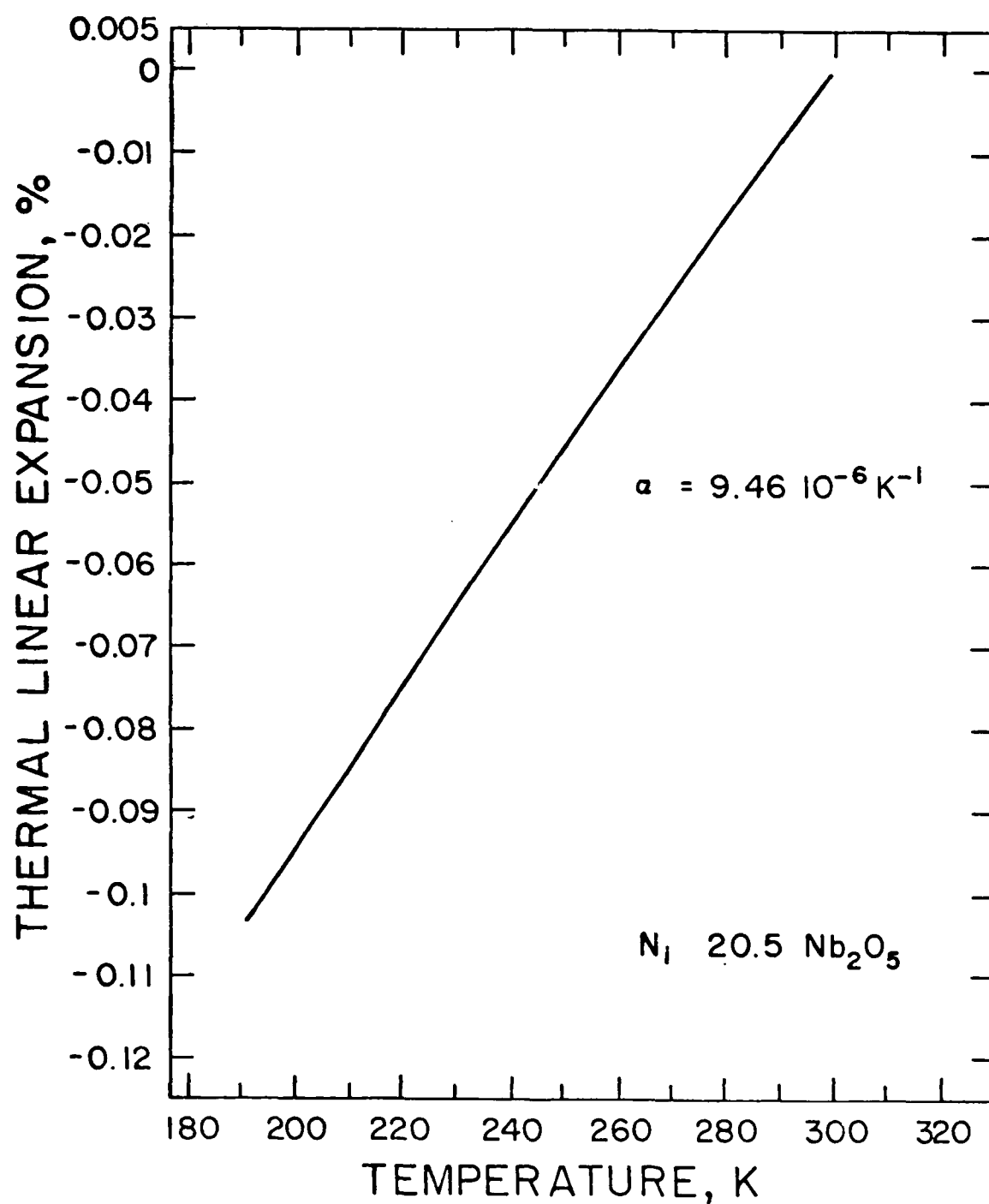


FIGURE 23. THERMAL LINEAR EXPANSION OF Ni-20.5 Nb_2O_5 vs TEMPERATURE

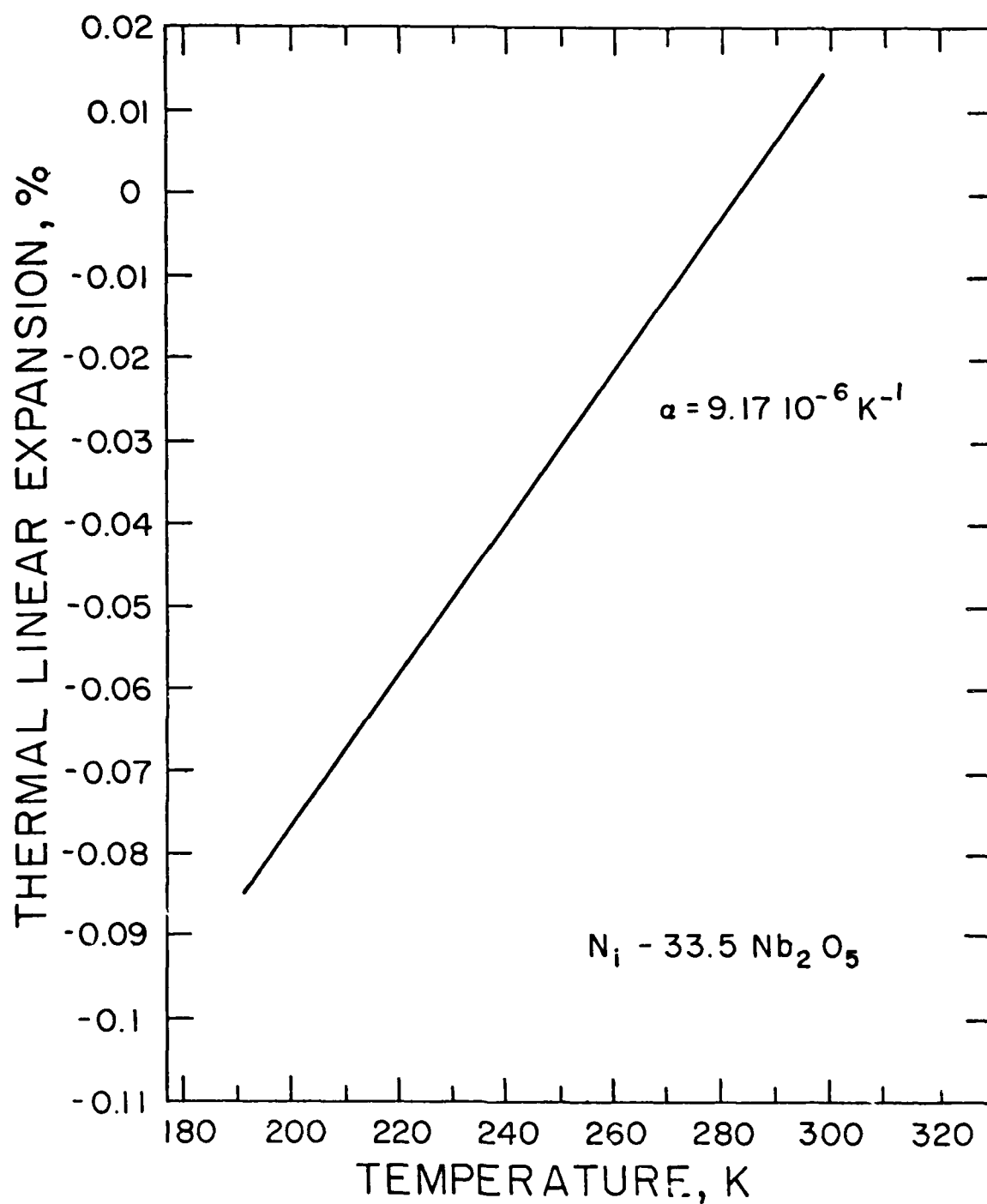


FIGURE 24. THERMAL LINEAR EXPANSION OF $\text{Ni}-33.5 \text{ Nb}_2\text{O}_5$
vs TEMPERATURE

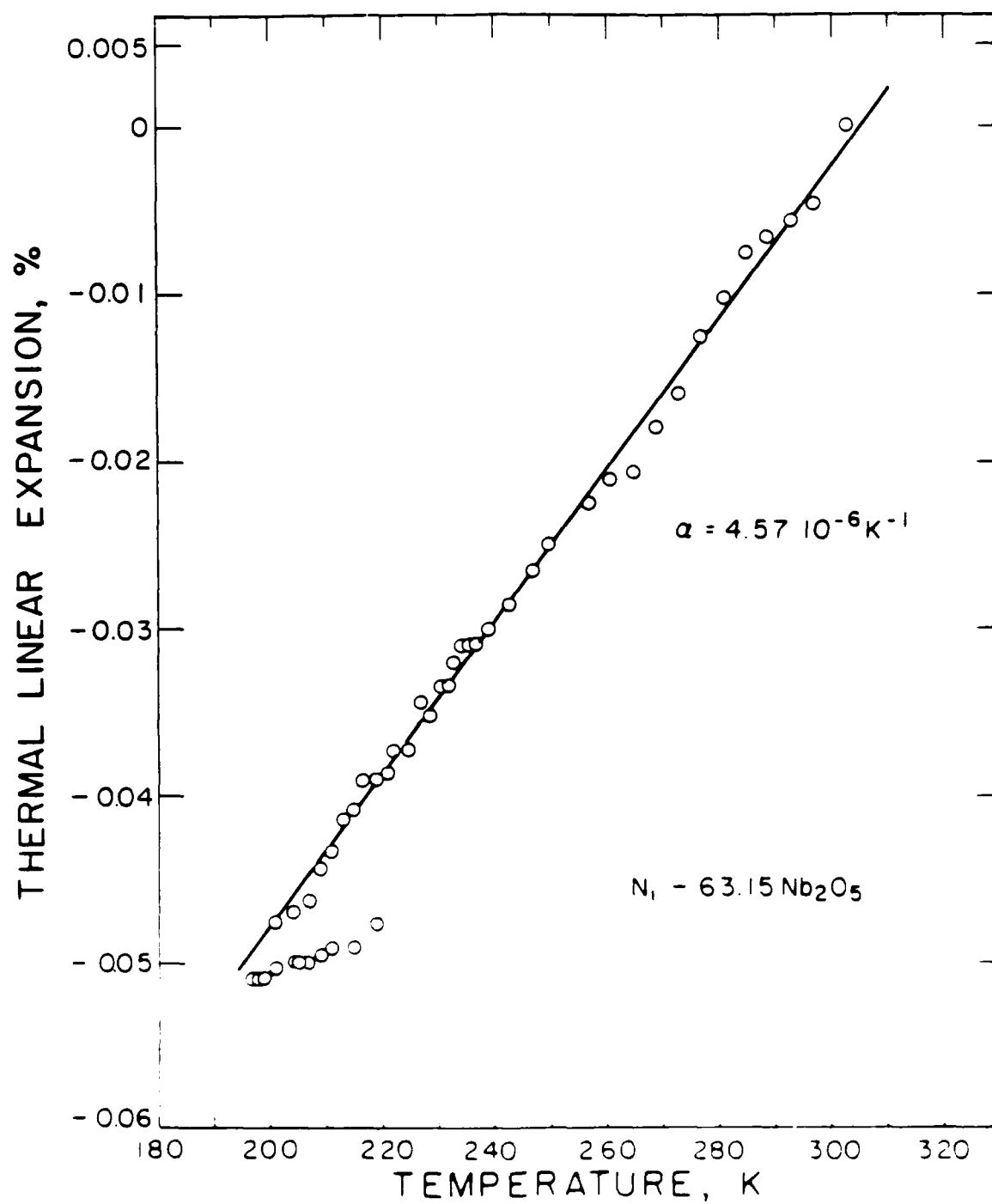


FIGURE 25. THERMAL LINEAR EXPANSION OF Nb-63.15 Nb₂O₅ VS. TEMPERATURE

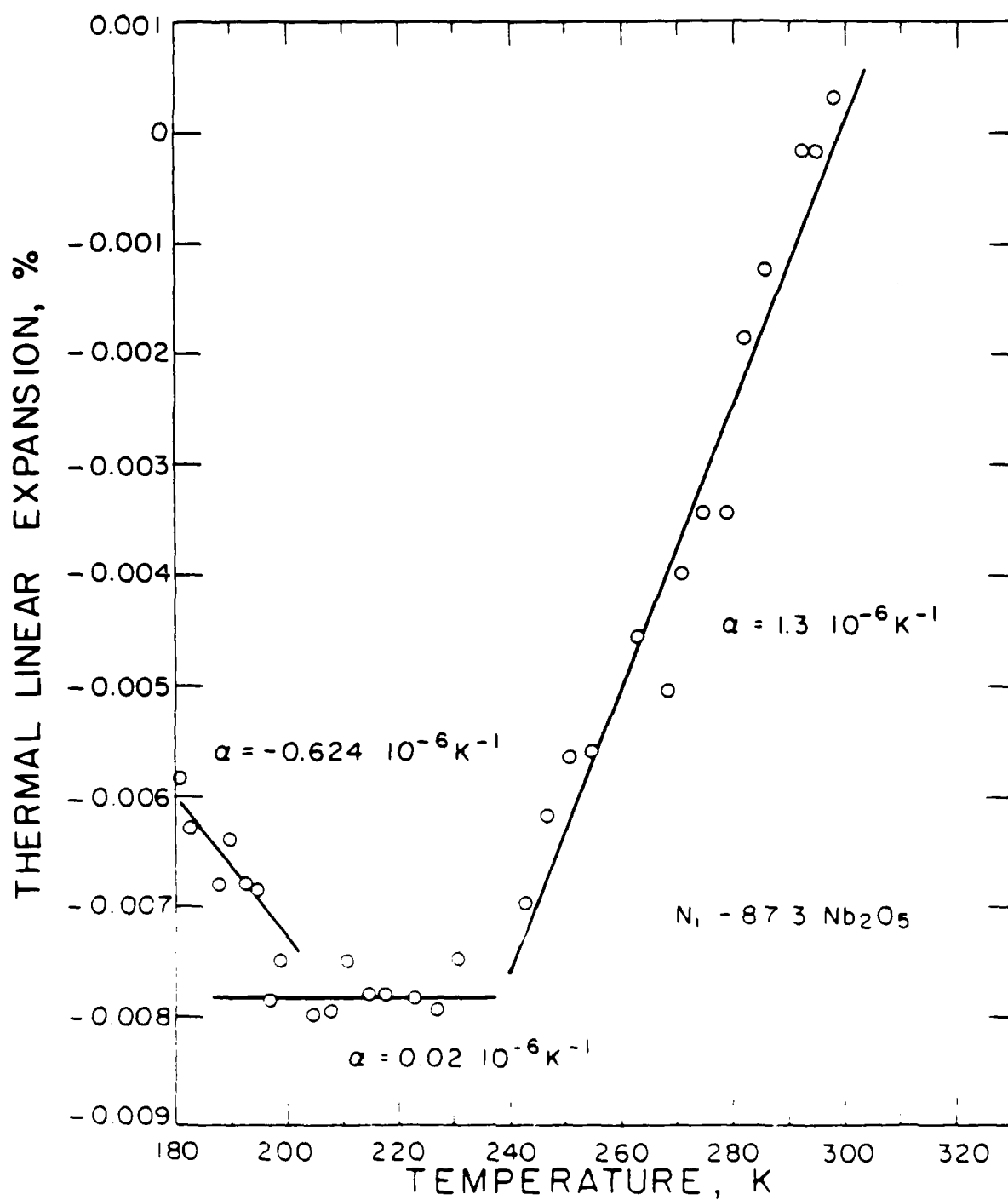


FIGURE 26. FIRST MEASUREMENT OF THE THERMAL LINEAR EXPANSION OF $Ni-87.3 Nb_2O_5$ vs TEMPERATURE

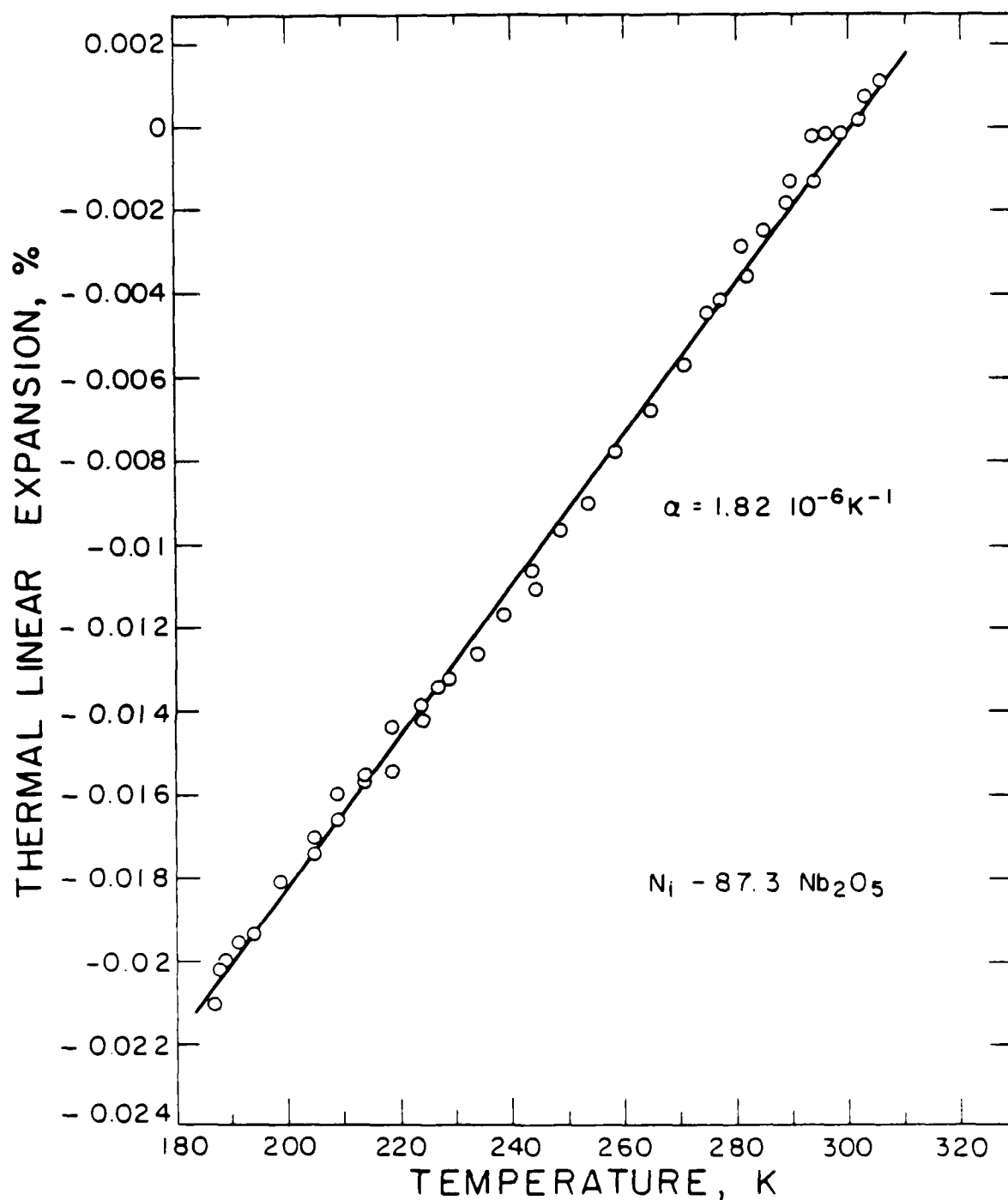


FIGURE 27. SECOND MEASUREMENT OF THE THERMAL LINEAR EXPANSION OF $\text{Ni}-87.3 \text{ Nb}_2\text{O}_5$ vs TEMPERATURE

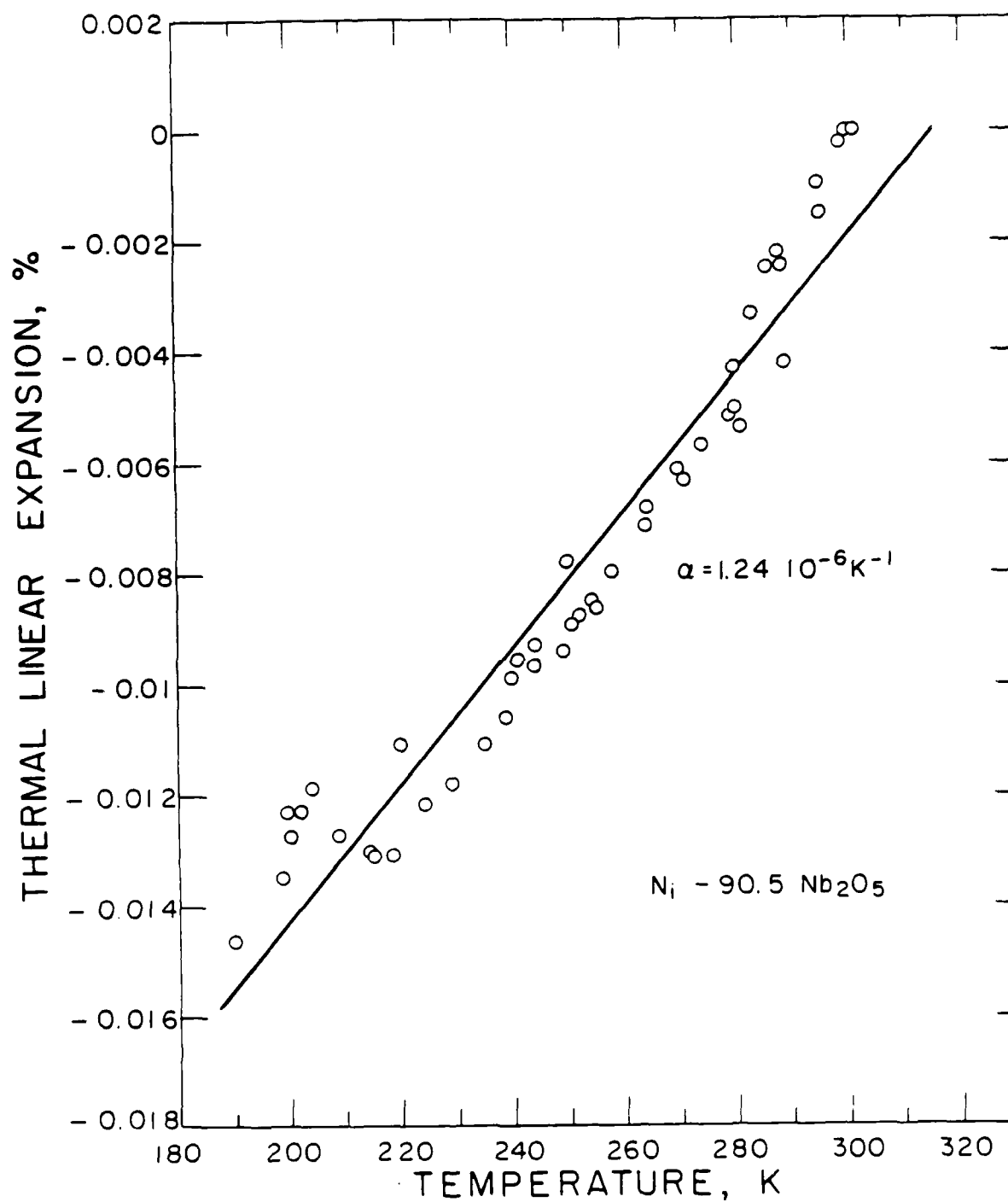


FIGURE 28. THERMAL LINEAR EXPANSION OF Ni - 90.5 Nb₂O₅
vs TEMPERATURE

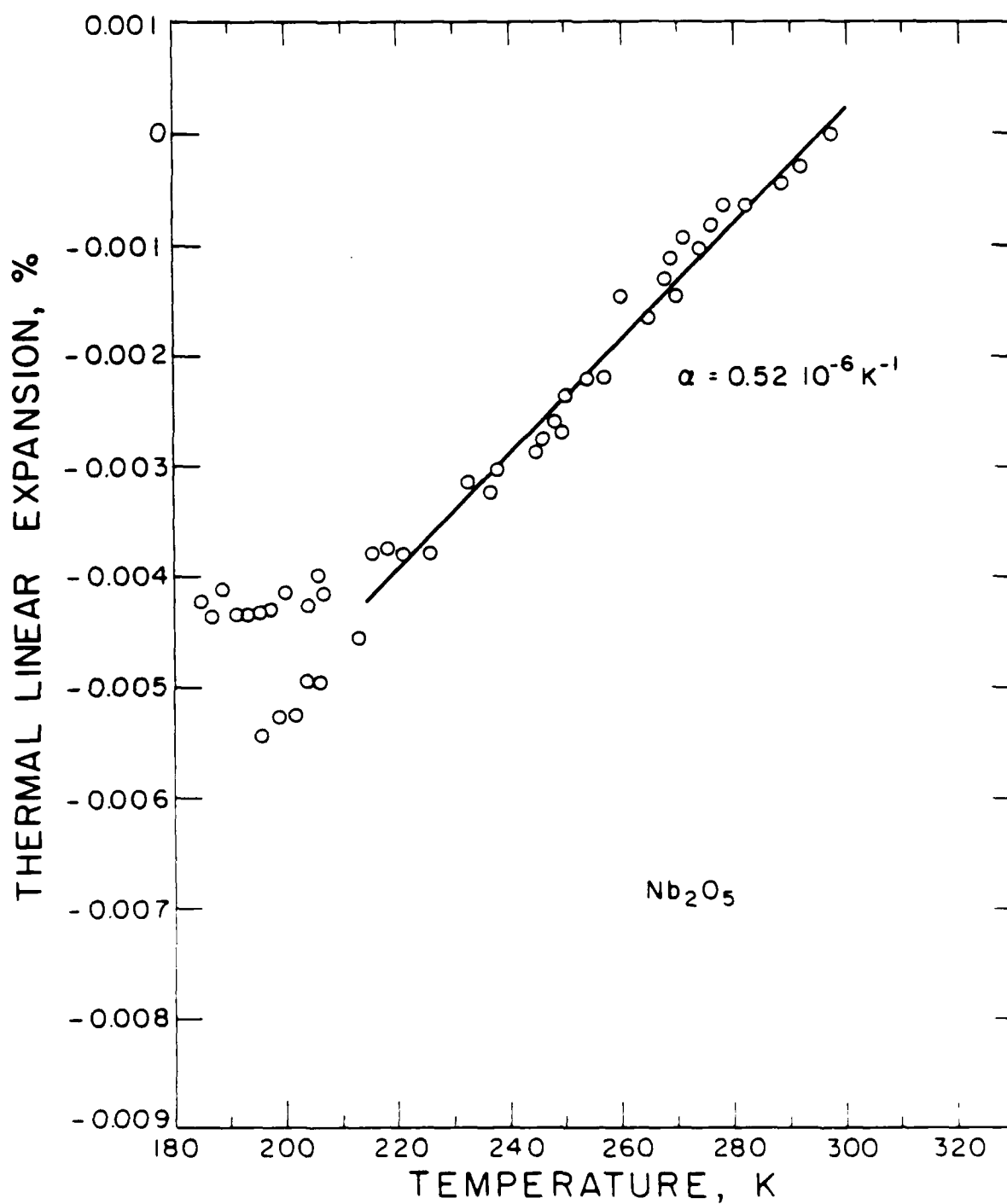


FIGURE 29. THERMAL LINEAR EXPANSION OF Nb_2O_5
vs TEMPERATURE

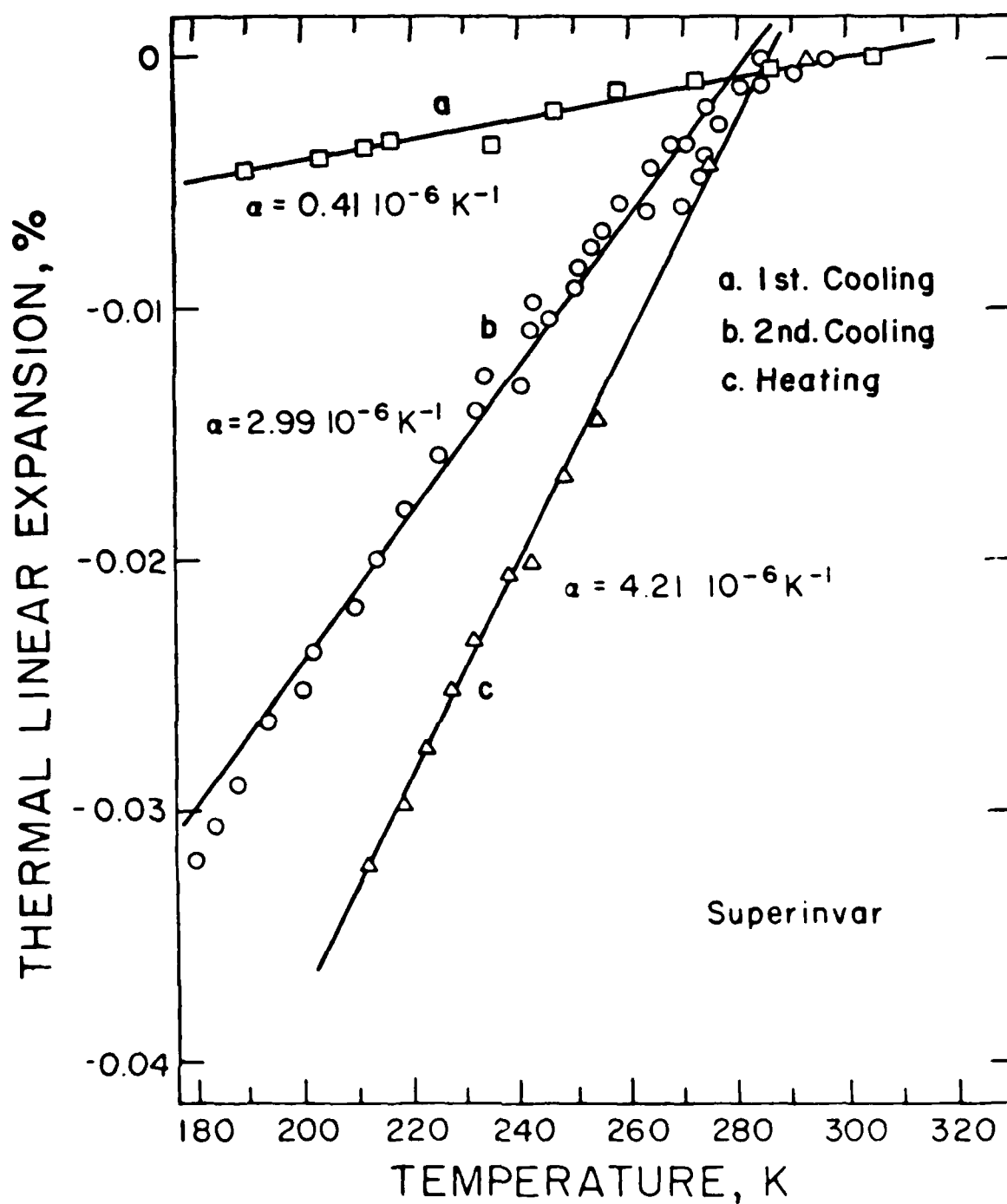


FIGURE 30. THERMAL LINEAR EXPANSION OF SUPERINVAR VS. TEMPERATURE

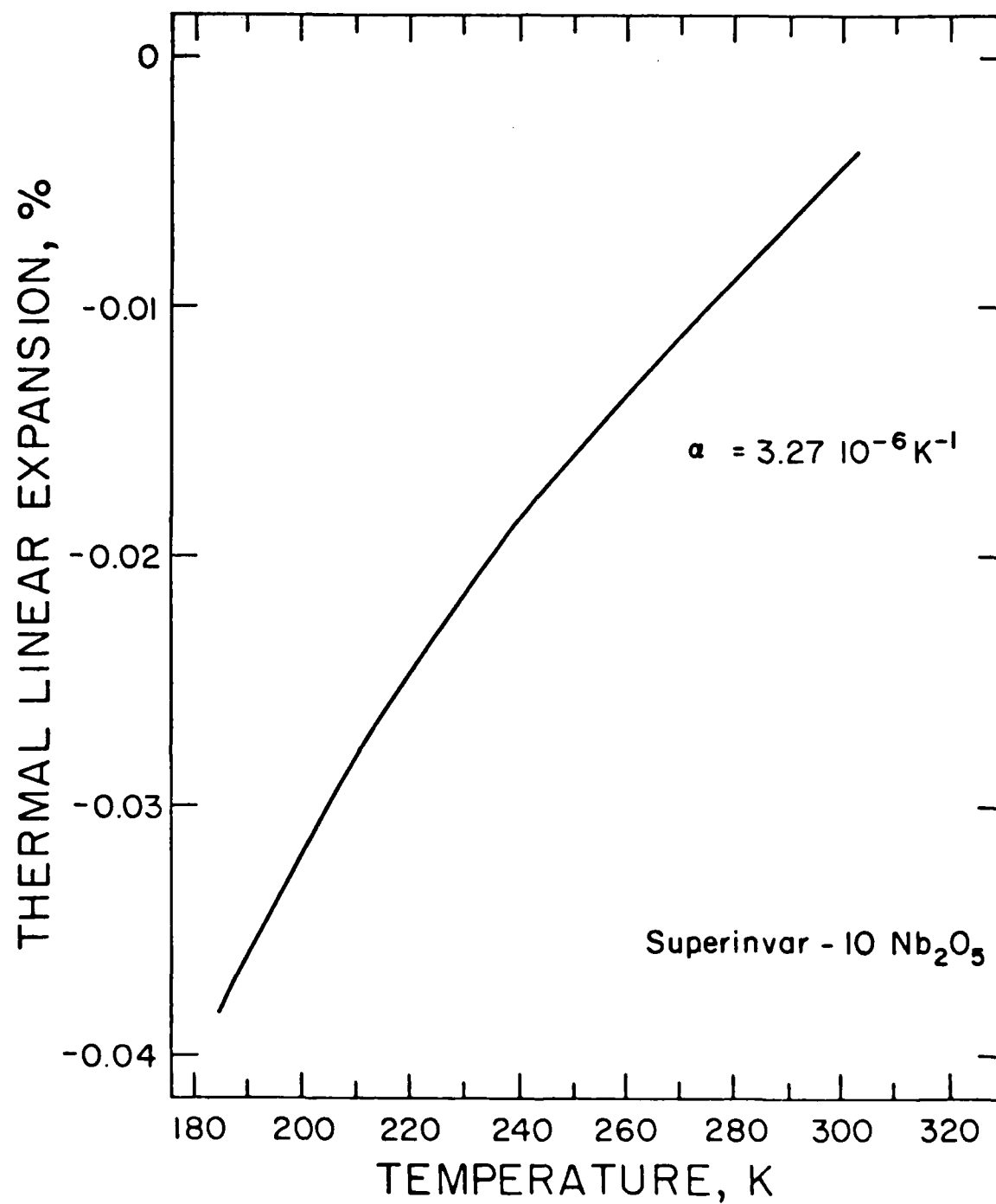


FIGURE 31. THERMAL LINEAR EXPANSION OF SUPERINVAR-
10Nb₂O₅ vs TEMPERATURE

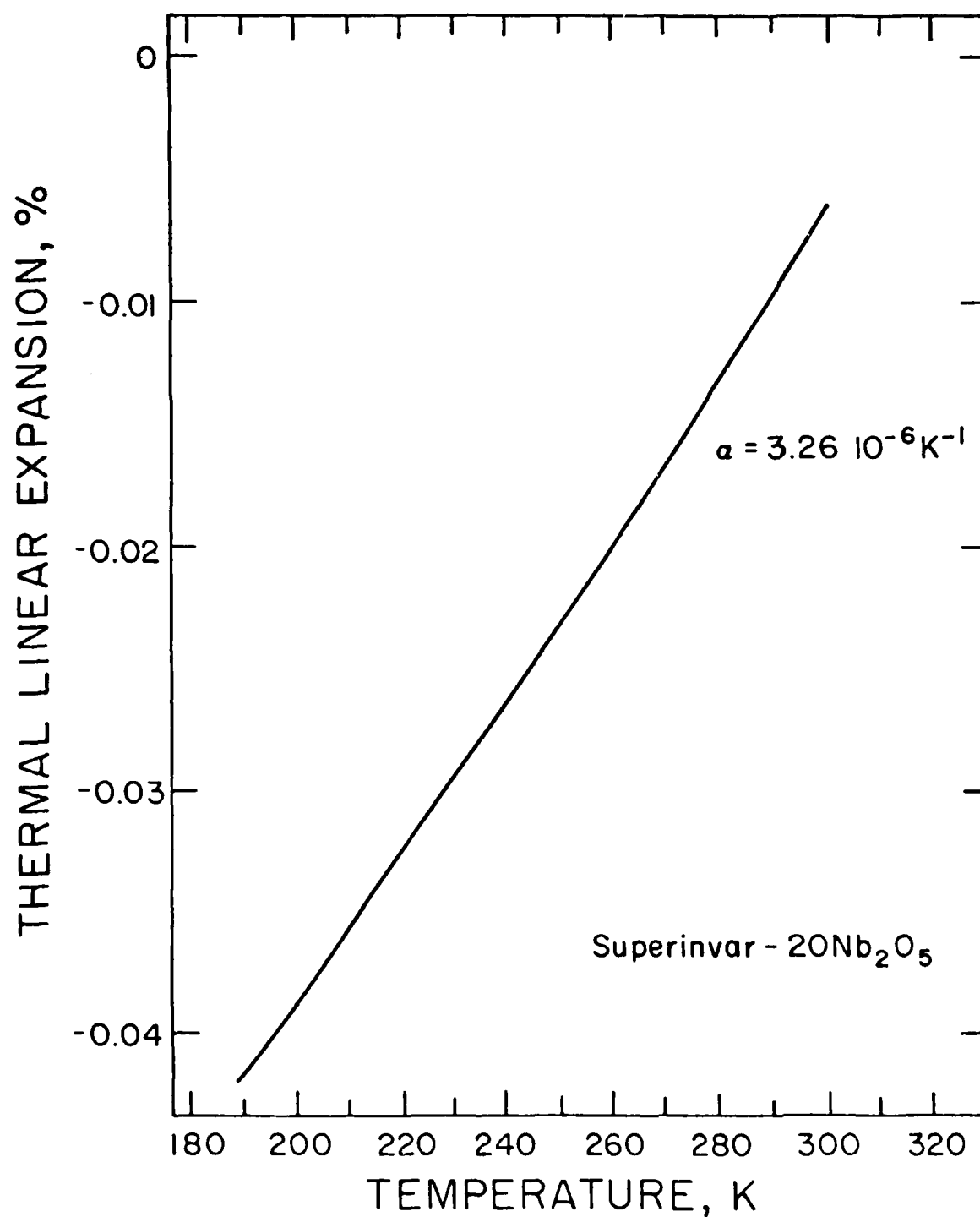


FIGURE 32. THERMAL LINEAR EXPANSION OF SUPERINVAR-20Nb₂O₅ vs TEMPERATURE

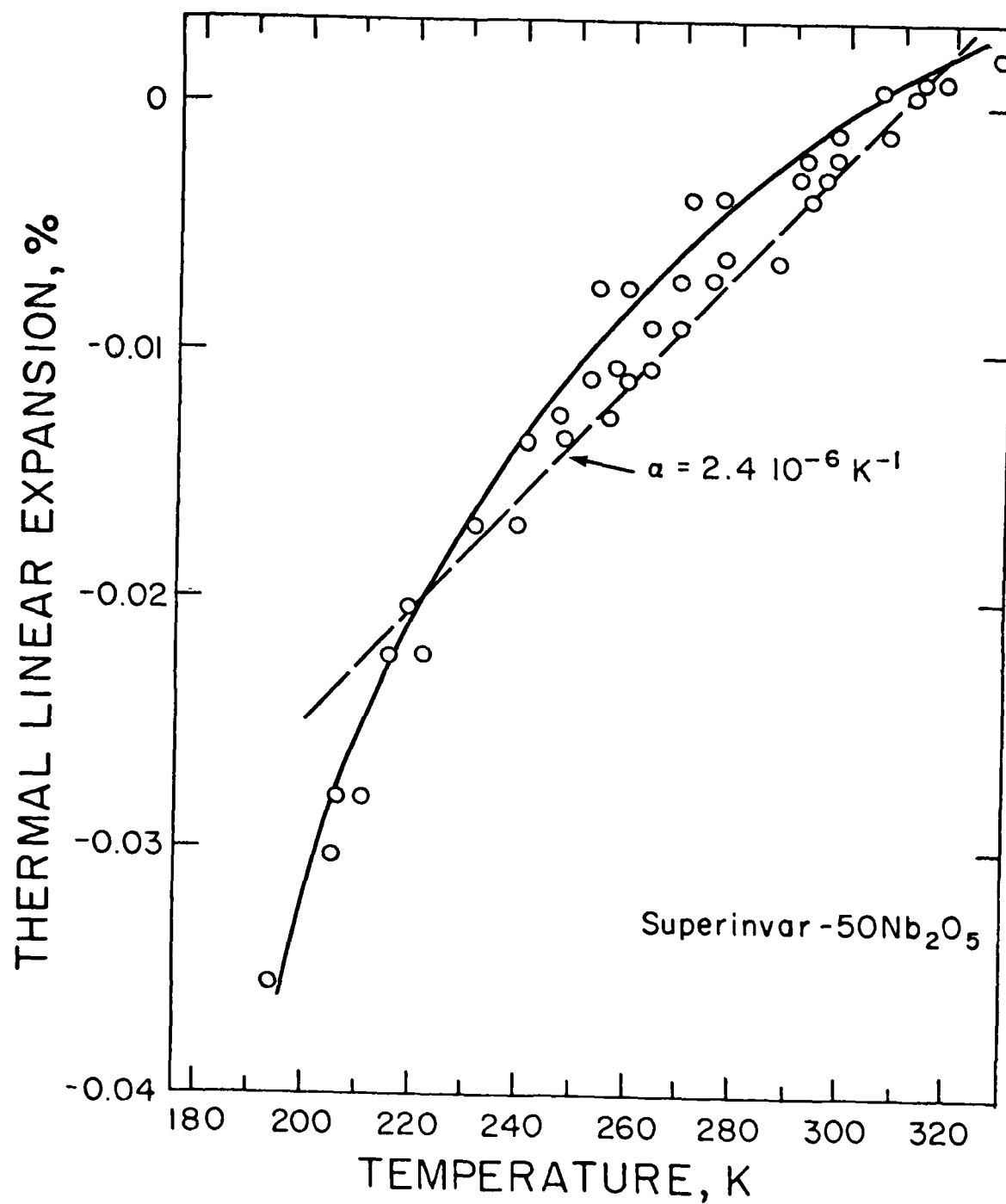


FIGURE 33. THERMAL LINEAR EXPANSION OF SUPERINVAR-50Nb₂O₅ vs TEMPERATURE

cooling [Figure 33b] from 300-180K and $4.21 \times 10^{-6} \text{K}^{-1}$ on heating [Figure 33c] in the same temperature range.

Another explanation for the behavior of the superinvar sample is the assumption of "discrete" antiferromagnetism [50], i.e., there should be a kind of antiferromagnetic interaction between atoms in the alloy. This explanation, however, is difficult to prove and should be further investigated.

It should be noted that Figures 25-30 and 33 were measured with a laser interferometer and expansion was recorded on both cooling and heating in the temperature range 180-300K. Figures 23-24 and 31-32, however were measured with a quartz dilatometer and expansion was recorded only during heating from 180-300K (after initial cooling) and the results are accurate to only within $\pm 5-10\%$.

Since most of the data seemed to fall on a straight line, a linear regression program was used to find the value of the coefficient of thermal expansion of the composites. Figures 34 and 35 summarize these results. The coefficient of thermal expansion of nickel in Figure 34 was obtained from Reference 7. The discussion of the results of Figures 34 and 35 will be taken up in the next chapter.

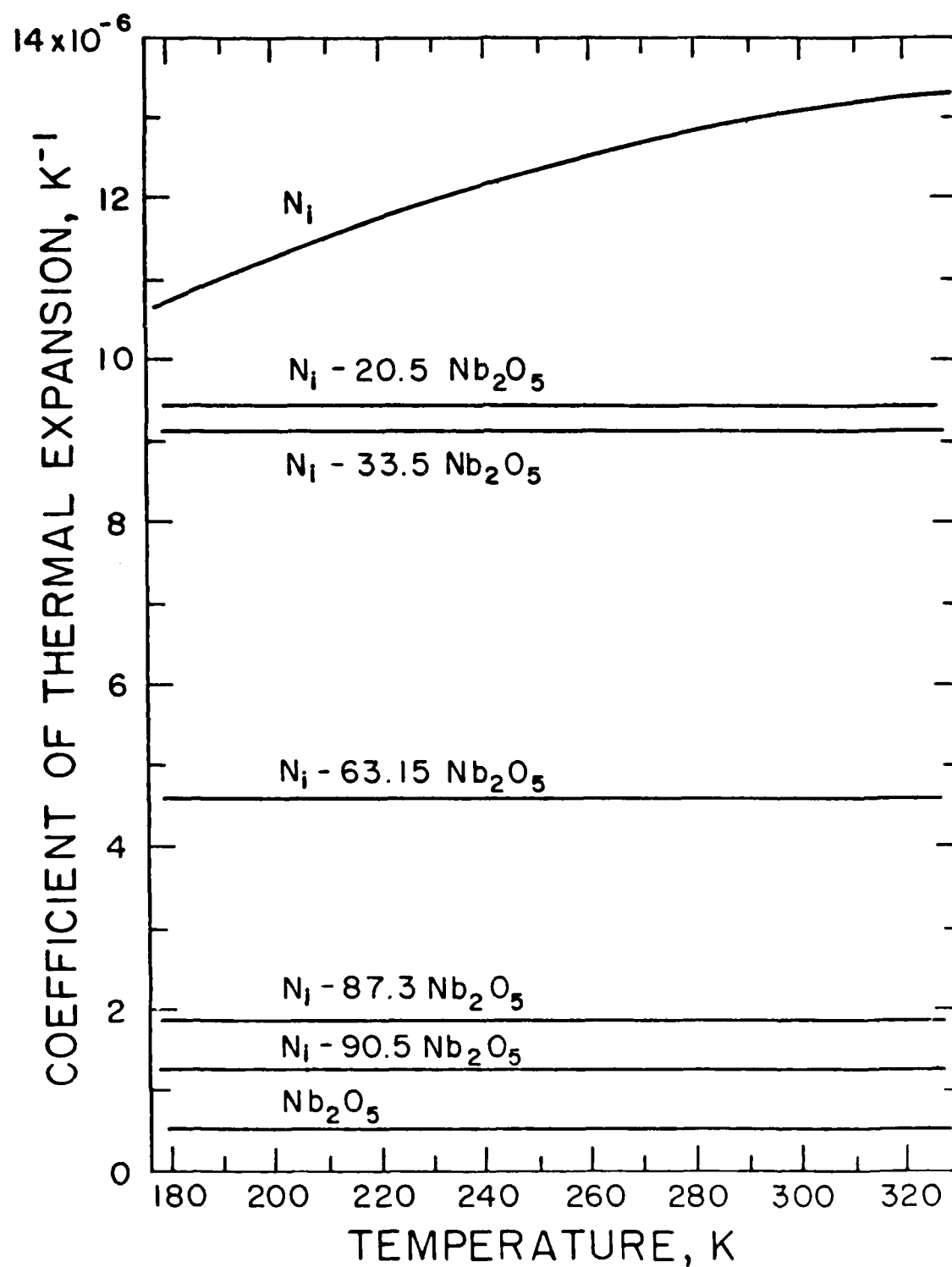
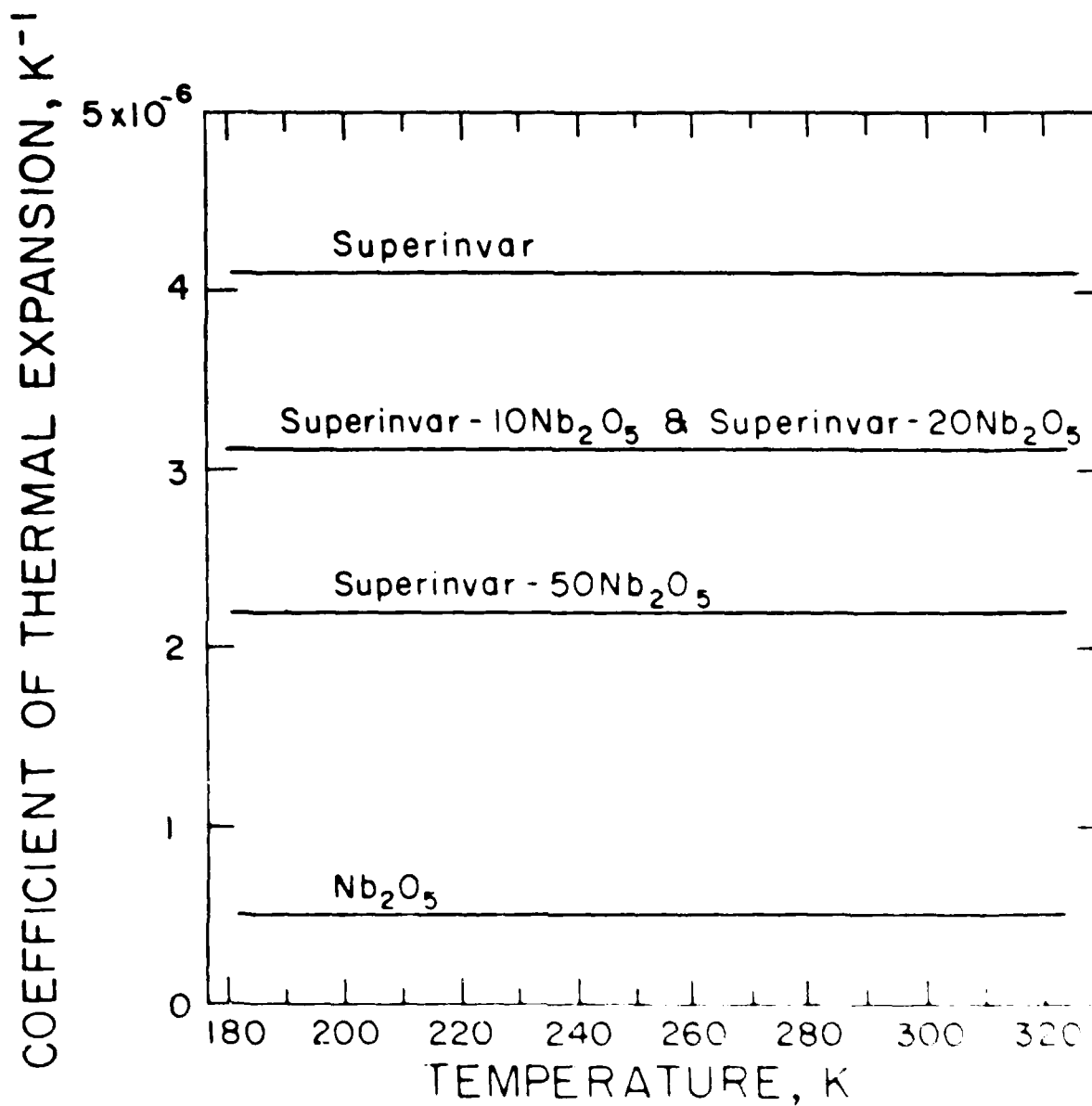


FIGURE 34. CTE OF $\text{Ni-Nb}_2\text{O}_5$ COMPOSITES vs TEMPERATURE



DISCUSSION

ULTRA-LOW EXPANSION METAL MATRIX COMPOSITES(U)
MASSACHUSETTS INST OF TECH CAMBRIDGE LAB FOR NFO AND
PRODUCTIVITY M P SUN ET AL APR 81 LMP/NTLS-81-84
NDA903-70-C-0417 F/G 11/4

U

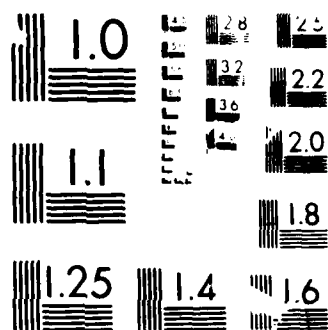
UNCLASSIFIED

MDA903-70-C-0417

F/G 11/4

1

[illegible]



1951-1952 RESOLUTION TEST CHART

A variety of microstructural factors can give rise to spurious effects when a specimen is subjected to CTE measurement. These microstructural factors include porosity, grain size, and anisotropy. Although dispersed pores in principle should not contribute to the thermal expansion of a solid, connected pores can open up when the specimen is cooled, especially in the case of samples with large cross-sectional area, or materials that do not have high thermal conductivity such as ceramics. This results in increase in length of the specimen when it is cooled and therefore an apparent negative CTE.

Similarly, anisotropic polycrystalline samples are also prone to cracking, even the absence of porosity, when they are heated or cooled. Because of different thermal expansion coefficients in different directions, when a polycrystalline aggregate is heated (or cooled) internal stresses will be developed in the grains due to constraints imposed by neighboring grains. These stresses, if high enough, can nucleate and propagate cracks within the grains and at the grain boundaries. While this may be unimportant in ductile metals, it is extremely important in ceramics and in metals that have cleavage planes. When these cracks nucleate and grow, they contribute to apparent CTE.

Because Nb_2O_5 has monoclinic and orthorhombic crystal structures, it is quite likely that the previously reported negative CTE in the sintered and even hot pressed specimens was due to microcracking at the grain boundaries and pores, or inside the grains. Unfortunately, it is not possible at present to isolate the effects of anisotropy and

porosity because the thermal expansion coefficients of Nb_2O_5 single crystals are not known for the range 200-300K. Further in majority of the cases studied in the past the microstructure of the specimens was not carefully characterized.

To investigate if there are any pores, the hot pressed Nb_2O_5 was observed in the SEM at 500 x. No pores were found. The thermal expansion coefficient of the Nb_2O_5 was also measured in the direction of loading (during hot pressing) and was found to be $0.5 \times 10^{-6} \text{K}^{-1}$. Since hot pressing should give samples that have planar isotropy this result indicates that the hot pressed Nb_2O_5 was essentially isotropic, even though single crystal Nb_2O_5 is anisotropic. This means that the grains were randomly oriented in the hot pressed specimens.

In summary, the hot pressed Nb_2O_5 used in this study gives the true thermal expansion of a polycrystalline Nb_2O_5 . Its value in the temperature range 200-300K is $0.52 \times 10^{-6} \text{K}^{-1}$. The negative values reported in the past were apparent values and do not reflect true CTE of Nb_2O_5 .

Nickel

Because of the purity of electroless Ni is 99.5 percent, the CTE value assumed for Ni is that of pure nickel, reported in Ref. 7. It is assumed that 0.25 percent boron in the electroless Ni does not affect the thermal expansion coefficient. Although this assumption seems justified as far as the room temperature CTE is concerned, the temperature variation of CTE for electroless Ni appears to be less

sensitive than that of pure Ni. This will be discussed in greater detail in a section on the composites.

Superinvar

From Figure 30 it is apparant that the CTE of superinvar is independent of temperature, but depends on the thermal history. Further the CTE value observed in this work is $4 \times 10^{-6} \text{K}^{-1}$, whereas the value reported in the literature [47-58] was $0.1-1 \times 10^{-6} \text{K}^{-1}$.

There are many reasons for this discrepancy. It has been reported that the thermal expansion coefficient of superinvar depends sensitively on the composition, especially the Co content. For example, changing Cobalt from 6.0 percent to 4.2 percent can change the thermal expansion coefficient by an order of magnitude. Similarly, small amounts of carbon can change the CTE of superinvar substantially. Generally an increase in carbon content results in an increase in CTE. Although Mn and Si also affect the CTE of superinvar, their effect is marginal.

The higher CTE values observed in this work are clearly due to higher Co and C in the specimen (Table 7).

The dependence of CTE of superinvar can be ascribed to $\gamma \rightarrow \alpha$ transformation during cooling and antiferromagnetic effects [47,49].

Ni-Nb₂O₅ Composites

Figures 23-25, 27 and 28 show that the coefficients of thermal expansion of Ni-Nb₂O₅ composites are almost independent of temperature. Only one test (on Ni-87.3 Nb₂O₄) showed that the composite had zero CTE in the temperature range 200-400K and negative CTE below 200K. Unfortunately, this behavior was not duplicated when measured again. Hence this result will be ignored in the rest of the discussion.

In Figure 36 the thermal expansion coefficients of both Ni-Nb₂O₅ and superinvar-Nb₂O₅ composites are shown along with the theoretical predictions using Equation (34) and the mixture rule. Because the thermal expansion coefficient of nickel increases slightly with temperature, two sets of curves are drawn for two temperatures, 200 and 300K.

It is interesting to note that all Ni-Nb₂O₅ composites, except the Ni-33.5 Nb₂O₅, fall on the theoretical curve (Equation 34) for 200K-300K. Hence, provided that the thermal expansion coefficient of electroless Ni is $11.3 \times 10^{-6} \text{K}^{-1}$, Equation (34) predicts the thermal expansion coefficients of Ni-Nb₂O₅ remarkably well. In fact, if the thermal expansion of coefficient of Ni is assumed to be between $11.3 \times 10^{-6} \text{K}^{-1}$ and $12.5 \times 10^{-6} \text{K}^{-1}$, which is a reasonable assumption, the argument between experiment and theory will be extremely good for the entire temperature range 200-300K.

Another interesting fact to be noted from Figure 36 is that the

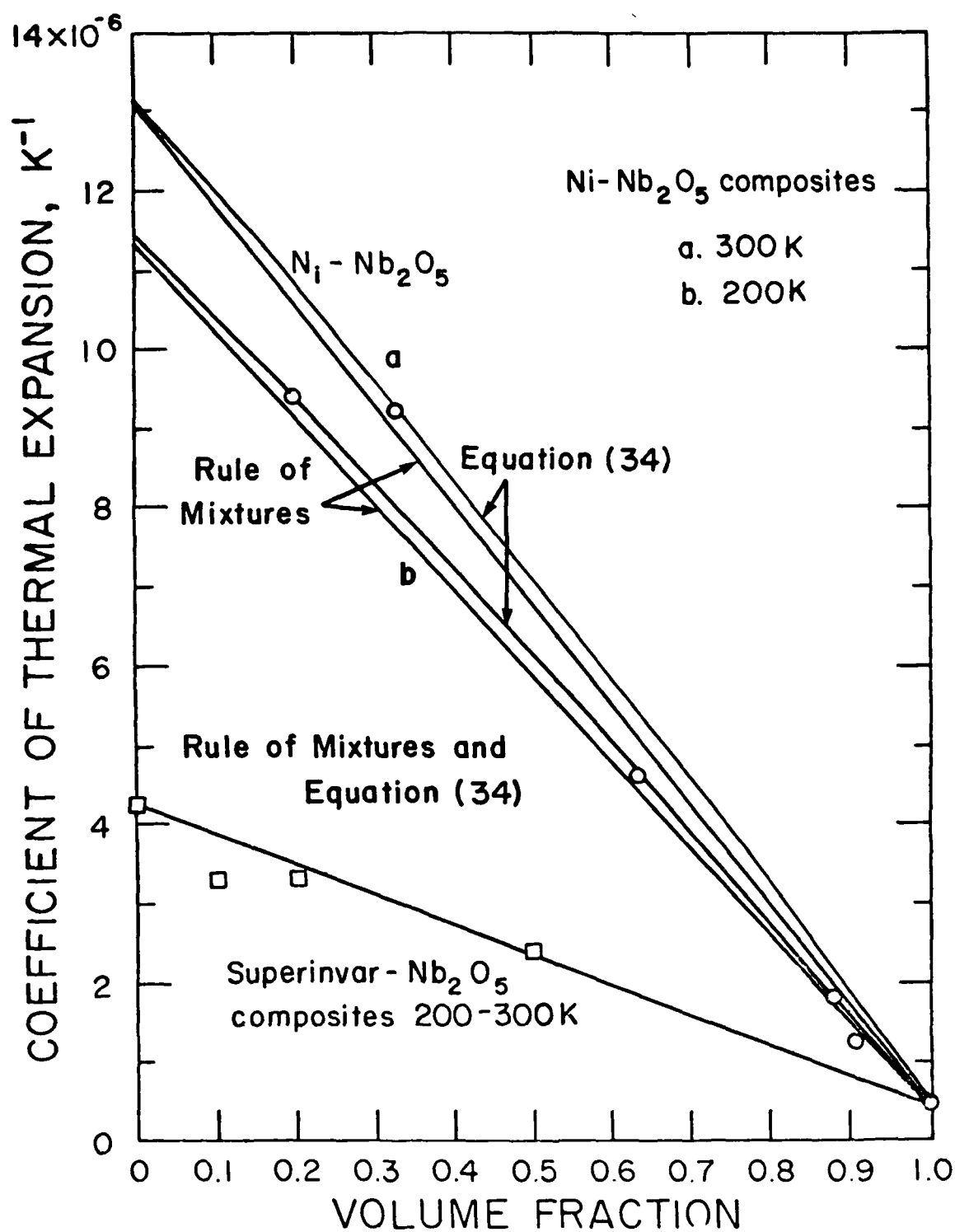


FIGURE 36. CTE OF $\text{Ni-Nb}_2\text{O}_5$ AND $\text{SUPERINVAR-Nb}_2\text{O}_5$ COMPOSITES vs VOLUME FRACTION OF Nb_2O_5

mixture rule predicts the thermal expansion coefficients of the $\text{Ni-Nb}_2\text{O}_5$ equally well, because the moduli and Poisson's ratio of Nb_2O_5 and Ni are not very different. However, when the moduli are substantially different, the mixture rule will not be able to predict the CTE as explained in the chapter on theoretical analysis.

From Figure 17c it can be seen that the Nb_2O_5 is the matrix phase and nickel the dispersed phase. Hence Equation (34) should be modified such that phase 2 refers to nickel and phase 1 to Nb_2O_5 . Accordingly, the thermal expansion of $\text{Ni-Nb}_2\text{O}_5$ composites are recalculated using nickel as the dispersed phase and Nb_2O_5 as the matrix phase. Table 10 gives CTE values calculated for various volume fractions of Nb_2O_5 using both Equation (34) which assumes Ni matrix and the modified version of Equation (34) which assumes Nb_2O_5 as matrix (for the same volume fraction of Nb_2O_5). It is interesting to note that the difference between these two values is at the most 1.3%. Hence it is really immaterial whether Ni or Nb_2O_5 is the matrix or dispersed phase as far as the thermal expansion is concerned. When the composite follows mixture rule (as in superinvar- Nb_2O_5) this difference is exactly zero.

Superinvar- Nb_2O_5 Composites

The superinvar- Nb_2O_5 -composites also follow the theoretical predictions. In this case the agreement is good for the entire temp-

TABLE 10. CTE PREDICTIONS OF Ni-Nb₂O₅
COMPOSITES AT 300K

VOLUME FRACTION OF Nb ₂ O ₅	Ni MATRIX	Nb ₂ O ₅ MATRIX	DIFFERENCE PERCENT
20.50	10.736	10.696	0.37
33.50	9.183	9.127	0.61
63.15	5.477	5.415	1.13
87.30	2.275	2.244	1.36
90.50	1.837	1.813	1.31

perature range 200-300K. It is also interesting to note that Equation (34) coincides with mixture rule in this case because the elastic modulus and Poisson's ratio are identically the same for superinvar and Nb_2O_5 .

Microstructural Effects

Although the agreement between the theoretically calculated and the experimentally measured values are remarkably good, the effect of some microstructure parameters on the thermal expansion coefficient of composites should be emphasized. Of particular importance are the effects of porosity and interfacial decohesion between the metal and ceramic phases.

First, it appears, again from the extremely good agreement between theory and experiment, that the porosity in the Nb_2O_5 particles did not seem to affect the CTE of the composites. As remarked earlier, small distributed pores should not affect the CTE of the Nb_2O_5 particles in the matrix.

Second, if debonding were a problem, the composite would have shown a thermal expansion coefficient of Nb_2O_5 while cooling when Nb_2O_5 is the matrix (i.e., for large volume fraction of Nb_2O_5) and that of the composite when heated. On the otherhand, when Ni is the matrix phase the coefficient of thermal expansion of the composite while cooling will be that of Ni and, again, the measured CTE during heating would be that of the composite. Same argument holds good for superinvar- Nb_2O_5 composites too. Because none of these effects was observed during the thermal ex-

pansion coefficient measurement, it can be assumed that the interfacial bonding was good, if not perfect.

Nevertheless, there is an indirect evidence to show that Ni did not bond well to the Nb_2O_5 particles. When the Ni coated powder was hot pressed, after electroless plating, the nickel segregated to the empty space between Nb_2O_5 particles. This indicates that Ni does not wet Nb_2O_5 readily and hence can be assumed that the bonding was not perfect.

Third, as pointed out earlier, the matrix material can yield and the dispersed oxide phase can fracture, which depend on the temperature difference, the volume fraction of the phases, elastic moduli, etc. It has already been shown that for superinvar and Ni matrices, i.e., when Nb_2O_5 is dispersed, yielding in the metallic phase and fracture of the ceramic phase are impossible. Similarly, when Nb_2O_5 happens to be the matrix and Ni and superinvar dispersed phases, it would still be impossible to induce yielding and fracture. When yielding and fracture occur it is expected that the thermal expansion coefficient will not agree with the theoretical curves.

Suggestions for Further Research

A few suggestions for producing ultra-low CTE composites with good mechanical properties can be given on the basis of this study. First, to produce an ultra-low CTE material it is necessary to start with a metal that has a low thermal expansion coefficient and a ceramic phase that has the largest possible negative CTE. Unfortunately,

literature search has shown that not many ceramics have large negative CTE. In fact most negative CTE values reported on ceramics in the literature are suspect because of the spurious effects due to micro-cracking. The most reliable CTE values are those obtained by low-temperature X-ray diffraction. Further literature search has shown that La_2O_3 has a negative thermal expansion coefficient of about $-4.0 \times 10^{-6} \text{K}^{-1}$ at room temperature. It appears therefore that La_2O_3 is the most promising candidate.

Second, it is necessary to improve the bonding between the metal and ceramic phase. This can be done by coating metal which forms an oxide that has lowest free energy of formation than the ceramic phase. It has been suggested [58] that Zr will be ideal for this purpose, for it forms a stable oxide (ZrO_2) when reacted with oxide ceramic phase and, therefore, bonding is expected to improve.

Third, as shown in the chapter on theoretical analysis the volume fraction of the metal and ceramic phase should be tightly controlled to get ultra-low CTE. This can be done by closely monitoring the volume fraction of the constituent phases during processing.

Fourth, the porosity in the ceramic phase should be eliminated so that even when it is under tension, the ceramic phase would be able to resist fracture.

Fifth, there is some scope for improvement in the theoretical analysis also. It has been assumed in the derivation of Equation (34) that the metal and ceramic phases are isotropic. In general small

ceramic particles ($\sim 50\mu\text{m}$) may not have many grains. As a result, the elastic properties of the ceramic will be anisotropic and therefore in the thermoelastic analysis it may be necessary to take this anisotropy into consideration.

Finally, Equation (34) was derived assuming that the thermal expansion coefficient of the composite is the same as that of the composite sphere which has the same value fraction as the composite. It is known, of course, that when spheres are packed together the resulting structure will have a porosity of about 25%. Further analysis is required to relate the CTE of two-layer sphere to two-phase composite.

CHAPTER VII

CONCLUSIONS

The following conclusions can be drawn on the basis of the thermoelastic analysis and experimental work on particle-dispersed metal-matrix composites.

(a) The theories of thermal expansion of particle-dispersed materials, published so far do not provide adequate guidance in the design of composites that are subjected to large temperature fluctuations (e.g. HALO/HELO substrates).

(b) The thermoelastic analysis presented in this thesis, in addition to predicting the CTE of particle-dispersed composites, gives exact expressions for displacements, strains and stresses in the composite. A knowledge of the stresses will enable one to design the composite against fracture in the ceramic phase and yielding in the metallic phase.

(c) To produce ultra-low or zero CTE metal-matrix composites it is necessary to use a metal that has the lowest positive thermal expansion coefficient, and a ceramic phase that has the largest negative thermal expansion coefficient.

(d) In addition, the amount of the metal and ceramic phases should be controlled to within a few percent. Failure to do so will produce either a large positive or negative CTE composites.

(e) The thermal expansion coefficient of hot pressed Nb_2O_5 in the temperature range 200-300K is positive ($+0.52 \times 10^{-6} \text{K}^{-1}$), contrary to the values reported in the literature.

(f) The agreement between the theoretically predicted thermal expansion coefficients and the experimentally measured values for $\text{Ni-Nb}_2\text{O}_5$ and superinvar- Nb_2O_5 is excellent.

(g) The coefficients of thermal expansion of the composites produced are an order of magnitude smaller than common metals and are comparable to invar and superinvar. Thermal expansion coefficients smaller than $0.52 \times 10^{-6} \text{K}^{-1}$ are not possible to obtain because the CTE of Nb_2O_5 is positive: ultra-low CTE can be obtained by choosing superinvar that has low carbon content and a ceramic phase that has the largest CTE (e.g. La_2O_3)

(h) Improved bonding between metal matrix, high negative CTE ceramic phase and high strength metal should be used to produce ZCTE composites.

REFERENCES

1. Wolff, E.G., "Dimensional Stability of Structural Composites for Spacecraft Applications," Metal Progress, Vol. 115, No. 6, June 1979, pp. 54-63.
2. McNamara, R.C., et al., "Materials for Large Space Optics, Phase I," Final Technical Report No. CASD-AFS-77-008, General Dynamics, Convair Division, January 1978.
3. Reiss, H., et al., Private Communication to Major Harry V. Winsor.
4. Kirby, R.K., "Thermal Expansion of Ceramics," National Bureau of Standards Special Publication 303, May 1969, pp. 41-61.
5. Yates, B., "Thermal Expansion," Plenum Press, New York-London, 1972, pp. 52-70.
6. Austin, J.B., "Thermal Expansion of Nonmetallic Crystals," Journal of the American Ceramic Society, Vol. 35, No. 10, 1952, pp. 242-253.
7. Touloukian, Y.S., et al., Ed., Thermophysical Properties of Matter, the TPRC Data Series, Thermal Expansion, Vols. 12, and 13, 1977.
8. Manning, W.R., et al., "Thermal Expansion of Nb_2O_5 ," Journal of the American Ceramic Society, Vol. 55, No. 7, 1972, pp. 342-347.
9. Dwivedi, G.L. and Subbarao, E.E., "Thermal Expansion of Monoclinic (Alpha) Nb_2O_5 ," Journal of the American Ceramic Society, Vol. 56, No. 8, 1973, pp. 443-444.
10. Durbin, E.A. and Harman, C.G., "An Appraisal of the Sintering Behavior and Thermal Expansion of Some Columbates," Report No. BMI-791, Batelle Memorial Institute, Columbus, Ohio, December 15, 1952.
11. Durbin, E.A., Wagner, H.E. and Harman, C.G., "Properties of Some Columbium Oxide-Basis Ceramics To United States Atomic Energy Commission," Report No. BMI-792, Batelle Memorial Institute, Columbus, Ohio, December 15, 1952.
12. Douglass, D.L., "The Thermal Expansion of Niobium Pentoxide and Its Effect on the Spalling of Niobium Oxidation Films," Journal of The Less-Common Metals, Vol. 5, 1963, pp. 151-157.

13. Bhide, V.G., Hegde, M.S. and Deshmukh, K., "Ferroelectric Properties of Lead Titanate," Journal of the American Ceramic Society, Vol. 51, No. 10, 1968, pp. 565-568.
14. Surendra, N.P. and Singh, S.H., "Thermal Expansion of La_2O_3 from 100 to 300K by an X-Ray Method," Ceramic Bulletin, Vol. 58, No. 2, 1979, pp. 184-186.
15. Holcombe, C.E., Jr. and Smith, D.D., "Characterization of the Thermally Contracting Tungstates $\text{Ta}_{22}\text{W}_4\text{O}_{67}$, Ta_2W_8 , $\text{Ta}_{16}\text{W}_{18}\text{O}_{94}$," Journal of the American Ceramic Society, Vol. 61, No 3-4, 1978, pp. 163-169.
16. Christosendo, V.G. and Novgorodsteva, V.I., "Microcrystalline Materials with Positive, Negative and Zero Coefficients of Thermal Expansion," The Structure of Glass, Vol. III, Catalysed Crystallization of Glass, Ed. Porai-Koshits, E.A., Trans. Uvarov, E.B., Consultants Bureau, New York, 1964, pp. 154-156.
17. Gillery, F.H. and Bush, E.A., "Thermal Contraction of β -Eucryptite ($\text{Li}_2\text{O}-\text{Al}_2\text{O}_3 - 2\text{SiO}_2$) by X-Ray and Dilatometer Methods," Journal of American Ceramic Society, Vol. 42, No. 4, 1959, pp. 175-177.
18. Hummel, F.A., "Thermal Expansion Properties of Some Synthetic Lithia Minerals," Journal of the American Ceramic Society, Vol. 34, No. 8, 1951, pp. 235-239.
19. Smoke, E.J., "Ceramics Compositions Having Negative Linear Thermal Expansion," Journal of the American Ceramic Society, Vol. 34, No. 3, 1951, pp. 87-90.
20. Ostertag, W., Fisher, G.R. and Williams, J.P., "Thermal Expansion of Synthetic β -Spodumene and β -Spodumene-Silica Solid Solutions," Journal of the American Ceramic Society, Vol. 51, No. 11, 1968, pp. 651-654.
21. Kosaka, Y., "Low Expansion Crystalline Glass," U.S. Patent No. 3,537,868, 1970.
22. Beall, G.H. and Martin, F.W., "Low Expansion Zinc Petalite-Beta Quartz, Glass-Ceramic Articles," U.S. Patent No. 3,681,097, 1972.
23. Confer, J.O. and Metaggart, G.D., "Ceramic Article and Method of Making It," U.S. Patent No. 3,715,220, 1973.
24. Muller, G., "Transparent Glass Ceramic with Small Thermal Expansion," U.S. Patent No. 3,977,866, 1976.

25. Baak, N.T.E.A., et al., "Low Expansion Glass Compositions," U.S. Patent No. 3,528,829, 1970.
26. Baak, N.T.E.A., et al., "Low Expansion Copper-Zinc-Aluminosilicate Glass Compositions, Composite Article and Mirror," U.S. Patent No. 3,498,876, 1970.
27. Petticrew, R.W., "New Thermally Crystallizable Glasses and Low Expansion Transparent, Translucent and Opaque Ceramics Made Therefrom," U.S. Patent No. 3,675,718, 1971.
28. Rittler, H.L., "AGCL-Nucleated Glass-Ceramic," U.S. Patent No. 3,854,963, 1974.
29. Rittler, H.L., "Highly Opaque, Ta_2O_5 Containing Glass Ceramic Articles," U.S. Patent No. 3,839,053, 1974.
30. Miller, D.M., "Sintered Cordierite Glass Ceramic," U.S. Patent No. 3,926,648, 1975.
31. Baak, N.I.E.A., " SiO_2 - $AlPO_4$ Glass Batch Compositions," U.S. Patent No. 3,942,991, 1976.
32. Jahn, W., "High-Temperature and Wear-Resistant Antifriction Material Having Low Thermal Expansions," U.S. Patent No. 3,954,479, 1976.
33. Lynch, C.T., Ed., Handbook of Materials Science, Vol. III, Non-Metallic Materials and Applications, CRC Press, 1975, pp. 3-79.
34. Lyman, T., Ed., Metals Handbook, Vol. 1, Properties and Selection of Metals, American Society for Metals, 1961.
35. Lynch, J.F., et al., "Engineering Properties of Ceramics," Technical Report No. AFML-TR-66-52, Battelle Memorial Institute, June 1966.
36. Turner, P.S., "Thermal-Expansion Stresses in Reinforced Plastics," Journal of Research National Bureau of Standards, Vol. 37, 1946, pp. 239-250.
37. Holliday, L. and Robinson, J., "Review: The Thermal Expansion of Composites Based on Polymers," Journal of Materials Science, Vol. 8, 1973, pp. 301-311.
38. Kerner, E.H., "The Elastic and Thermo-Elastic Properties of Composite Media," Proceedings of the Physical Society, Vol. 69, 1956, pp. 808-813.

39. Arthur G. and Coulson, J.A., "Physical Properties of Uranium Dioxide-Stainless Steel Cermets," Journal of Nuclear Materials, Vol. 13, No. 2, 1964, pp. 242-253.
40. Cribb, J.L., "Shrinkage and Thermal Expansion of a Two Phase Material," Nature, Vol. 220, 1968, pp. 576-577.
41. Budiansky, B., "Thermal and Thermoelastic Properties of Isotropic Composites," Journal of Composite Materials, Vol. 4, July 1970, pp. 286-295.
42. Tummala, R.R. and Friedberg, A.L., "Composites, Carbides, Thermal Expansion of Composite Materials," Journal of Applied Physics, Vol. 41, 1970, pp. 5104-5107.
43. Wang, T.T. and Kwei, T.K., "Effect of Induced Thermal Stresses on the Coefficients of Thermal Expansion and Densities of Filled Polymers," Journal of Polymer Science, Part A-2, Vol. 7, 1969, pp. 889-896.
44. Fahmy, A.A. and Ragai, A.N., "Thermal-Expansion Behavior of Two-Phase Solids," Journal of Applied Physics, Vol. 41, 1970, pp. 5108-5111.
45. Timoshenko, S.P. and Goodier, J.N., "Theory of Elasticity," Third Edition, McGraw Hill Book Company, New-York, 1970, pp. 452-456.
46. Mendelson, A., "Plasticity: Theory and Application," MacMillan Company, New York, 1970, p. 74.
47. Lement, B.S., Averbach, B.L. and Cohen, M., "The Dimensional Behavior of Invar," Transactions of the American Society of Metals, Vol. 43, 1951, pp. 1072-1097.
48. Scott, H., "Expansion Characteristics of Low-Expansion Nickel Steels," Transactions of the American Society of Steel Treatment, Vol. 13, 1928, pp. 829-847.
49. Scott, H., "Expansion Properties of Low-Expansion Fe-Ni-Co Alloys," Transactions of the American Institute of Mining, Metallurgical and Petroleum Engineers, Vol. 89, 1930, pp. 506-537.
50. Zakharov, A.I. and Fedotov, L.N., "Low-Temperature Thermal Expansion of Invar," Phys. Metals Metallogr., Vol. 23, No. 4, 1967, pp. 201-203.

51. Bol'shakov, Y.V., Zakharov, A.I., Pozvonkov, F.M., Solov'eva, N.A. and Fridman, V.G., "Thermal Expansion of Alloy 36 Nkh AT 4.2-300K," Metal Science and Heat Treatment, Vol. 3, 1971, p. 234.
52. Hunter, M.A., "Low Expansion Alloys," Metals Handbook, Vol. I, American Society of Metals, 1961, pp. 816-819.
53. Zakharov, A.I., Perepelkina, A.M. and Shiryayeva, A.N., "Effect of Alloying on Thermal Expansion of Superinvar Alloy," Metal Science and Heat Treatment, Vol. 6, 1972, pp. 539-541.
54. Waring, J.L., Roth, R.S. and Parker, H.S., "Temperature-Pressure Phase Relationships in Niobium Pentoxide," Journal of Research of the National Bureau of Standards, Vol. 77A, No. 6, 1973, pp. 705-711.
55. Roth, R.S., "Phase Equilibrium Relations in the Binary System Lead Oxide-Niobium Pentoxide," Journal of Research of the National Bureau of Standards, Vol. 62, No. 1, 1959, pp. 27-38.
56. Goldschmidt, H.J., "A High-Temperature X-Ray Investigation On Niobium Pentoxide and Some Problems Concerning the Oxidation of Niobium," Journal of the Institute of Metals, Vol. 87, 1958-59, pp. 235-239.
57. Gatehouse, B.M. and Wadsley, A.D., "The Crystal Structure of the High Temperature Form of Niobium Pentoxide," Acta Crystallographica, Vol. 17, 1964, pp. 1545-1554.
58. Suh, N.P. and Fillion, P.D., "Optimization of Cutting Tool Properties Through the Development of Alumina Cermet," Wear, to appear.

APPENDIX I

THERMAL EXPANSION COEFFICIENT OF COMPOSITES: LITERATURE REVIEW

A simple equation for the thermal expansion coefficient of a composite, α_c , is obtained by the rule of mixtures as

$$\alpha_c = \alpha_1 x_1 + \alpha_2 x_2 + \dots + \alpha_n x_n \quad (I.1)$$

This equation assumes that the elastic properties (e.g. E and ν) of the constituent phases are equal. However, because all materials do not have the same elastic properties, elastic interaction between phases is bound to occur and hence the need for a more rigorous equation.

For the past thirty-five years many researchers have investigated this problem. The first was Turner [1]. He assumed that with temperature changes each phase in the composite is constrained to expand or contract the same rate as the aggregate and that the shear deformation is negligible. Using this assumption he derived the following equation

$$\alpha_c = \frac{\alpha_1 K_1 x_1 + \alpha_2 K_2 x_2 + \dots + \alpha_n K_n x_n}{K_1 x_1 + K_2 x_2 + \dots + K_n x_n} \quad (I.2)$$

Or, for two-phase composite

$$\alpha_c = \frac{\alpha_m K_m x_m + \alpha_d K_d x_d}{K_m x_m + K_d x_d} \quad (I.3)$$

Turner realized that his equation might not fit the experimental data because the shape and size of various phases could have an effect on the coefficient of thermal expansion. However it was found in fact that Turner's equation agrees quite well with the thermal expansion of fiber-reinforced composites [2].

In 1956 Kerner [3] developed an equation by assuming that the composite is isotropic and homogeneous (on a large scale) and that the dispersed phases are in the form of randomly distributed spherical grains suspended in, and bonded to, a uniform medium. He also assumes some average state of stress or strain in the grains and that an average grain is surrounded by an average shell of the suspending medium. He further assumes that when the volume fraction of the suspending fluid goes to zero, in the limit, its properties are equal to the properties of the composite. According to this model the thermal expansion of a composite is given by

$$\alpha_c = \frac{4G_c}{K_c} + 3 \sum_{i=1}^n \left(\frac{\alpha_i x_i}{4 \frac{G_c}{K_i} + 3} \right) \quad (I.4)$$

Using the same model Kerner found the same bulk modulus of the composite to be

$$K_c = \frac{\sum_{i=1}^n K_i x_i / (3K_i + 4G_i)}{\sum_{i=1}^n x_i / (3K_i + 4G_i)} \quad (I.5)$$

so if a two phase composite is considered where phase d is dispersed in matrix m then

$$G_c = G_m \quad (1.6)$$

Substituting equations (1.5) and (1.6) in equation (1.4)

$$\alpha_c = \frac{\alpha_m K_m x_m / (4G_m + 3K_m) + \alpha_d K_d x_d / (4G_m + 3K_d)}{K_m x_m / (4G_m + 3K_m) + K_d x_d / (4G_m + 3K_d)} \quad (1.7)$$

It was found that Kerner's equation agrees quite well with experimental values obtained on matrices containing spherical filler particles, even though the assumption of isostatic stress throughout the composite is not clearly an acceptable one.

Holliday and Robinson [2] refer to an empirical equation proposed by Thomas in 1960; the equation is

$$\alpha_c = x_m \alpha_m^a + x_d \alpha_d^a \quad (1.8)$$

where a varies from -1 to $+1$ depending on the particular system. If a is small

$$\ln \alpha_c = x_m \ln \alpha_m + x_d \ln \alpha_d \quad (1.9)$$

$$a = -1 \quad \frac{1}{\alpha_c} = \frac{x_m}{\alpha_m} + \frac{x_d}{\alpha_d}$$

$$a = +1 \quad \alpha_c = x_m \alpha_m + x_d \alpha_d \quad (1.10)$$

The empirical nature of this equation makes it suitable for most composites provided the adjustable constant a is known, but it is devoid of any physical significance.

Arthur and Coulson [4] refer to an equation of Blackburn

$$\alpha_c = \alpha_d + \frac{3(1 - \nu_d)(\alpha_m - \alpha_d)x_d}{(1 + \alpha_d) + 2x_m(1 - 2\alpha_d) + 2x_d(1 - 2\alpha_m)} \frac{E_d}{E_m} \quad (I.11)$$

This equation was derived for the case of spherical particles in a matrix at low concentration.

In 1968 Cribb [5] developed the following equation

$$\alpha_c = \frac{K_m(K_c - K_d)}{K_c(K_m - K_d)} \alpha_m + \frac{K_d(K_m - K_c)}{K_c(K_m - K_d)} \alpha_d \quad (I.12)$$

This equation assumes the phases to be homogeneous and isotropic, but there were no limitations on size or shape of the particles. This equation requires that the bulk modulus of the composite is known a priori.

Similar equations, equations where G_c , K_c , E_c and α_c are known a priori, were published by Budiansky [6] in 1970. He assumed that the composite consists of random mixtures of n isotropic phases and that at least $(n-1)$ of these phases are distributed in a particulate fashion, with the particles roughly spherical in shape.

$$\alpha_c = \left[\sum_{i=1}^n x_i (K_i/K_c) \alpha_i [1 - a + a(K_i/K_c)] \right]^{-1} \quad (I.13)$$

$$\text{where } a = \frac{1}{3} \left[\frac{1 + \nu_c}{1 - \nu_c} \right] \quad (\text{I.14})$$

$$\text{and } \nu_c = \frac{3K_c + 2G_c}{6K_c + 2G_c} \quad (\text{I.15})$$

For a two-component composite these equations yield

$$\frac{\alpha_c - \alpha_d}{\alpha_m - \alpha_d} = \frac{K_c^{-1} - K_d^{-1}}{K_m^{-1} - K_d^{-1}} \quad (\text{I.16})$$

It is obvious therefore that Cribb's and Budiansky's equations cannot be used to directly calculate the coefficient of thermal expansion of the composite because K_c and G_c are not known a priori. This difficulty is circumvented by iterative procedures.

Tummala and Friedberg [7] published the following equation for a two-phase particle-dispersed composite in 1970

$$\alpha_c = \alpha_m - \frac{(\alpha_m - \alpha_d)x_d (1 + \nu_m)/2E_m}{[(1 + \nu_m)/2E_m] + [(1 - 2\nu_d)/E_d]} \quad (\text{I.17})$$

where it was assumed that the composite's thermal expansion coefficient is the sum of the matrix thermal expansion coefficient modified by the effect of the dispersed phase upon the expansion of the matrix, and the expansion coefficient of the dispersed phase modified by the effect of matrix on the expansion of the dispersed phase. Examination of the term

$$\frac{(1 + \nu_m)/2E_m}{[(1 + \nu_m)/2E_m] + [(1 - 2\nu_d)/E_d]} \quad (I.18)$$

shows that it is a constant for a given system since it is independent of the volume fraction of either phase. Equation (I.17) represents a straight line, emphasizing that it can only be valid over a limited range where the volume fraction of the dispersoid is low (<0.25). It is interesting to note also that when $E_d \gg E_m$ Equation (I.18) approaches unity and hence Equation (I.17) will be the same as Equation (I.1).

Finally, Wang and Kwei [8] in 1969 and Fahmy and Ragai [9] in 1970 independently derived the following equation

$$\alpha_c = \alpha_m - \frac{3(\alpha_m - \alpha_d)(1 - \nu_m)x_d}{2 \frac{E_m}{E_d} (1 - 2\nu_d)x_m + 2x_d(1 - 2\nu_m) + (1 + \nu_m)} \quad (I.19)$$

In this model spherical particles were assumed to be dispersed. The derivation was made for a single spherical composite particle where each sphere from one phase is surrounded by a spherical shell of the other phase. This one-particle model was then extended for the final composite where a number of those composite particles of various sizes are assembled together. It is assumed that filler particles are more or less evenly distributed in the matrix without coming into physical contact.

Equation (I.19) is the same as that derived in Chapter III of this thesis and it is the one used to compute the value of α_c for different volume fractions of the dispersed phase.

Perhaps it is worth reminding here that all the above equations were derived on the assumption that only elastic deformation takes place and that bonding between the phases is perfect. So, if the matrix deforms plastically or if poor adhesion between the phases is encountered, then the equations are no longer valid. Also, these equations do not take into account the size of the particles. There is no immediate evidence that the size of the particles will affect the coefficient of thermal expansion, but it will affect the stresses in the various phases hence fracture might occur. Hence the size of the particles might have an effect on the coefficient of thermal expansion.

None of these equations agreed with data obtained on all composites although it was found [2] that Turner's equation applies quite well to composites in which the filler is fibrous whereas equations in derived by Kerner [3], Wang and Kwei [8] and Fahmy and Ragai [9] apply quite well to composites containing spherical filler particles.

APPENDIX I - REFERNECES

- I-1. Turner, P.S., "Thermal-Expansion Stresses in Reinforced Plastics," Journal of Research National Bureau of Standards Vol. 37, 1946, pp. 239-250.
- I-2. Holliday, L. and Robinson, J., "Review: The Thermal Expansion of Composites Based on Polymers," Journal of Materials Science, Vol. 8, 1973, pp. 301-311.
- I-3. Kerner, E.H., "The Elastic and Thermo-Elastic Properties of Composite Media," Proceedings of the Physical Society, Vol. 69, 1956, pp. 808-813.
- I-4. Arthur G. and Coulson, J.A., "Physical Properties of Uranium Dioxide-Stainless Steel Cermets," Journal of Nuclear Materials, Vol. 13, No. 2, 1964, pp. 242-253.
- I-5. Cribb, J.L., "Shrinkage and Thermal Expansion of a Two Phase Material," Nature, Vol. 220, 1968, pp. 576-577.
- I-6. Budiansky, B., "Thermal and Thermoelastic Properties of Isotropic Composites," Journal of Composite Materials, Vol. 4, July 1970, pp. 286-295.
- I-7. Tummala, R.R. and Friedberg, A.L., "Composites, Carbides, Thermal Expansion of Composite Materials," Journal of Applied Physics, Vol. 41, 1970, pp. 5104-5107.
- I-8. Wang, T.T. and Kwei, T.K., "Effect of Induced Thermal Stresses on the Coefficients of Thermal Expansion and Densities of Filled Polymers," Journal of Polymer Science, Part A-2, Vol. 7, 1969, pp. 889-896.
- I-9. Fahmy, A.A. and Ragai, A.N., "Thermal-Expansion Behavior of Two Phase Solids," Journal of Applied Physics, Vol. 41, 1970, pp. 5108-5111.

APPENDIX II
FLAME SPRAYING

The thermospray system used was MetCo 6P-H hand-held manual spray gun. Approximate schematic diagram [1] of the thermospray system is shown in Figure II-1. (The thermospray gun shown is the MetCo 5P model; the only difference between the two models is that in the MetCo 6P-H gun the powder is fed from the back of the gun instead of the top). The powder emerged through the center of the head. The feed rate was about 450-900g per hour. A temperature of 4000K was provided by an oxy-acetylene flame.

The size of the Nb_2O_5 particles was 38-63 μm . Particles larger than 63 μm did not melt and particles smaller than 38 μm stuck together and did not flow evenly through the gun. The powder was sprayed in a water bath and was collected by filtration. Then it was dried for two days in air at room temperature and baked at 373K for two hours to get the remaining moisture out. The size of the flame-sprayed particles was about the same as that of the initial particles.

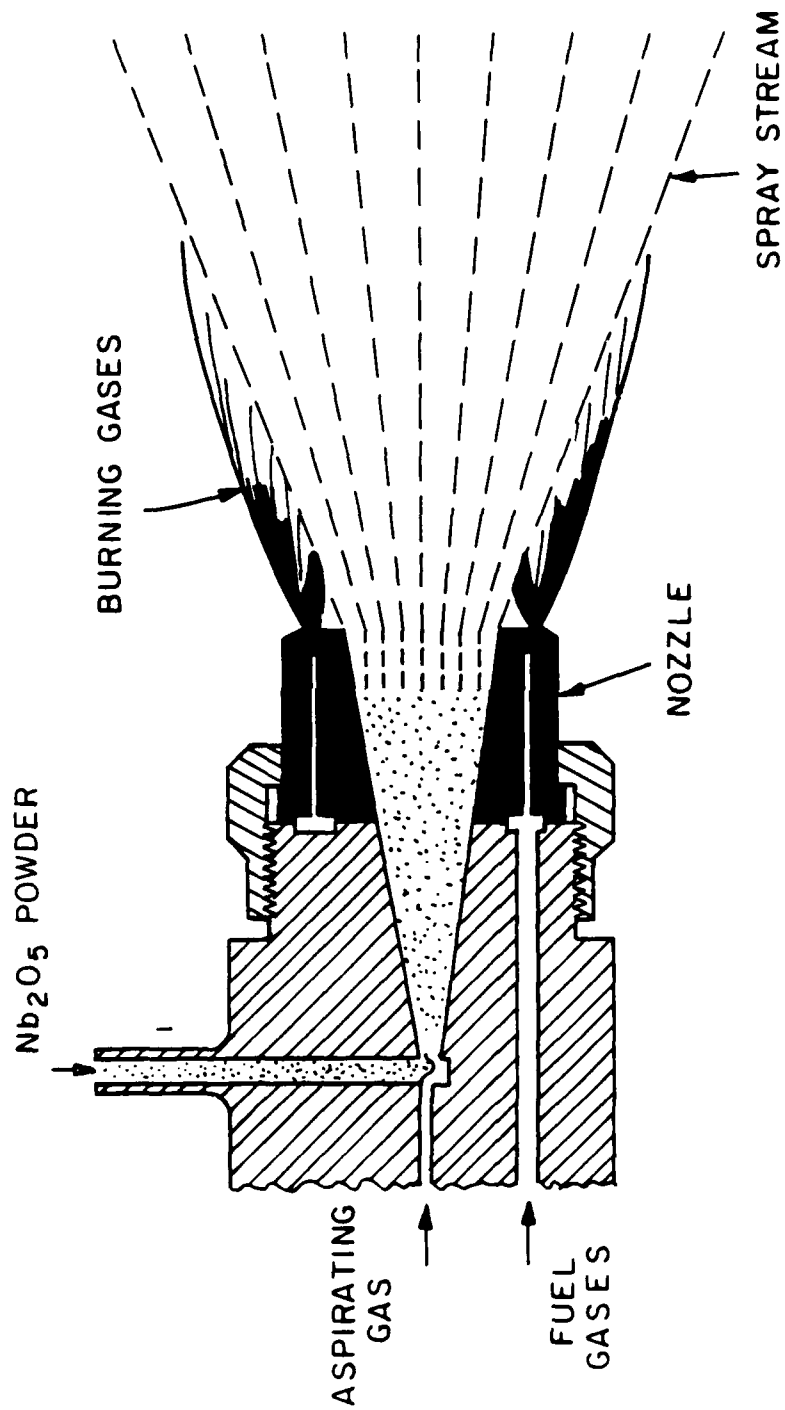


FIGURE II.1: SCHEMATIC DIAGRAM OF THE THERMOSPRAY SYSTEM

APPENDIX II - REFERENCE

1. Ingham, H.S. and Shephard, A.P., "Flame Spray Handbook, Vol. II, Powder Process," Second Edition, METCO, Inc., New York, 1964.

APPENDIX III
ELECTROLESS PLATING

For coating each Nb_2O_5 particle with nickel a commercial electroless nickel plating process was used. This process is employed in industry for plating high purity nickel on metals, semiconductors and insulators.

The composition of the plating bath is given in Table III-1. Unfortunately, it was not possible to obtain the exact chemical composition of the bath, except that it contains nickel sulfate and uses dimethylamine borane (DMAB) $[(\text{CH}_3)_2\text{NHBH}_3]$ as a reducing agent.

About 6g of flame sprayed Nb_2O_5 powder (38-63 μm) was soaked in PdCl_2 catalyst (1g PdCl_2 per 500 ml of distilled water) for 15 minutes, rinsed twice with distilled water and poured into a liter of electroless plating solution held at 338K in a Pyrex beaker. Depending on the volume fraction of the nickel required the plating was carried out for 2-17 hours. While nickel was being plated on Nb_2O_5 , hydrogen bubbles were released. When the evolution of hydrogen ceased, which indicates that the plating rate was not appreciable, the plating bath was replaced by a fresh one every 2-3 hours of plating time. Table III-2 gives the plating time and the number of times a fresh solution was used for different volume fractions of nickel.

A magnetic stirrer was used to reduce the temperature gradients in the bath and to keep the Nb_2O_5 particles suspended. This

TABLE III-1. COMPOSITION OF THE NIPOSIT 468
ELECTROLESS PLATING BATH*

CONSTITUENT	VOLUME PERCENT
Niposit 468A	4
Niposit 468B	4
Niposit 468M	2.5
Distilled water	88.5

* Supplied by Shipley Co., Danvers, MA
One liter of plating solution contains 4.4g of Ni.

TABLE III-2. PLATING TIME vs NICKEL VOLUME FRACTION*

CUMULATIVE PLATING TIME, hours	NUMBER OF TIMES FRESH SOLUTION USED	VOLUME FRACTION OF Ni
2	1	0.095
4	2	0.127
8	3	0.368
17	6	0.665

*Amount of Nb_2O_5 used is about 6g.

prevented the particles from settling down to the bottom of the beaker and allowing them to be uniformly coated.

The pH of the bath was maintained between 6.8 and 7.5. When the temperature of the bath reached 338K, the pH dropped to 6.55. Because low pH reduces the plating rate substantially, about 5m% of NH_4OH per liter of the plating solution was added to the bath which brought the pH back to 7.3 and kept the plating rate constant. A schematic of the experimental apparatus is shown in Figure (III-1).

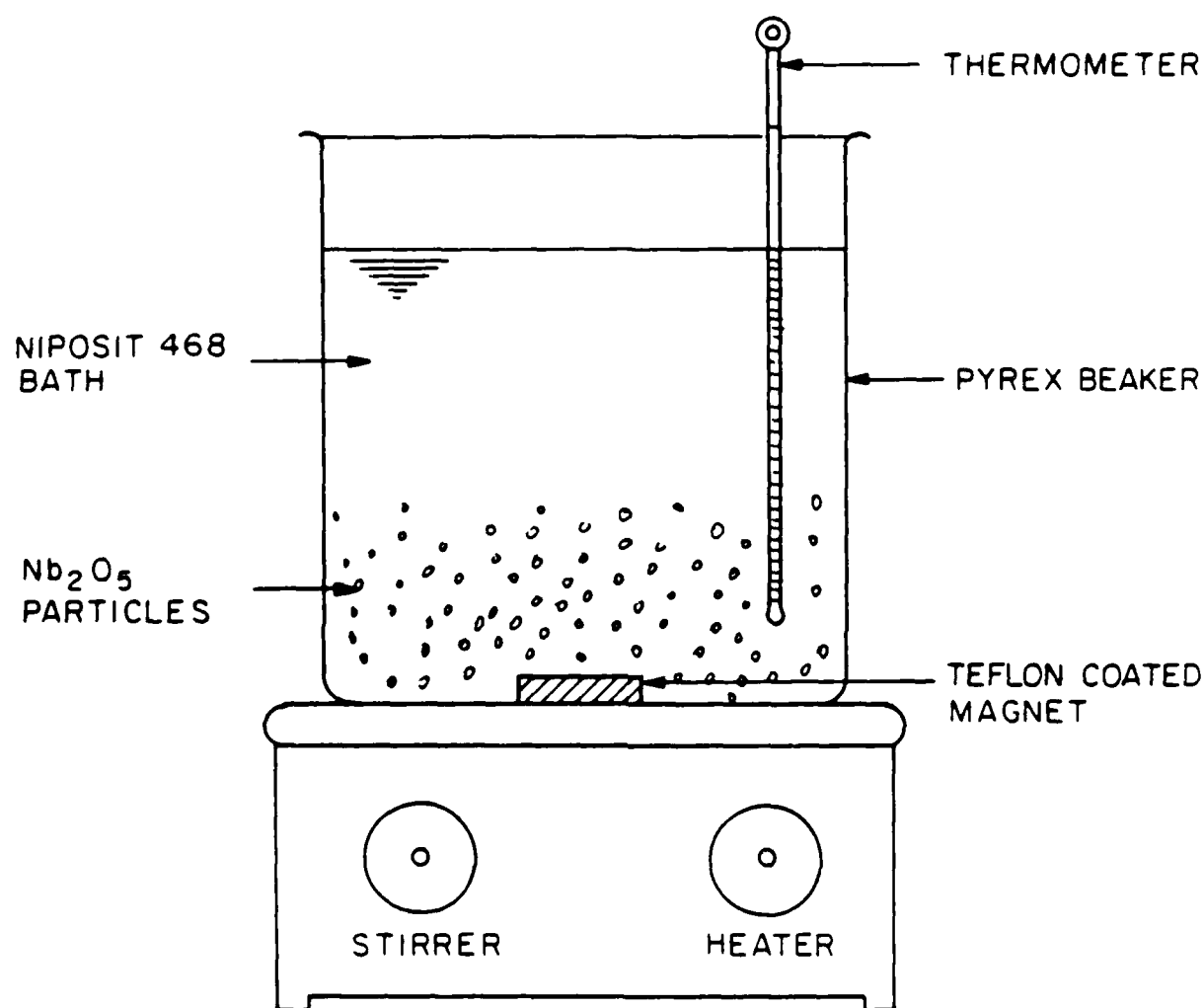


FIGURE III.1. SCHEMATIC DIAGRAM OF THE ELECTROLESS NICKEL PLATING APPARATUS

APPENDIX IV

HOT PRESSING

The coated and mixed powders were compacted by uniaxial hot pressing. This appendix will discuss the equipment used, the choice of the hot pressing parameters and the environment.

Equipment

Hot pressing was done by means of a large hydraulic press in a Poco graphite die which was heated inductively. The apparatus is shown in Figure IV-1, and Figure IV-2 shows the schematic diagram of the hot pressing die.

The pressure was applied by a hydraulic press capable of delivering loads up to 100 tons on a 15 cm ram. A hydraulic pump was used to maintain constant pressure on the specimen during the run. A 7.5 KVA Lepel induction unit supplied the power. The graphite die, which rested on Transite discs, was located in a water cooled vacuum chamber. The die was surrounded by a water cooled induction coil connected to the induction unit. Kaowool insulation was used between the coil and the die. The pressure was transmitted to the specimen through the stainless steel rods and graphite plungers. Transite discs served as insulation between the stainless steel rods and graphite plungers. A vacuum pump and an argon supply tank were connected to the chamber. The temperature was measured by means of a Pt/Pt-10% Rh thermocouple.



FIGURE 1. Evaporation setup.

1. The rate of evaporation is measured by the change in mass of the liquid.

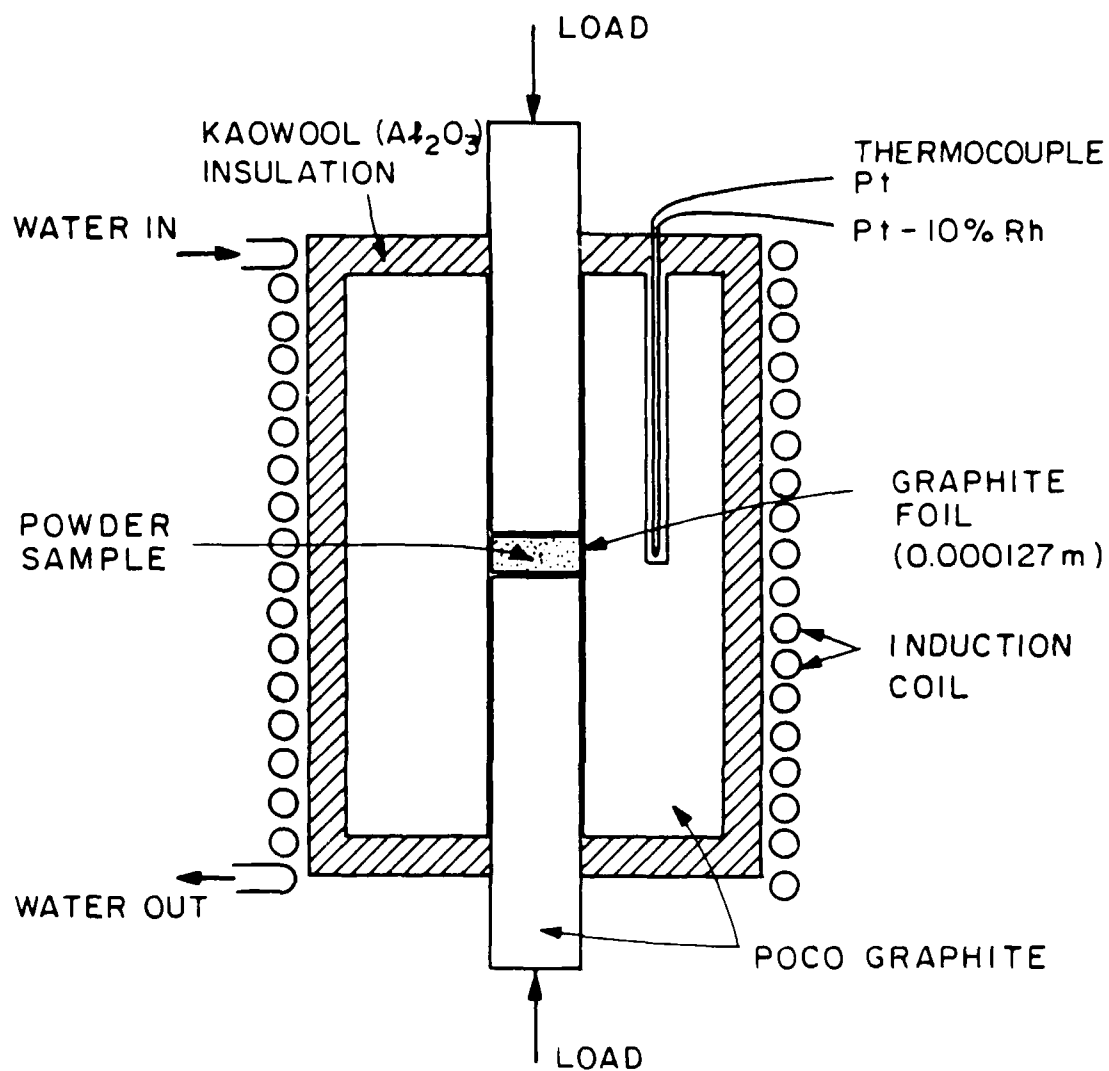


FIGURE IV.2. SCHEMATIC DIAGRAM OF HOT PRESSING DIE

Environment

To prevent oxidation of the powders, graphite die and graphite plungers hot pressing was carried out in an inert atmosphere [1]. Using a mechanical pump a vacuum of 0.5 Torr was first obtained. Then the chamber was filled with argon and a continuous flow was maintained throughout the run.

Process Parameters

The primary processing parameters are pressure, temperature and time. Some researchers have attempted to optimize these parameters [2-4] considering that the principal mechanism of densification is either diffusion or plastic deformation. However, the theoretical predictions did not always agree with the experimental results especially with materials that develop nonstoichiometry, or go through structure changes. So the choice of the parameters was not done according to any of those theories, but rather by using the results in those articles as a guideline.

For oxides, such as Al_2O_3 and ZrO_2 , the pressing temperature was about 1600-2000K that is about 80% of the oxide's melting temperature, or higher. Hence, for nickel, Nb_2O_5 and superinvar samples, whose melting temperatures are in the range 1720-1920, a temperature of 1473K was used.

In the graphite die the maximum allowed pressures are about 69 MPa (10,000 psi). In a trial run a pressure of 34.5 MPa (5000 psi) was chosen. After the first sample was hot pressed it was found that

this pressure was adequate, hence it was used for the rest of the samples.

The hot pressing time can vary from five minutes to one hour depending on the pressing temperature. The higher the temperature the lower could be the pressing time. Thirty minutes was chosen as the hot pressing time since the temperature is not near the melting point.

In summary, the sample was heated to a temperature of 1473K. Then a pressure of 34.5 MPa was applied to 30 minutes after which time pressure was released and the specimen was furnace cooled. The hot pressing conditions are shown in Figure IV-3.

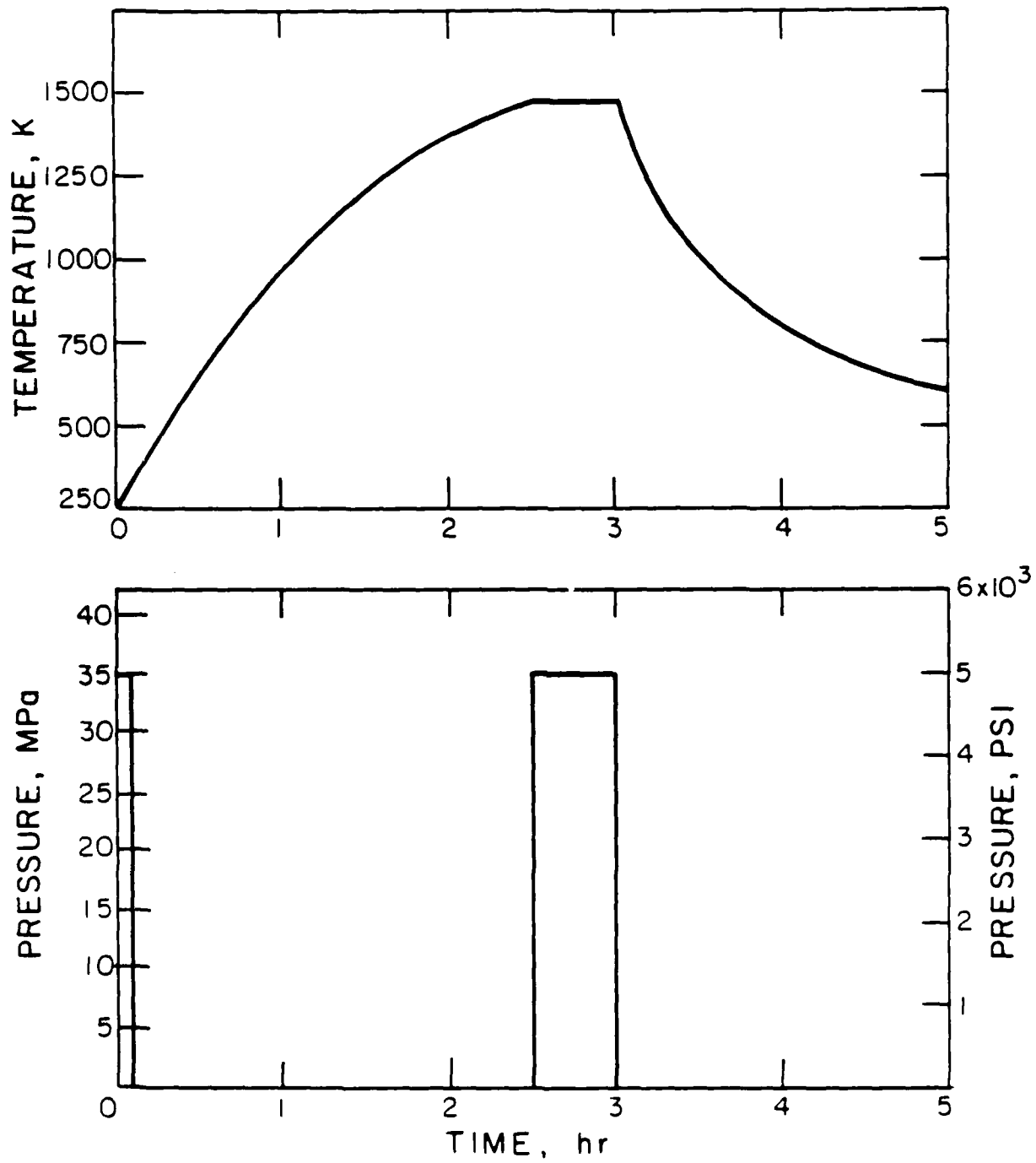


FIGURE IV.3. HOT PRESSING CONDITIONS

APPENDIX IV - REFERENCES

1. Leipold, M.H., "Hot Pressing", Treatise on Materials Science and Technology, Vol. 9, Ed. Wang, F.F.Y., Academic Press, Inc., London, 1976, pp. 95-134.
2. Murray, P., Livey, D.T., and Williams, J., "The Pressing of Ceramics", Ceramic Fabrication Processes, Ed., Kingery, W.D., The M.I.T. Press, Cambridge, MA 1963, pp. 147-171.
3. Palmour, H., III, and Johnson, D.R., "Phenemenological Model for Rate Controlled Sintering", Sintering and Related Phenomena, Ed. Kuczynski, G.C., Hooton, W.A. and Gibbon, C.F., Gordon and Breach, New York, 1967, pp. 779-791.
4. Vasilos, T. and Spriggs, R.M., "Pressure Sintering of Ceramics", Progress in Ceramic Science, Vol. 4, Ed. Burke, J.E., Pergamon Press, New York, 1966, pp. 90-132.

APPENDIX V

CTE MEASUREMENT

The coefficient of thermal expansion of the composites was measured by the contactless laser interferometric technique at the Aerospace Corporation, El Segundo, CA. The advantages of this controlled measurement technique [1] are:

- (a) contactless methods reduce microcreep, thermal lag, need for corrections, surface abrasions or contamination, extra fabrication steps, temperature range restrictions, environmental restrictions and contact fastening induced stresses, and
- (b) contactless methods allow arbitrary sample size or shape, separate heating and gaging circuits, moving or vibrating systems and studies of surface effects.

Contactless length measurement can be performed by several methods, but the most accurate one is the Michelson interferometry [2]. Figure IV-1 shows the double Michelson interferometer used for ultra-low CTE measurement of small samples. The laser beam, L, is split at a beam splitter (not shown in Figure V-1). The resulting beams then go through their respective paths through mirrors, m, beam splitters, B/S, lenses, L, and finally to photo detectors, PD. The change of length of the sample is then the difference between the two changes in optical path lengths. Those two paths are the one that appears to pass through the sample and the one that does not [3].

Also, an apparatus for heating the samples is shown in Figure V-2.

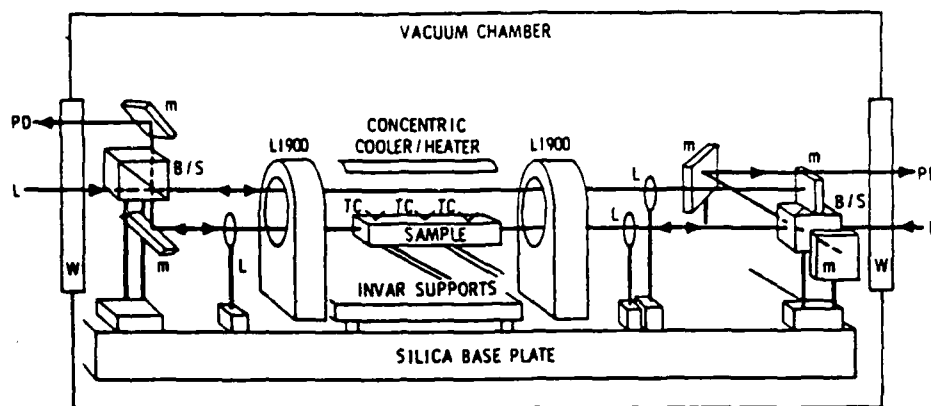


FIGURE V.1. DOUBLE MICHELSON INTERFEROMETER FOR SMALL SAMPLE CTE MEASUREMENTS

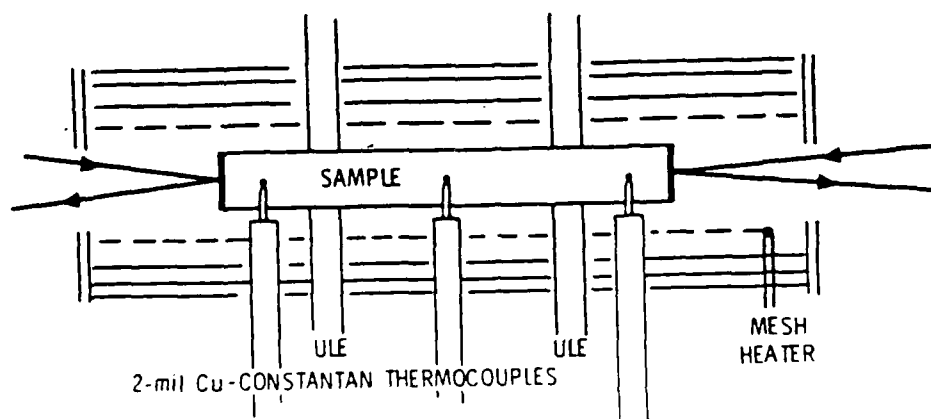
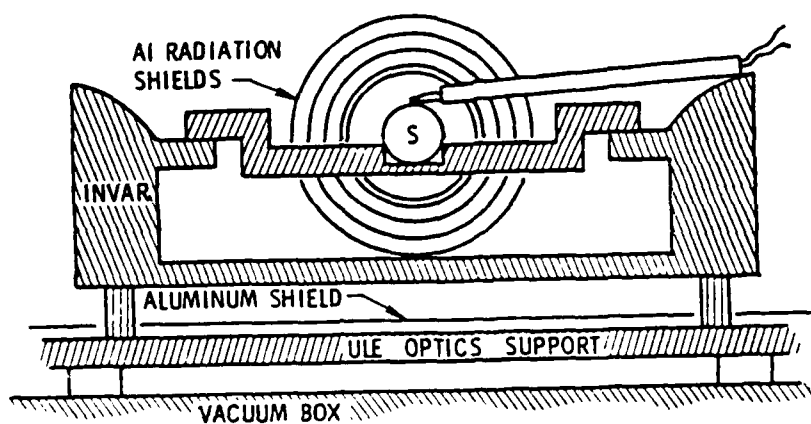


FIGURE V.2. APPARATUS FOR HEATING CYLINDRICAL SAMPLES

For the samples that had high metal volume fraction, a quartz dilatometer was used to measure the coefficient of thermal expansion. Even though this method is not as good as the laser interferometry and it is only accurate within $\pm 5-10\%$, it is quite acceptable for measuring high values of the coefficients of thermal expansion (larger than $1 \times 10^{-6} \text{K}^{-1}$). This method is not very sensitive hence it cannot be used to measure low coefficients of thermal expansion.

APPENDIX V REFERENCES

1. Wolff, E.G., "Measurement Technique for Low Expansion Materials", Society for Advancement of Material and Process Engineering, Vol. 9, 1977, pp. 57-72.
2. Wolff, E.G. and Eselun, S.A., "Absolute Length Changes by Remote Interferometry", Interim Report prepared for Space and Missile Systems Organization Air Force Systems Command, Aerospace Corporation, El Segundo, CA 1975.
3. Wolff, E.G. and Eselun, S.A., "Double Michelson Interferometer for Contactless Thermal Expansion Measurements", Interferometry, SPIE Proceedings, Vol. 192, 1979, pp. 204-208.

END

DATE

FILMED

FEB.

1988